National Library of Canada

Acquisitions and Bibliographic Services Branch

395 Wellington Street
Ottawa, Ontario
K1A 0N4

Bibliothèque nationale du Canada

Direction des acquisitions et des services bibliographiques

395, rue Wellington
Ottawa (Ontario)
K1A 0N4

Your file Votre référence

Our file Notre référence

NOTICE

The quality of this microform is heavily dependent upon the quality of the original thesis submitted for microfilming. Every effort has been made to ensure the highest quality of reproduction possible.

If pages are missing, contact the university which granted the degree.

Some pages may have indistinct print especially if the original pages were typed with a poor typewriter ribbon or if the university sent us an inferior photocopy.

Reproduction in full or in part of this microform is governed by the Canadian Copyright Act, R.S.C. 1970, c. C-30, and subsequent amendments.

AVIS

La qualité de cette microforme dépend grandement de la qualité de la thèse soumise au microfilmage. Nous avons tout fait pour assurer une qualité supérieure de reproduction.

S'il manque des pages, veuillez communiquer avec l'université qui a conféré le grade.

La qualité d'impression de certaines pages peut laisser à désirer, surtout si les pages originales ont été dactylographiées à l'aide d'un ruban usé ou si l'université nous a fait parvenir une photocopie de qualité inférieure.

La reproduction, même partielle, de cette microforme est soumise à la Loi canadienne sur le droit d'auteur, SRC 1970, c. C-30, et ses amendements subséquents.

Canada

UNIVERSITY OF ALBERTA

A study of an end-on inductively coupled plasma optical emission spectrometer (ICP-OES); and the addition of nitrogen into an argon inductively coupled plasma mass spectrometer (ICP-MS).

by

Diana Lee Smith

©

A thesis submitted to the Faculty of Graduate Studies and Research in partial fulfillment of the requirements for the degree of Master of Science.

DEPARTMENT OF CHEMISTRY

Edmonton, Alberta
Fall 1994

National Library
of Canada

Acquisitions and
Bibliographic Services Branch

395 Wellington Street
Ottawa, Ontario
K1A 0N4

Bibliothèque nationale
du Canada

Direction des acquisitions et
des services bibliographiques

395, rue Wellington
Ottawa (Ontario)
K1A 0N4

Your file Votre référence

Our file Notre référence

The author has granted an irrevocable non-exclusive licence allowing the National Library of Canada to reproduce, loan, distribute or sell copies of his/her thesis by any means and in any form or format, making this thesis available to interested persons.

L'auteur a accordé une licence irrévocable et non exclusive permettant à la Bibliothèque nationale du Canada de reproduire, prêter, distribuer ou vendre des copies de sa thèse de quelque manière et sous quelque forme que ce soit pour mettre des exemplaires de cette thèse à la disposition des personnes intéressées.

The author retains ownership of the copyright in his/her thesis. Neither the thesis nor substantial extracts from it may be printed or otherwise reproduced without his/her permission.

L'auteur conserve la propriété du droit d'auteur qui protège sa thèse. Ni la thèse ni des extraits substantiels de celle-ci ne doivent être imprimés ou autrement reproduits sans son autorisation.

ISBN 0-315-95113-3

Canada

UNIVERSITY OF ALBERTA

RELEASE FORM

NAME OF AUTHOR: Diana Lee Smith

TITLE OF THESIS: **A study of an end-on inductively coupled plasma optical emission spectrometer (ICP-OES); and the addition of nitrogen into an argon inductively coupled plasma mass spectrometer (ICP-MS)**

DEGREE: Master of Science

YEAR THIS DEGREE GRANTED: 1994

Permission is hereby granted to the University of Alberta Library to reproduce single copies of this thesis and to lend or sell such copies for private, scholarly or scientific research purposes only.

The author reserves all other publication and other rights in association with the copyright in the thesis, and except as hereinbefore provided thesis nor any substantial portion thereof may be printed or otherwise reproduced in any material form whatever without the author's prior written permission.

Diana Lee Smith

111 Raglan Ave #2104
Toronto Ontario Canada
M6C 2K9

Date: Sept 6 1994

UNIVERSITY OF ALBERTA

FACULTY OF GRADUATE STUDIES AND RESEARCH

The undersigned certify that they have read, and recommend to the Faculty of Graduate Studies and Research for acceptance, a thesis entitled **"A study of an end-on inductively coupled plasma optical emission spectrometer (ICP-OES); and the addition of nitrogen into an argon inductively coupled plasma mass spectrometer (ICP-MS)"** submitted by Diana Lee Smith in partial fulfillment of the requirements for the degree of Master of Science.

Gary Horlick.

Professor G. Horlick

Professor L. Li

Professor J.D. Dale

Date: Sept. 6, 1994

ABSTRACT

The effect of the addition of nitrogen into the various gas flows of the inductively coupled plasma, detected by a mass spectrometer (ICP-MS), upon the background species argon oxide, hydroxide, and dimers, and upon the signals of the analytes, iron and selenium, with which these species interfere, has been studied. The most benefit was obtained from the introduction of nitrogen into the coolant flow. Compared with the signals in an argon plasma, when nitrogen is introduced into the coolant flow, and the nebulizer flow is increased and the sampling distance is decreased, the background signals were reduced to approximately half their intensity, while iron signals were tripled and selenium signals increased sixfold when the forward power was also increased. The signal to noise ratios were at least tripled, while the signal to background ratios were increased fourfold.

The sample extraction zone of the ICP-MS was studied using optical emission spectrometric (OES) detection. The zone which was observed through a sampling orifice was found to be similar to an ICP viewed end-on along its axis. The effect of the addition of nitrogen into the coolant gas upon the atomic emission of magnesium and lead was studied. Compared with the signals in an argon plasma, the ionic and atomic emission intensity for lead and magnesium and the background continuum emission were increased when nitrogen was introduced into the coolant. The signal response to the addition of nitrogen differed somewhat from responses generally seen for both ICP-MS and ICP-OES. An attempt to view the zone of expansion showed very weak analyte emission and much reduced background continuum emission.

ACKNOWLEDGEMENT

This thesis is dedicated to my partner, Lyle Burton, in loving recognition of his playfulness, generosity, support, and unstinting lovingkindness.

A sincere thank you to my supervisor, Gary Horlick, for his guidance and cheerful tolerance through the past several years.

A special thank you to the machinists, the glassblowers, and the electronics specialists, who have been generous and helpful.

I would like to acknowledge the financial support of the Natural Sciences and Engineering Research Council of Canada.

TABLE OF CONTENTS

page

Abstract

Acknowledgements

Table of Contents

List of Tables

List of Figures

Chapter 1
INTRODUCTION 1

1.1 Objectives 1

1.2 Introduction to ICP-MS 3

1.3 Instrumentation 6

1.3.1 ICP 6

1.3.2 Sampling Interface 8

1.3.3 Detection 10

1.4 Overview of Thesis 12

Chapter 2
EXPERIMENTAL 13

2.1 Experimental Apparatus 13

2.2 Mass Spectrometric Detection 15

2.3 Optical Spectrometric Detection 19

Chapter 3
MASS SPECTROMETRIC MEASUREMENTS 25

3.1 Introduction 25

3.2 Results 27

3.2.1 Argon plasma 27

3.2.2 Introduction of nitrogen into the plasma 33
3.2.2.a Addition of nitrogen into the coolant gas 33
3.2.2.b Addition of nitrogen into the nebulizer gas 50
3.2.2.c Addition of nitrogen into all plasma gases 54
3.3 Conclusions 61

Chapter 4
OPTICAL MEASUREMENTS 63
4.1 Introduction 63
4.2 Results 65
4.2.1 End-on view of the ICP-sampler interface 65
4.2.2 End-on view of the ICP 80
4.2.3 Side-on view of the ICP 85
4.3 Conclusions 91

Chapter 5
CONCLUSIONS 92

REFERENCES 94

LIST OF TABLES

Table	Description	page
2.1	Experimental details	17
2.2	Details of the optical detection system	24
3.1	Operating parameters as nitrogen is added to the coolant gas flow	42
3.2	Operating parameters as nitrogen is added into all gas flows	56
4.1	Species, wavelengths, and upper energy levels of the spectral line transitions monitored by ICP-OES	66

LIST OF FIGURES

Figure	Description	page
1.1	A schematic diagram of the inductively coupled plasma (ICP) torch.	7
1.2	A sketch of ICP-MS sampling interface, showing sampler, skimmer, and torch.	9
1.3	A schematic of the Sciex Elan 250 Mass Spectrometer.	11
2.1	A block diagram of the experimental set-up used in this work.	14
2.2	A schematic diagram of the ICP-MS system.	16
2.3	A schematic diagram of the ICP-OES system, "end-on" viewing set-up.	20
2.4	A schematic diagram of the ICP-OES system, (a) "end-on" viewing, no sample extraction set-up and (b) "side-on" viewing.	22
3.1	Mass spectrum of water in 2% nitric acid in 100% argon plasma (10–40 amu).	28
3.2	Mass spectrum of water in 2% nitric acid in 100% argon plasma (40–85 amu).	29
3.3	Dependence of the normalized signal intensity for 100 ppb Rh upon sampling distance, nebulizer gas flow rate, and forward power. (a) Forward power of 1.25 kW. Sampling distance varied. (b) Sampling distance of 15 mm. Forward power varied.	31

3.4 Dependence of the normalized signal intensity for 100 ppb Rh upon sampling distance, nebulizer gas flow, and constitution of the plasma as nitrogen added to the coolant. 34
(a) Forward power 1.25 kW, 15 mm sampling distance.
(b) Forward power 1.25 kW, 12 mm sampling distance.
(c) Forward power 1.5 kW, 15 mm sampling distance.

3.5 Dependence of the normalized signal intensity for 100 ppb Rh upon sampling distance, nebulizer gas flow rate, and forward power, as 10% nitrogen added to the coolant. 37

3.6 Dependence of the normalized net signal intensity for 100 ppb Fe^+ and the background species ArO^+ at m/z 56 upon the nebulizer flow rate and the constitution of the plasma as nitrogen added to the coolant at two forward powers. 39
(a) ArO^+, forward power 1.25 kW, 15 mm sampling distance.
(b) ArO^+, forward power 1.5 kW, 15 mm sampling distance.
(c) Fe^+, forward power 1.25 kW, 15 mm sampling distance.
(d) Fe^+, forward power 1.5 kW, 15 mm sampling distance.

3.7 Dependence of the normalized net signal intensity for 100 ppb Se^+ and the background species Ar_2^+ at m/z 78 upon the nebulizer flow rate and the constitution of the plasma as nitrogen added to the coolant at two forward powers. 40
(a) Ar_2^+, forward power 1.25 kW, 15 mm sampling distance.
(b) Ar_2^+, forward power 1.5 kW, 15 mm sampling distance.
(c) Se^+, forward power 1.25 kW, 15 mm sampling distance.
(d) Se^+, forward power 1.5 kW, 15 mm sampling distance.

3.8 Effect of the addition of nitrogen into the coolant upon the net signal intensities for 100 ppb analytes at two forward powers. Sampling distances are as shown in Table 3.1. The left hand axis shows absolute net signal level in counts/second. The right hand axis shows normalized values. (a) Rhodium at m/z 103. (b) Iron at m/z 56. (c) Iron at m/z 57. (d) Selenium at m/z 76. (e) Selenium at m/z 78. (f) Selenium at m/z 82. 44

3.9 Effect of the addition of nitrogen into the coolant upon the background signal intensities at two forward powers. Sampling distances are as shown in Table 3.1. The left hand axis shows absolute background signal level in counts/second. The right hand axis shows normalized values. (a) Background at m/z 103. (b) ArO^+ at m/z 56. (c) $ArOH^+$ at m/z 57. (d) Ar_2^+ at m/z 76. (e) Ar_2^+ at m/z 78. (f) Ar_2^+ at m/z 82. 45

3.10 Effect of the addition of nitrogen into the coolant upon the ratio of net signal/background signal (SBR) at two forward powers. Sampling distances are as shown in Table 3.1. The left hand axis shows absolute SBR. The right hand axis shows normalized values. (a) SBR at m/z 103. (b) SBR at m/z 56. (c) SBR at m/z 57. (d) SBR at m/z 76. (e) SBR at m/z 78. (f) SBR at m/z 82. 46

3.11 Effect of the addition of nitrogen into the coolant upon the ratio of net signal/background noise (SNR) at two forward powers. Sampling distances are as shown in Table 3.1. The left hand axis shows absolute SNR. The right hand axis shows normalized values. (a) SNR at m/z 103. (b) SNR at m/z 56. (c) SNR at m/z 57. (d) SNR at m/z 76. (e) SNR at m/z 78. (f) SNR at m/z 82. 47

3.12 Dependence of the normalized signal for 100 ppb Rh upon nebulizer flow rate and sampling distance as nitrogen added to the nebulizer gas at two forward powers, and varying the sampling distance. (a) Forward power 1.25 kW, varying sampling distance. (b) Forward power 1.5 kW, varying sampling distance. 51

3.13 Effect of the addition of 3% nitrogen into the nebulizer gas at 1.25 kW forward power at two sampling distances upon: (a) the normalized net signal intensity, (b) the normalized background intensity, (c) the normalized SBR, and (d) the normalized SNR. 53

3.14 Dependence of the normalized signal intensity for 100 ppb Rh upon nebulizer flow rate, sampling distance, and constitution of the plasma as nitrogen added to all gas flows. (a) Forward power 1.25 kW, 15 mm sampling distance. (b) Forward power 1.25 kW, 12 mm sampling distance. (c) Forward power 1.5 kW, 15 mm sampling distance. 55

3.15 Effect of the addition of nitrogen into all gas flows upon the normalized net signal intensities for 100 ppb analytes at two forward powers. Sampling distances are as shown in Table 3.2. (a) Rhodium at m/z 103. (b) Iron at m/z 56. (c) Iron at m/z 57. (d) Selenium at m/z 76. (e) Selenium at m/z 78. (f) Selenium at m/z 82. 57

3.16 Effect of the addition of nitrogen into all gas flows upon the normalized background signal intensities at two forward powers. Sampling distances are as shown in Table 3.2. (a) Background at m/z 103. (b) ArO^+ at m/z 56. (c) $ArOH^+$ at m/z 57. (d) Ar_2^+ at m/z 76. (e) Ar_2^+at m/z 78. (f) Ar_2^+at m/z 82. 58

3.17 Effect of the addition of nitrogen into all gas flows upon the ratio of net signal/background signal (SBR) for 100 ppb analytes at two forward powers. Sampling distances are as shown in Table 3.2. The axis on the left hand side shows absolute SBR. The right hand axis shows normalized values. (a) SBR at m/z 103. (b) SBR at m/z 56. (c) SBR at m/z 57. (d) SBR at m/z 76. (e) SBR at m/z 78. (f) SBR at m/z 82. 59

3.18 Effect of the addition of nitrogen into all gas flows upon the ratio of net signal/background noise (SNR) at two forward powers for 100 ppb analytes. Sampling distances are as shown in Table 3.2. The axis on the left hand side shows absolute SNR. The right hand axis shows normalized values. (a) SBR at m/z 103. (b) SBR at m/z 56. (c) SBR at m/z 57. (d) SBR at m/z 76. (e) SBR at m/z 78. (f) SBR at m/z 82. 60

4.1 Optical emission spectrum of 100% argon and water, end-on plasma with chamber. 1.25 kW, 15 mm sampling distance, 50 μm monochromator entrance slit. (275–500 nm) 67

4.2 Optical emission spectrum of 100% argon and water, end-on plasma with chamber. 1.25 kW, 15 mm sampling distance, 50 μm monochromator entrance slit. (500–660 nm) 68

4.3 Optical emission spectrum of water in argon and 3% nitrogen in the coolant, end-on plasma with chamber. 1.25 kW, 15 mm sampling distance, 50 μm monochromator entrance slit. (275–500 nm) 70

4.4 Optical emission spectrum of water in argon and 3% nitrogen in the coolant, end-on plasma with chamber. 1.25 kW, 15 mm sampling distance, 50 μm monochromator entrance slit. (500–660 nm) 71

4.5 Effect upon net spectral line emission intensity for 100 ppm Mg in water at (a) 279.6 nm (b) 280.3 nm, and (c) 285.2 nm as nebulizer flow varied and as the fraction of nitrogen in the coolant increased to 15% nitrogen as shown. 1.25 kW, 15 mm sampling distance, 50 μm monochromator entrance slit. 73

4.6 (a) Optical emission spectra from 279 to 286 nm for 100 ppm Mg in 100% argon and as 3 to 15% nitrogen added into the coolant. (b) Normalized net analyte signal intensities at 279.6, 280.3, and 285.3 nm. 1.25 kW, 15 mm sampling distance, 50 μm monochromator entrance slit. 75

4.7	Effect upon optical emission signal intensity for 100 ppm lead at various wavelengths (Pb (I) 261, Pb (I) 280, Pb (I) 283, Pb (I) 364, Pb (I) 368, Pb (I) 406, and Ar (I) 404 (for comparison)) as nitrogen increased in the coolant. (a) Normalized net signal intensities,(b) SNR, (c) SBR. 1.25 kW, 15 mm sampling distance, 50 μm monochromator entrance slit.	77
4.8	Scans comparing the optical emission signals for 100 ppm lead in 100% argon with signals as10% nitrogen is added into the coolant for wavelength regions as shown. 1.25 kW, 15 mm sampling distance, 50 μm monochromator entrance slit.	79
4.9	Dependence of the net spectral line emission intensity at 279.6, 280.3, and 285.2 nm for 100 ppm Mg in water upon nebulizer flow for 100% argon plasma. Viewed "end-on" with no sampling plate or expansion chamber. 1.25 kW, 50 μm monochromator entrance slit.	81
4.10	Scans comparing the optical emission signal intensities for 1000 ppm lead in argon viewed "end-on" with sampler and expansion chamber (on left) to the "end-on" view without sampler (on right).	83
4.11	Comparison of the optical emission signals for 1000 ppm lead, viewed "end-on" with and without sampler and chamber. (a) Ratios of net signal emission intensities *i.e.*, net signal without plate and chamber/net signal with plate and chamber; (b) SNR; (c) SBR.	84
4.12	Optical emission spectrum of argon and water, viewed "side-on" through expansion chamber. 1.25 kW, 15 mm sampling distance, 100 μm monochromator entrance slit (300–660 nm).	86

4.13 Dependence of the spectral line emission intensity at 279 nm for 1000 ppm Mg upon nebulizer flow rate for 100% argon plasma. 1.25 kW, 15 mm sampling distance. 88

4.14 Optical emission spectra of various analytes in argon, viewed "side-on" through expansion chamber. (a) 1000 ppm Sr (I) from 458 to 462 nm. (b) 1000 ppm Sr (II) from 407 to 422 nm. (c) 1000 ppm Ca (II) from 393 to 398 nm. (d) 1000 ppm Ca (I) from 421 to 424 nm. (e) 1000 ppm Mg (II) from 279 to 286 nm. 89

CHAPTER 1

INTRODUCTION

1.1 Objectives

Since its development, inductively coupled plasma-mass spectrometry (ICP-MS) has been applied to a wide variety of sample types. The method is used in the detection of trace elements in a wide variety of environmental and biological samples, including analysis of soils and sediments, natural waters, biological reference materials, as well as clinical analysis and analysis of ultra-pure materials.

There are several features of ICP-MS which have led to its widespread use in such diverse areas, including low detection limits for many of the elements, simple spectra which can uniquely identify elements, and the ability to obtain accurate and precise isotope ratio data. In addition, spectra can be acquired rapidly and with little consumption of sample.

Despite these advantages, there still remain unresolved problems in the use of ICP-MS. Serious spectral overlaps exist, arising especially from species formed by the nebulization of water into an argon ICP and from the sample matrix including any acids used for sample dissolution. A persistent problem is the formation of oxides, about whose origins there is still debate. There have been suggestions that oxides may be formed beyond the sampled region, as the sample plume travels towards the mass spectrometer [1], but more recent calculations [2] have suggested that there are far too few collisions here to be responsible for the oxide levels typically found in ICP-MS. Some calculations show that the level of oxides observed by ICP-MS for some refractory species can be attributed to levels consistent with their dissociation equilibria in the plasma [3]. Although it is not clear that this is the only source of oxide formation,

there have been studies whose approach is to alter the plasma composition to reduce oxides.

In this work the plasma composition was changed by addition of nitrogen into the various gas flows of the ICP in an attempt to reduce these oxide levels. The effect of this nitrogen may be at least twofold: to act as a scavenger for oxygen (*i.e.*, forming NO) and to provide more excitation of the sample in the plasma. Temperatures in nitrogen containing plasmas are higher than in pure argon plasmas [4], which may increase both element ionization and dissociation, and the NO^+ formed in the plasma may additionally ionize some species by charge transfer.

Another difficult problem unique to ICP-MS has been named the "matrix effect": the usual effect is suppression of the desired analyte signal by high concentrations of concomitant elements (the matrix). Although it has been suggested that the matrix effect may arise during the extraction of the ICP into the mass spectrometer [5, 6], it is more generally believed that it arises from the passage of ions through the mass spectrometric ion lens system [7] as a result of strong mutual repulsion in the positively charged ion beam. The overall observed effect may arise from a combination of these along with other factors.

Virtually no characterization of the sampling zone has been published. A thorough understanding of both the ion extraction step and the processes occuring in this zone is of importance in order to improve the analytical utility of ICP-MS. Without a knowledge of the causes of the matrix interference, it is difficult to improve the sampling interface to reduce its effect. An optical view of this region may be used to discover which of the reported interelement effects are due to the mass spectrometer itself. In this work a preliminary optical study of this region was begun. The region just in front of the extraction zone was observed along the plasma axis and compared with that region when there was

no plasma extraction. A small vacuum chamber was built with optical ports in order to observe optical signals of the sample by emission, and, it was hoped, by absorbance and fluorescence. The intention was to monitor the species distribution of analyte and oxide species in the presence and absence of matrix elements. Unfortunately it was not possible to accomplish this with the experimental set-up used, so only preliminary results will be presented.

1.2 Introduction to ICP-MS

After little more than a decade of development and application, inductively coupled plasma-mass spectrometry (ICP-MS) is now established as an important tool for elemental analysis [8]. The combination of an inductively coupled plasma as ion source with a quadrupole mass spectrometer for mass filtering and detection, has strengths which have given the technique its current importance, despite its high cost in comparison to other competing techniques such as ICP optical emission spectroscopy (ICP-OES). ICP-MS has detection limits of 1-100 pg/mL (part per trillion, ppt) for many elements in solution [8], two or three orders of magnitude better than current detection limits achieveable by other multi-element methods, with wider coverage of the periodic table than electrothermal atomic absorption. The background spectrum is clean and spectral overlaps are relatively few. The mass spectrum of an element is simple, unique, and predictable, corresponding to its natural isotopic abundance. Isotopic ratios can be obtained [9] and the technique of isotopic dilution can be used in analysis. ICP-MS has a wide linear dynamic range, has multi-element capability, and is reasonably rapid. It is widely used in geological study, especially for the analysis of heavy elements [10] which are notorious for the complexity of their optical spectra, and in analysis of environmental and

biological materials, including foods and clinical analysis, which demand ever lower detection limits.

There are disadvantages and problems in ICP-MS which limit its wider applicability. A major disadvantage is, of course, its instrumental complexity and attendant high cost. Unlike ICP-OES in which sample emission is viewed as it passes an observation spot in the plasma, ions must be physically transported from an atmospheric pressure plasma into a vacuum, mass selected, and focussed to physically strike a detector. Sampling of the plasma is accomplished with a narrow sampling orifice situated between the plasma and the mass spectrometer and, ideally, should be carried out so that sampled material reflects sample composition in the plasma itself. The orifice can also be blocked by deposition of salt from samples in high concentration matrices.

A more complex type of matrix interference than orifice blockage arises from molecular ions such as oxides, hydroxides, dimers, and clusters formed from the solvent, sample matrix constituents, entrained air, and plasma support gases. If the major isotope of a desired analyte, M^+, overlaps with the mass of a background species, the quadrupole resolution will likely be insufficient to resolve the signals. If the analyte has other sufficiently abundant isotopes, one of these may be monitored instead. Some of the species which suffer from this interference include $^{28}Si^+$ (interference by N_2^+), $^{31}P^+$ (NOH^+), $^{40}Ca^+$ (Ar^+), $^{56}Fe^+$ and $^{57}Fe^+$ (ArO^+ and $ArOH^+$), $^{76}Se^+$, $^{78}Se^+$, and $^{80}Se^+$ (isotopes of Ar_2^+), $^{51}V^+$ (ClO^+ in HCl solution), $^{75}As^+$ ($ArCl^+$ in HCl). There may be further interference arising from the various possible isotopic combinations and hydrides. The intensities of these background species vary and do not present the same severity of interference in all cases. The detection limits for $^{56}Fe^+$ and $^{82}Se^+$ are degraded by signals from ArO^+ and $Ar_2H_2^+$ to 1 ppb in comparison with ppt detection limits attainable for many other elements [8]. Phosphorus and

arsenic are monoistopic, hence there are no other isotopes to monitor; vanadium's only other isotope is just 0.25% abundant and cannot be monitored at low concentrations. These interferences may also cause difficulty in correcting for isobaric overlap: for example ^{58}Fe interferes with the determination of ^{58}Ni. In order to correct for the iron interference, its total concentration must be known, but its isotopes at the mass to charge ratios (m/z) 54, 56, and 57 are all overlapped by background species ArN^+, ArO^+, and $ArOH^+$ and thus, may preclude an accurate determination of nickel. Species which readily form oxides may interfere with a heavier analyte species, in addition to having their own M^+ signal lowered.

There is an additional matrix effect unique to ICP-MS which has been widely observed: a high concentration of almost any species will interfere with the observation of many others, the so-called "matrix effect interference". Usually a signal suppression is observed, and is most severe when the interferent is of heavier mass than the analyte and is present in highly ionized solutions in a molar ratio of interferent/analyte of at least 1000/1 [11, 12, 6]. It is believed that this matrix effect does not originate in the sampling step, but rather in the transport of the ions through the mass spectrometer [7, 13, 14]. The ICP suffers from fluctuations and drift, which limit precision. The usual channetron electron multiplier detector is not able to simultaneously monitor more than one mass, and thus cannot be used to detect transient signals. Although for most elements the level of ionization in the ICP is quite high, making it useful as an atomic ion source for the mass spectrometric detector, only about one percent of sample actually enters the ICP during the nebulization process and of that, only about one percent is carried past the sample interface into the mass spectrometer, and of that, only about 0.01 percent reaches the detector to give a signal [15], making for low sampling efficiency.

1.3 Instrumentation

1.3.1 ICP

A schematic diagram of the ICP torch is given in Figure 1.1, along with typical radiofrequency (rf) power and flow rates used in this work. The plasma is generated by wrapping an induction coil about a quartz tube containing an argon flow. A Tesla discharge plants a seed of free electrons in the tube. The induction coil is connected to an rf generator whose oscillating current generates an oscillating magnetic field perpendicular to the load coil, which in turn induces an eddy current of free electrons which circulate in closed annular paths inside the quartz tube space. These electrons meet with resistance and heating occurs which ionizes the argon, to form a plasma.

The plasma is sustained and centred by the plasma gas which flows axially through the outer tube of the quartz torch as shown. This gas flow, generally argon, is called the plasma gas, the support gas, the outer gas, or the coolant gas because it also thermally isolates the hot plasma from the quartz tubing. In this work, up to fifteen percent nitrogen is introduced into this flow and mixed with the argon as the coolant. The auxiliary gas flow lifts the plasma slightly above the quartz tubing and is not strictly necessary for a pure argon plasma, but is necessary when nitrogen is added to the coolant, as the plasma heats and shrinks and is pulled down towards the load coil. Sample in solution is introduced into a nebulizer and spray chamber, as shown in Figure 2.2, where up to 99% of the sample is lost to the drain. The aerosol is then carried into the injection channel in the centre of the torch by the nebulizer gas. The sample is desolvated, vapourized, dissociated, excited, and ionized by the ICP.

As shown in Figure 1.1, an optical emission spectrum is generally observed ninety degrees to the torch in the region called the "normal analytical zone" (NAZ). It has been shown [16] that an ICP consists of different excitation

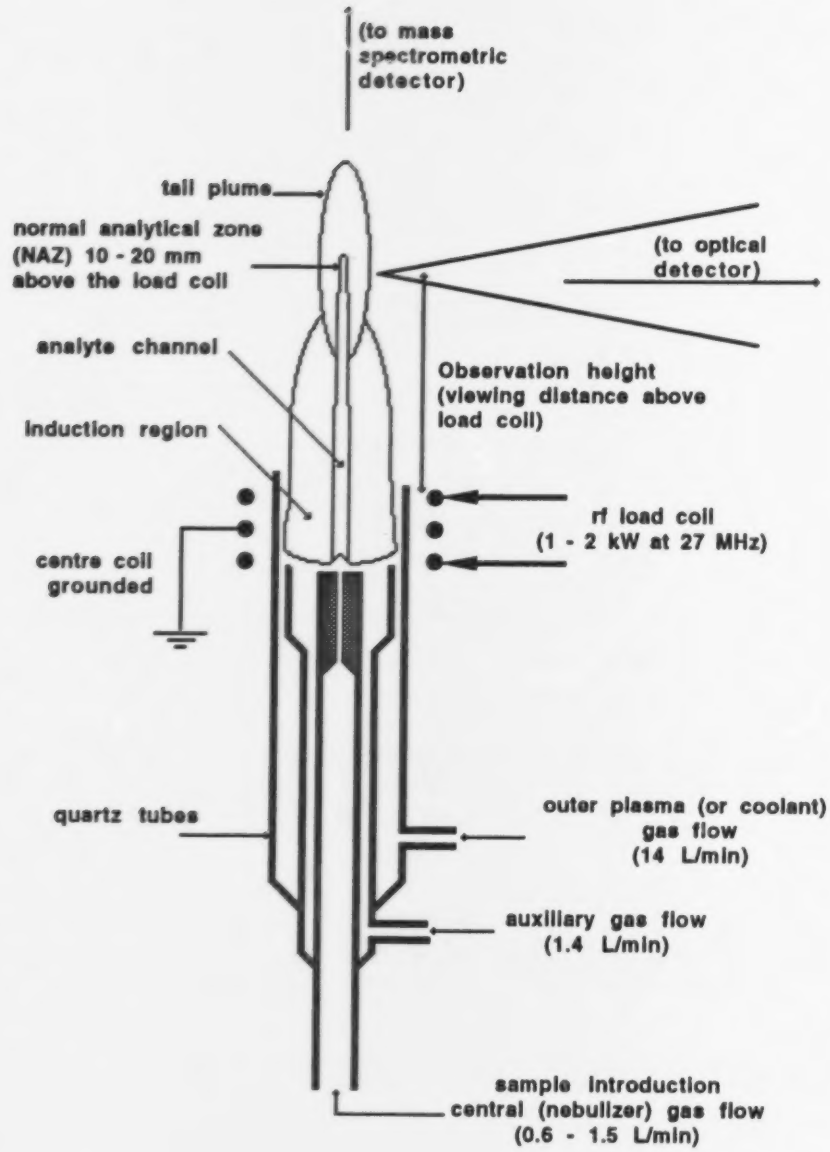
(to mass spectrometric detector)
tail plume
normal analytical zone (NAZ) 10 - 20 mm above the load coil
(to optical detector)
analyte channel
Observation height (viewing distance above load coil)
induction region
rf load coil (1 - 2 kW at 27 MHz)
centre coil grounded
quartz tubes
outer plasma (or coolant) gas flow (14 L/min)
auxiliary gas flow (1.4 L/min)
sample introduction central (nebulizer) gas flow (0.6 - 1.5 L/min)

Figure 1.1
A schematic diagram of the inductively coupled plasma (ICP) torch.

regions above the load coil, and that analytical performance depends upon operating parameters [17, 18]. The NAZ is typically in a region about 20 to 25 mm above the load coil (alc), where ionic emission is normally viewed; the Initial Radiation Zone (IRZ) is typically about 10 to 15 mm above the load coil and is the usual zone for observation of atomic emission [19], if desired. Lower down is the induction region with intense continuum emission and, above the NAZ, the plasma cools and molecular species begin to form. The exact dimensions of these zones vary with the particular conditions of the plasma under observation. Increasing the power or the level of excitation in the plasma tends to pull the plasma down closer to the induction region. If the observation height is held constant, the IRZ and NAZ can effectively be shifted upwards by increasing the nebulizer flow within the central channel; hence atomic emission may be viewed at the same observation height normally associated with the NAZ and ionic emission, although this will also change the plasma conditions by cooling the plasma.

1.3.2 Sampling Interface

Ions are transferred from the plasma at atmospheric pressure into the mass spectrometer vacuum in two stages using an interface as shown in Figure 1.2. The plasma gas expands through the first sampler cone into a mechanically pumped 1 to 5 torr zone and the core of this expansion beam passes through the second skimmer cone into a vacuum of about 10^{-5} torr. These cones have orifices of approximately 1 mm diameter in order to sample the bulk plasma with minimum orifice clogging or the formation of a cool boundary layer which creates oxides at the sampler plates [20]. The sampled species form a collision-free supersonic jet [2, 21] ("zone of silence") bounded by shock waves where the directed expansion scatters as it collides with the background gas. Provided the skimmer is placed at the front of this expansion (at the "Mach disc") or slightly

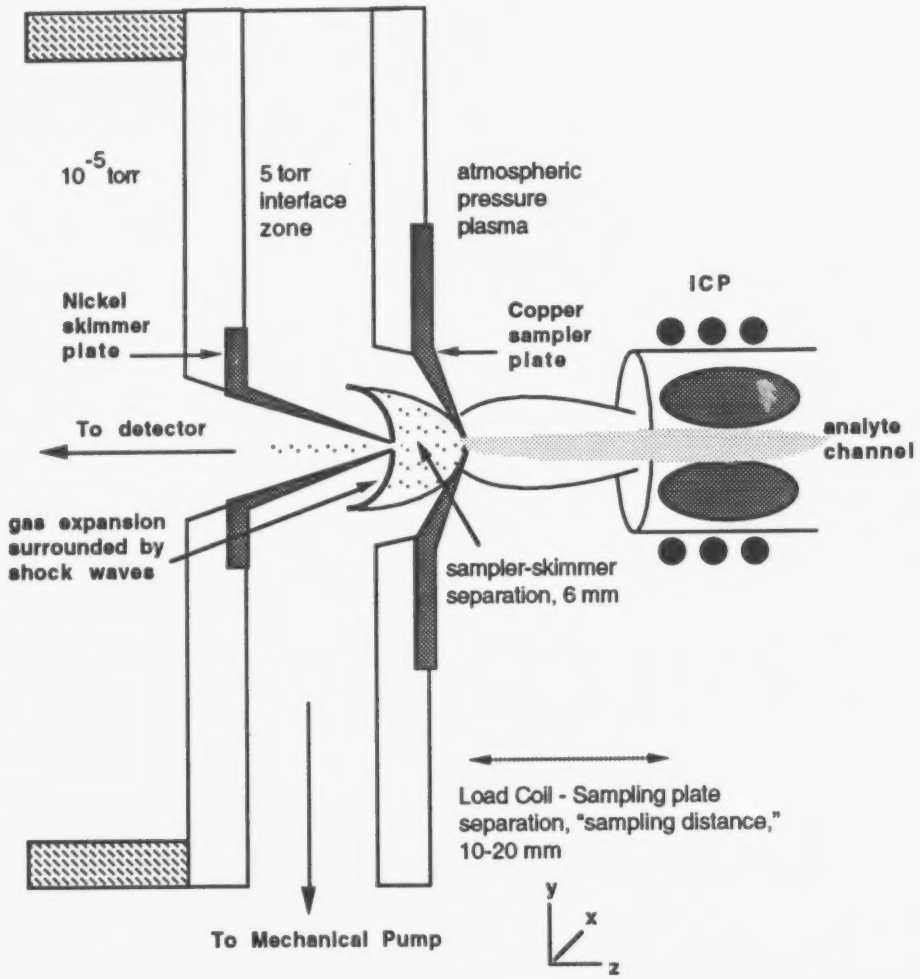

Figure 1.2
A sketch of the ICP-MS sampling interface, showing sampler, skimmer, and torch.

within the zone of silence [2, 22], about one percent of this flow is further sampled by the skimmer plate and directed towards the detector system.

Much of the discussion about the origin of oxide species and the effort to educidate their causes has focussed upon the sample interface, *i.e.*, sample and skimmer orifice diameter [23, 20, 24], skimmer and sampler separation [22], sampler cone shape, etc. Oxides have also been investigated by changing the plasma conditions by various means [74], as will be discussed further in Chapter 3.

1.3.3 Detection

After passing through the skimmer, ions enter the mass spectrometer vacuum proper and are electrostatically focussed and transmitted to the quadrupole and detector, shown in the schematic of Figure 1.3, for the Sciex Elan 250 which was used for this work. In this instrument the positively charged ion beam must pass through the centre axis of a series of negatively charged cylindrical plates, the so-called Einzel lenses, and through the Bessel box apertures as shown in the figure, in order to reach the quadrupole rods. A quadrupole mass spectrometer serves as a relatively low resolution mass filter to separate ions according to the ratio of mass to charge. Since the detector is sensitive to photons as well as ions, photons are physically blocked within the mass spectrometer, and the detector is mounted off-axis to further prevent photons from striking it. It is in the ion focussing step that the interference of heavy matrix elements upon a light analyte species is believed to occur [25, 26, 27], although there has been research suggesting that the plasma may also contribute to the observed matrix effects [28]. Qualitative calculations [29,7] show that the ion current is of sufficient intensity that mutual repulsion of ions in the positive ion beam causes defocussing of the ions from the centre of the beam.

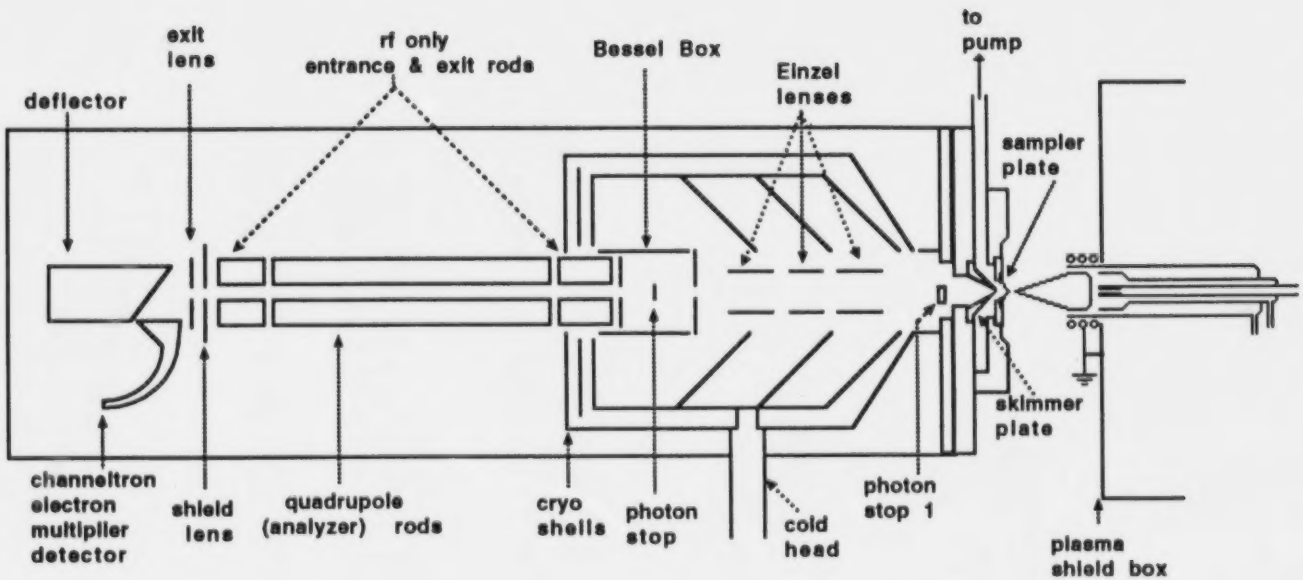

Figure 1.3
A schematic of the Sciex Elan 250 Mass Spectrometer.

Lighter ions are defocussed more readily and if defocussed off-axis, do not reach the quadrupole.

1.4 Overview of Thesis

In the next chapter, a brief description of the experimental system used will be given. Chapter 3 presents a study of the addition of nitrogen into variously, the outer plasma gas flow, the nebulizer gas flow, and all of the gas flows. The main conclusions are that nitrogen addition is most effective for reduction of argon oxide and dimer background species if nitrogen is added into the outer gas flow; that analyte signals and figures of merit for selenium and iron are also most enhanced by addition of nitrogen into the outer gas flow. The sampling distance must be reduced and the nebulizer flow rate must be increased in order to see these signal enhancements.

Chapter 4 presents the results of a preliminary study of the first stage of the sampling zone of the ICP-MS observed optically. This work shows that the sampler plate does not alter the optical spectrum obtained and indicates a low level of excitation in the zone of silence. Further study is required in order to understand this region and determine its effect upon the signal detected by the mass spectrometer.

CHAPTER 2

EXPERIMENTAL

2.1 Experimental Apparatus

A block diagram of the instrumentation employed in all this work is shown in Figure 2.1. Aerosol sample is introduced into an ICP, coupled to a sample extraction zone. This consists of one or two cones with orifices which extract the flow of the plasma into a reduced pressure zone, as described in the introduction, and the signal obtained is then detected. This block diagram is shown to emphasize the similarity between the various experimental arrangements used in this work. The instrumentation used in the experiments differ from one another in the details of the extraction method and the detection method employed. The remainder of the blocks shown in the diagram were essentially unchanged between experiments.

The inductively coupled plasma used in all this work consisted of a three-turn centre grounded load coil and cross-flow (MAK) type torch, mounted horizontally, and operated at a forward power of 1.25 or 1.5 kW at 27.12 MHz generated by a Plasma-Therm radio frequency generator and matching network. An ICP is shown in Figure 1.1 of the introductory chapter.

Using a peristaltic pump (Rabbit, Rainin Instrument, Woburn, MA), aqueous samples were pumped at a constant rate of 1 mL per minute. They were nebulized into a Scott-type spray chamber with a concentric Meinhard type nebulizer and then introduced into the central nebulizer gas flow of the plasma. A mass flow controller (Matheson, Model 8240-0423, Brooks Instrument Division, Emerson Electric, Hatfield, PA) was added to the nebulizer gas line to provide finer control over the flow rate and to keep the flow constant.

The ICP was always ignited using one hundred percent industrial grade argon. In some of the work reported here, a mixture of argon and nitrogen was

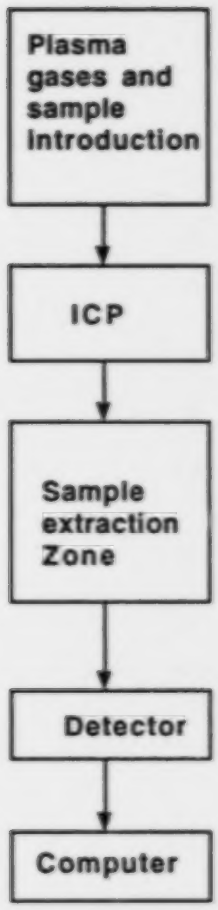

Figure 2.1
A block diagram of the experimental setup used in this work.

introduced into one or all of the gas flow inlets. Once the plasma stabilized, up to fifteen percent nitrogen was gradually mixed with argon (if added too rapidly, the plasma could be extinguished) and admitted into the desired gas inlet using a Matheson rotameter (7300 Series, Matheson Gas Products).

The overall schematic shown in Figure 2.2 shows as, an example, nitrogen introduced into the plasma gas. The tube sizes used in the gas proportioner depended upon which gas inlet was being fed the mixed gas and the total flow rate required. The gases then mix together in the central tube and are admitted as the plasma gas into the torch. In order to switch the gas inlet into which nitrogen was introduced it was necessary to shut down the plasma. The total outer flow of argon, or mixed argon-nitrogen, was kept at 14 L/min, the auxiliary flow at 1.4 L/min, and the nebulizer flow was varied between 0.6 L/min and 1.6 L/min, as shown in Figure 1.1.

2.2 Mass Spectrometric Detection

A schematic diagram of the ICP-Mass Spectrometer (ICP-MS) data acquisition and detection system used for part of this work is shown in Figure 2.2. The ICP-MS used was a conventional commercially available Sciex Elan 250 (Sciex, Thornhill, ON) and was shown in a schematic in Figure 1.3. The ion lens voltages were set at compromise values in order to obtain maximum signal intensity over a wide mass range.

The sampling interface between the icp and the mass spectrometer is sketched in Figure 1.2 and consists of two plates separated by 6.1 mm: a nickel skimmer plate and a copper sampling plate. The orifice diameters and other experimental details of this system are shown in Table 2.1. The sampling distance refers to the separation of the sampling plate from the ICP load coil along the z direction, as shown in the figure, and was measured using a precision dial gauge mounted on the torch box undercarriage. The usual

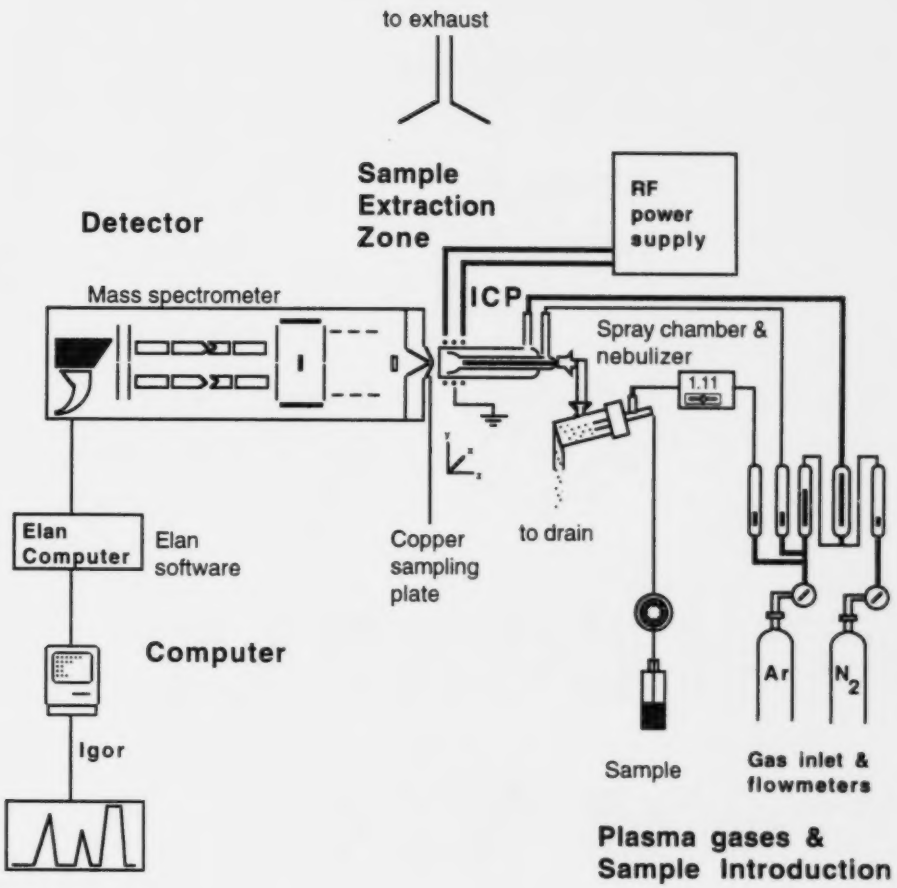

Figure 2.2
A schematic diagram of the ICP-MS system.

TABLE 2.1 EXPERIMENTAL DETAILS

skimmer plate	nickel, orifice diameter 0.89 mm.	
sampler plate	copper, orifice diameter usual range 0.63 to 1.02 mm. The orifice diameter for ICP-MS measurements was 0.89 mm and was 0.76 mm for the ICP-OES.	
sampling distance	10 to 18 mm from tip of sampling cone to load coil. Usual distance was 15 mm.	
forward power	1.25 kW or 1.5 kW, as given. Reflected power < 25 W.	
gas flow rates	Total Coolant:	14 L/min
	Auxiliary:	1.4 L/min
	Nebulizer:	0.5 to 1.6 L/min.

sampling distance was 15 mm. The torch mounting apparatus was modified slightly to use a torch of the same length typically used for ICP-OES, and to shorten the minimum sampling distance possible to 10 mm. The torch position was centred with respect to the sampler plate by optimizing the $^{103}Rh^{+}$ signal. The interface region was mechanically pumped to establish a vacuum in the range of one to ten torr. The ion lens and detector regions were cryogenically pumped to a vacuum with a working range of approximately 10^{-6} to 10^{-5} torr as measured while the plasma was running.

All multi-element analyte solutions were prepared from 1000 parts per million (ppm) stock solutions (Spex Industries Inc., Edison, NJ, USA) and diluted to 100 parts per billion (ppb) standard solutions in two percent reagent grade nitric acid in distilled deionized water, except as noted. Analyte intensities were measured using the peak hopping mode of the mass spectrometer using dwell times of 0.3 to 1.0 seconds, as noted. Where appropriate, blanks of distilled water in two percent nitric acid were obtained. Reported net signal values are background (blank) subtracted and are the mean of 5 to 16 replicate measurements, as noted. Signal intensity is measured as ion counts/sec. The values reported as noise are a single standard deviation from these mean values. The signal to noise ratio (SNR) was calculated as the background subtracted signal divided by the standard deviation of the blank. The signal to background ratio (SBR) was the background subtracted signal divided by the signal of the blank.

The resultant intensities along with the respective masses, were transferred from the Elan computer to a Macintosh. The data were processed on a Macintosh IIsi using programs written in Pascal, and further manipulated using commercially available software (Excel 3.0 (Microsoft) and Igor Pro 2.0 (WaveMetrics, Lake Oswego, OR)).

2.3 Optical Spectrometric Detection

For the remainder of this work, an optical detection system was used to observe sample emission. The ICP, copper sampling plate, gas flow controls, and sample uptake equipment were removed from the mass spectrometer system and mounted in front of a scanning monochromator. The torch was mounted horizontally, using the usual ICP-MS orientation. Schematic diagrams of the ICP-OES data acquisition and detection systems used are shown in Figures 2.3 and 2.4. The sample and gas introduction are identical to those shown in Figure 2.2 for the ICP-MS set-up. Shown in Figure 2.3 is the "end-on" viewing set-up for this thesis. This orientation differs from usual optical set-up as shown in Figure 1.1, by viewing horizontally along the plasma axis and through a sampling orifice.

The copper sampling plate from the ICP-MS system was mounted to the front of a cylindrical glass chamber (of approximate diameter 10 cm and length 18 cm). An aluminium plate with a quartz viewing window was mounted at the back. The skimmer plate used in ICP-MS was omitted from these experiments. This arrangement was made to approximately simulate the ICP-sampler interface zone of the ICP-MS. The chamber was mechanically pumped to maintain a vacuum of approximately two to five torr monitored with a dial gauge. The sampling orifice was 0.76 mm in diameter, smaller than the orifice used in mass spectrometric measurements. This was necessary in order to keep the pressure in the chamber acceptably low since there was no cryogenic pump beyond this chamber to help reduce its pressure.

The sampling distance between the copper plate and the load coil was set to be approximately the same as for the ICP-MS experiments, generally 15 mm. A quartz biconvex lens of focal length 10 cm was inserted midway between the sampling zone and the entrance slit of the monochromator for 1:1 imaging of

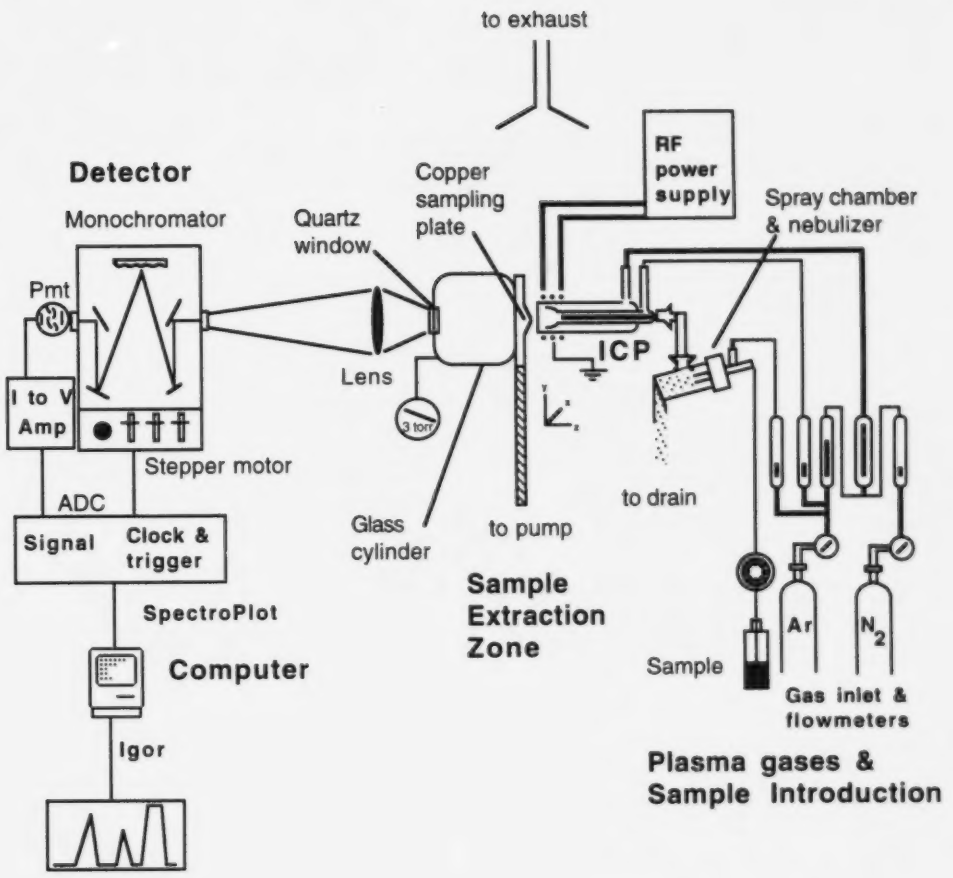

Figure 2.3
A schematic diagram of the ICP-OES system, "End-on Viewing" set-up.

the plasma as it was extracted into the sampling plate. The intent was to view only the nebulization channel down the centre of the plasma as it entered the sampling orifice and, hence an aperture of 1.6 mm was inserted in front of the entrance slit of the monochromator to block background emission from the surrounding plasma.

Some additional observations of the plasma were made in the absence of the chamber-sampler extraction zone, that is, of the plasma axis viewed "end-on," as shown in Figure 2.4 (a). This contrasts with the normal viewing orientation perpendicular to the torch, as shown in Figure 1.1. An air cut-off stream was inserted approximately 40 mm beyond the load coil, near the tip of the plasma torch to reduce self absorption and to prevent heating the optical components. The lens was kept in place in order to view the same plasma region 1:1 as was viewed previously, *i.e.*, that region of the plasma along its axis which entered the sampling plate approximately 15 mm beyond the load coil. An aperture 1 mm in diameter was inserted in front of the 50 μm entrance slit to the monochromator in order to block the brilliant plasma emission surrounding the nebulizer channel.

Figure 2.4 (b) shows another variant on the described arrangement. The main difference between this arrangement and the others is that optical observation is at right angles to the ICP torch and sampling cylinder, and is called "side-on" viewing in this thesis. The viewing angle is the same as the more usual observation in optical emission detection of the normal analytical zone (NAZ) of the ICP. The critical difference here is that the plasma enters a sampling orifice and expands into a stainless steel chamber; it is the expansion zone as the plasma enters the chamber, rather than the plasma itself, which is observed through a quartz viewing port. The ICP was blocked from the monochromator so that only the emission within the chamber was observed. It

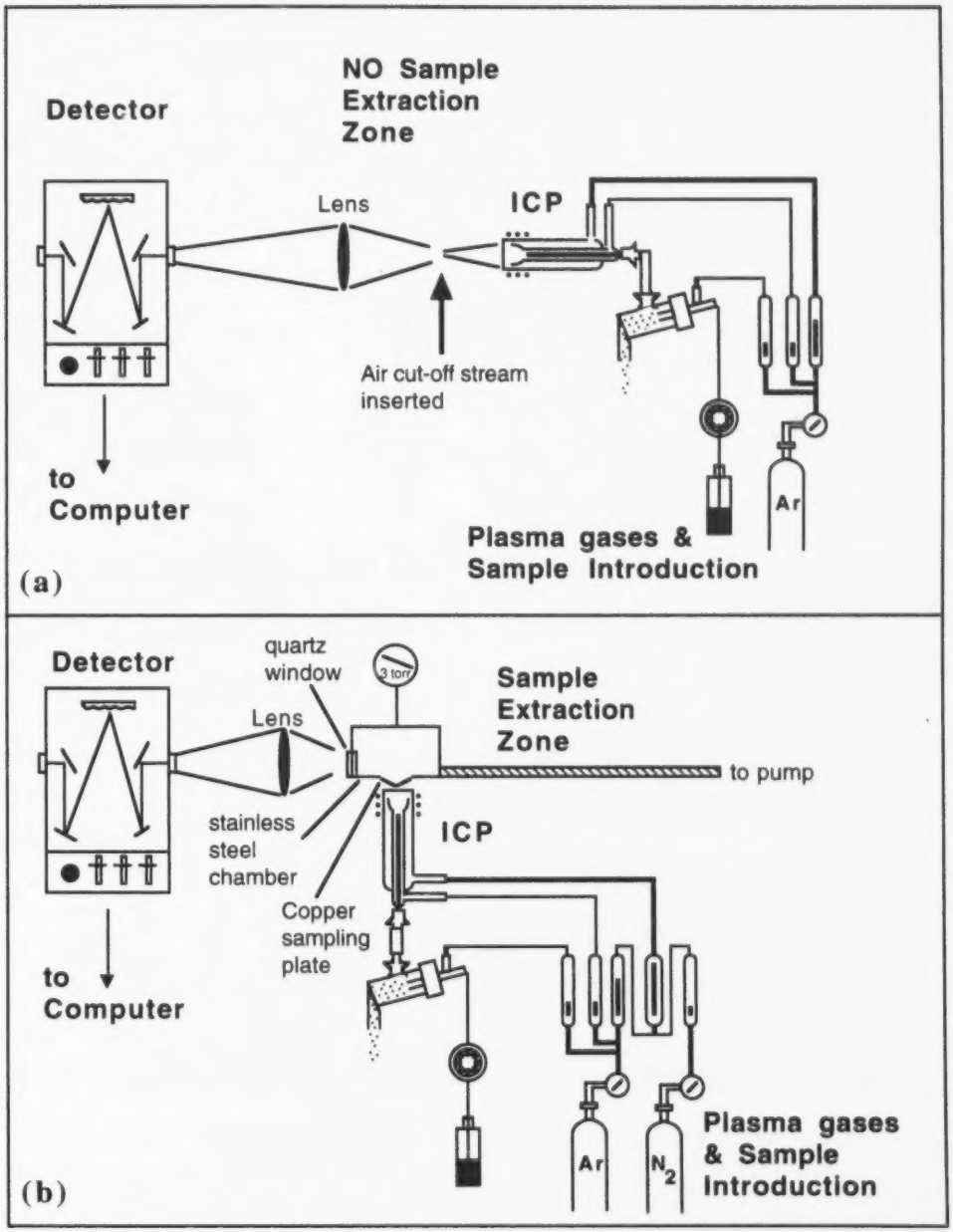

Figure 2.4
A schematic diagram of the ICP-OES system,
(a) "End-on" viewing, no sample extraction set-up, and
(b) "Side-on" viewing.

was necessary to dim the room lights during data acquisition since emission was very weak.

An Heath EU-700 scanning monochromator was used to disperse the incoming light. Details of the dispersion and detection system are given in Table 2.2. The control unit of the monochromator which supplies electronic pulses to drive the scanning mechanism was used as an external clock pulse and trigger, to time the computer acquisition of the signal from the amplifier to ensure its synchronization with the scanning of the monochromator. A photo multiplier tube (pmt) was used as the detector; its signal output was then amplified by a current-to-voltage converter (Keithley K427 or 414, Keithley Instrument, Inc:, Cleveland, OH) and digitized by a 12 bit analog-to-digital converter (National Instruments). The gain was set so that the intensity of the most intense desired spectral line was as large as possible without saturating the amplifier. In this chapter the reported signal intensity uses arbitrary intensity units, but the scale of the scans and the signals are as consistent with one another as possible. A filter was used to block second order spectral lines from 500 to 660 nm except as noted. Spectra have not been corrected for the spectral response of the pmt detector. The resultant data were acquired by a Macintosh IIsi using SpectroPlot (King and Horlick [30]) and processed further using commercial software.

For this study, most samples were prepared from reagent grade chloride salts into 100 ppm solutions. Lead was prepared from a nitrate salt. Higher concentrations were required than for the mass spectrometric study because of the reduced sensitivity and increased background and noise of the emission experiments. All solutions were prepared in distilled deionized water in reagent grade two percent nitric acid.

TABLE 2.2	DETAILS OF THE OPTICAL DETECTION SYSTEM
monochromator	Heath, model EU-700 Czerny-Turner. The focal length was 350 mm. The entrance and exit slit width was 50 μm, except as noted, and the slit height was 12 mm.
grating	Plane grating with 1180 lines/mm; this resulted in a reciprocal linear dispersion of 2 nm/mm.
detector	Photo multiplier tube, Hamamatsu 1P28A. Bias voltage -600 V.
data acquisition	Monochromator scan rate 0.2 nm/sec. Data acquired at 20 Hz. One data point was acquired for each scan step.
amplifier	Keithley K427 or K414 (Keithley Instrument, Inc., Cleveland, OH). Rise time for the K427 of 3 ms. Rise time for the K414 depended on signal (gain). When this amplifier was used, scan rate and data acquisition rate were reduced.

CHAPTER 3

MASS SPECTROMETRIC MEASUREMENTS

3.1 Introduction

The problem of oxide formation in ICP-MS was discussed in the introductory chapter. The simplest solution, background subtraction, may not be sufficient in cases where the background and the signal are of similar intensity. To reduce the level of oxides detected, the interface zone has been altered by varying the sampler and skimmer orifice diameters and separation [23, 22, 21], and plasma conditions themselves have also been altered. In certain circumstances these background species may be reduced by changing the plasma conditions, in particular, by changing the acid used for sample dissolution and pretreatment [31] (although this may be of minimal benefit in many cases), desolvating the aerosol to reduce the water level in the plasma [32, 33, 34] (and hence reduce the main source of oxygen), introducing the sample aerosol as a hyride [35], adding xenon [36], oxygen or nitrogen, or an organic solvent into the sample aerosol [37, 38], and mixing nitrogen with the plasma gas [75, 39]. For practical use, desolvation combined with addition of nitrogen into the plasma gas is straightforward and the use of nitrogen has the additional benefit of reducing plasma operating costs.

Various effects have been attributed to the addition of nitrogen into the plasma. Lam and Horlick [75] reported that the addition of nitrogen into the outer gas of the ICP enhances analyte signal and reduces the background species ArO^+ by an order of magnitude. The level of analyte enhancement was correlated to the analyte oxide bond strength for analytes of low ionization potential. The background equivalent concentration (BEC) for ArO^+ as iron at 56 amu was reduced from 160 ng/mL in argon to 7 ng/mL in 12% nitrogen, while the BEC for Ar_2^+ as selenium at 80 amu was reduced from 2.3 µg/mL to 0.5

µg/mL. These effects were seen using high nebulizer flow rates with five to twelve percent nitrogen added to the coolant. With the addition of more than twenty percent nitrogen to the plasma analyte signals decreased. Addition of nitrogen to the nebulizer flow decreased analyte signals for most species observed. Lam and McLaren [32] who added eight percent nitrogen in the coolant in combination with aerosol desolvation, also saw a reduction in the BEC of ArO^+ and state only that the analyte signal for ^{56}Fe "did not deteriorate much." Oxides were reduced at lower nebulizer flow rates, in agreement with other reports [40]. They suggest that nitrogen competes with analyte and matrix species for oxygen to form NO^+, that charge transfer with the NO^+ species (I.P. = 9.26 eV) may provide additional excitation, that the low nebulizer flow rates increase the residence time in the plasma to enhance dissociation of refractory oxides, and that the effect of desolvation is to enhance a spatial shift of the oxide containing zones from the sampled zone.

Beauchemin and Craig [39] on the other hand, who did not vary the nebulizer flow rate as nitrogen was added to the coolant, report a fivefold decrease in analyte sensitivity for iron and selenium at 1.2 kW and five percent nitrogen, but a fourfold improvement in the detection limits gained as nitrogen was added, due to a reduction in background noise. Evans and Ebdon [41] added three percent nitrogen into the nebulizer gas at 1.8 kW and 10.5 mm sampling distance and measured the intensities of the background species $ArCl^+$, Ar_2^+ (at m/z 76), ArO^+, $ArOH^+$, and the analyte species indium. They cite an improvement of two to two hundredfold in the various indium to background species ratios, resulting from the reduction in intensity of the background species by one to three orders of magnitude despite a reduction in indium sensitivity to about 75% of that in a pure argon plasma. The signal intensities of arsenic, iron, and selenium were not monitored and any similar such

improvement in their signal to background ratios would apply to these species only if their behaviour were similar to that of indium as nitrogen is added.

3.2 Results

In this work, the constitution of the plasma was altered by the addition of nitrogen into the various gas flows and the resulting signals of various analytes and background species are compared. The experimental set-up is shown in Figure 2.3. Nitrogen was introduced into either the outer plasma gas, or into the nebulizer gas flow, or into all the gas flows (outer, nebulizer, and auxiliary gas lines) as described previously. All analyte concentrations were 100 ppb.

The features of an argon only plasma and its dependence upon various operating parameters will be described first. Next, the effect of the addition of up to ten percent nitrogen into the plasma gas upon the background species ArO^+, $ArOH^+$, Ar_2^+, and $Ar_2H_2^+$ and the analyte ions iron and selenium at the same masses will be described. The effect of three percent nitrogen in the nebulizer gas upon the same species is next discussed, followed by the effect of the addition of up to two percent nitrogen into all of the gas flows. There are a number of plots of signal intensity versus nebulizer flow rate and also plots in which the nebulizer flow rate is not shown. In these cases, the signals are obtained at the nebulizer rate which was optimal for rhodium in the same circumstances.

3.2.1 Argon plasma

The mass spectrum of an element is very simple in comparison with an optical ICP spectrum. For elements which form strong oxide bonds, an MO^+ signal on the same order of magnitude as the M^+ signal may be observed, especially at high nebulizer flow rates; low levels of M^{+2} may be observed for those species with low ionization potential. The elemental mass spectrum is superimposed upon the background spectrum from water, air, and argon

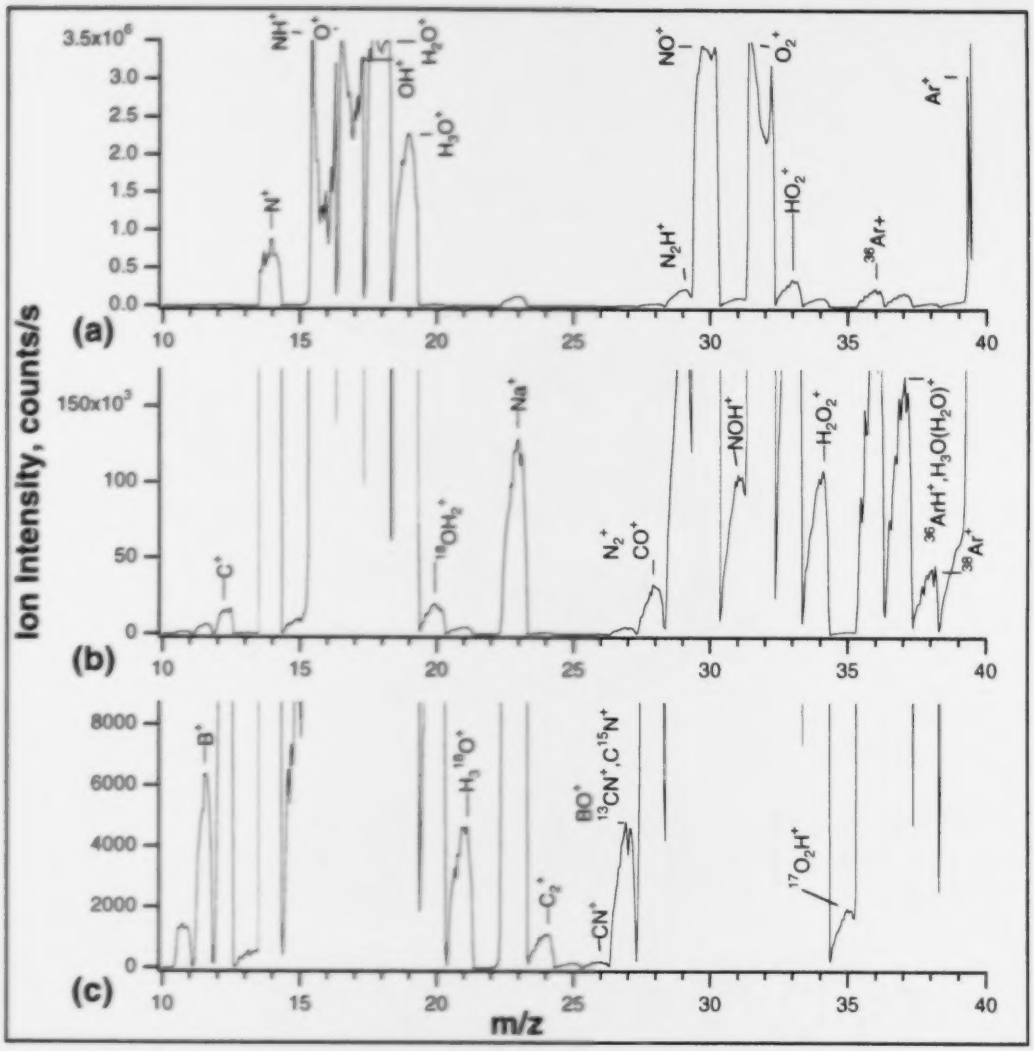

Figure 3.1
Mass spectrum of water in 2% nitric acid in 100% argon plasma.

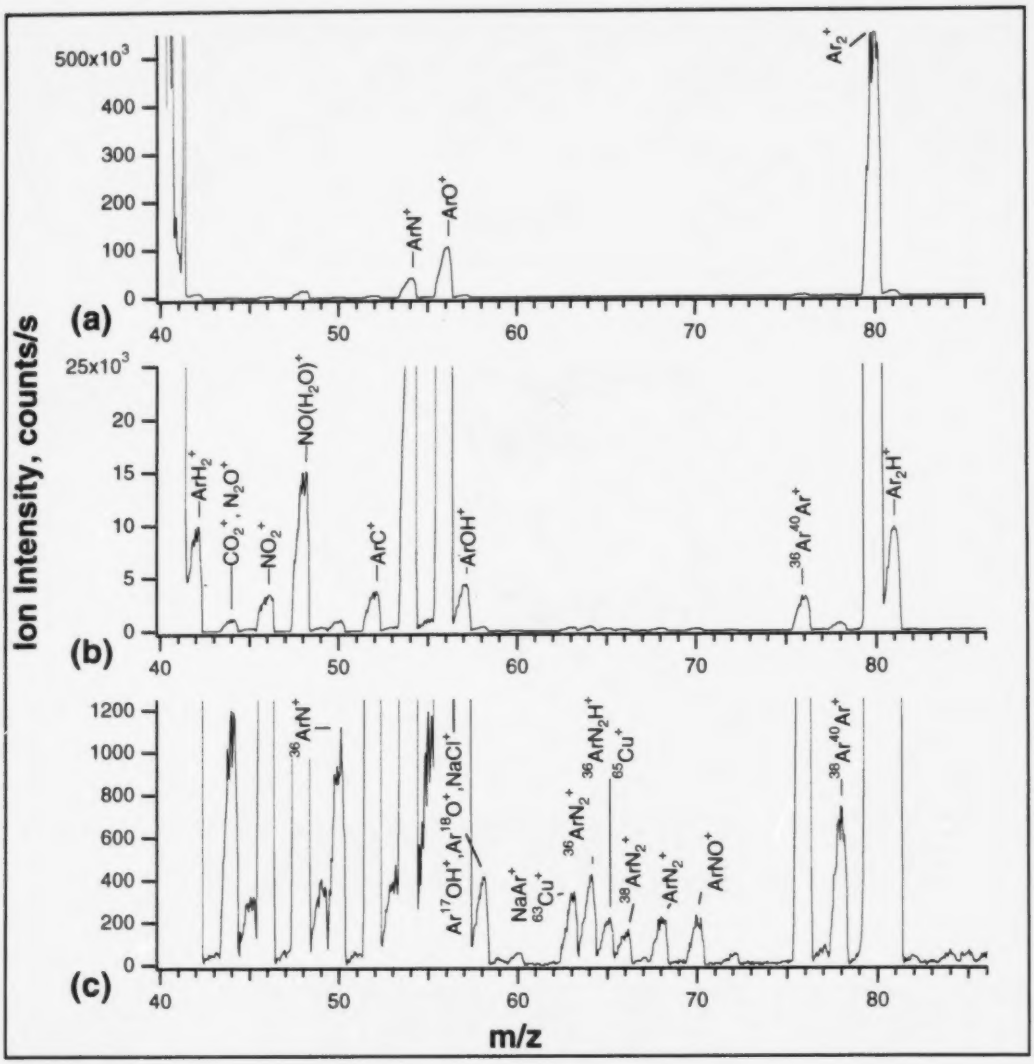

Figure 3.2
Mass spectrum of water in 2% nitric acid in 100% argon plasma.

species from the plasma. Figures 3.1 and 3.2 show the background spectra of water in two percent nitric acid solution from 10 to 85 atomic mass units (amu) in an argon plasma. The scale is expanded twenty times from plot to plot in each figure to show the background of water, air, and argon species. Major features which have been identified [31, 42] are labelled. In order to scan the intense nitrogen, water, oxygen, and argon regions of the spectrum which normally saturate the detector, the ion transmission was reduced during acquisition and several spectra were summed [43]. It is evident that below 40 amu the background is too intense for most analytical purposes. Sodium and copper contamination in the acid are noticeable; the B^+ peak at m/z 11 and BO^+ at m/z 27 are probably not acid contamination but indicate the quartz tube melting slightly in the plasma.

Although still intense, the background in the range 42 to 85 amu is much more manageable. In this region the most intense background species are the dimers of argon isotopes and their hydrides around m/z 80, ArO^+ and $ArOH^+$ species around m/z 56, and ArN^+ and $ArNH^+$ species around m/z 54. Beyond the region 85 m/z, the background is very quiet with background levels well below 100 counts per second, depending upon operating conditions. Nitric acid solutions are generally preferred for use in ICP-MS since their spectra are very similar to that of water itself. Other acid solutions have more complex mass spectra, in particular with interferences with many of the first row transition metals [31].

The most easily adjusted variable operating parameters which most affect signal intensity are nebulizer gas flow rate, forward power, and sampling distance [44, 45]. Examples of the interdependence of these parameters and their effect upon the net signal for 100 ppb Rh at m/z 103 are shown in Figure 3.3. These plots are typical of ICP-MS in that there is generally a single optimal

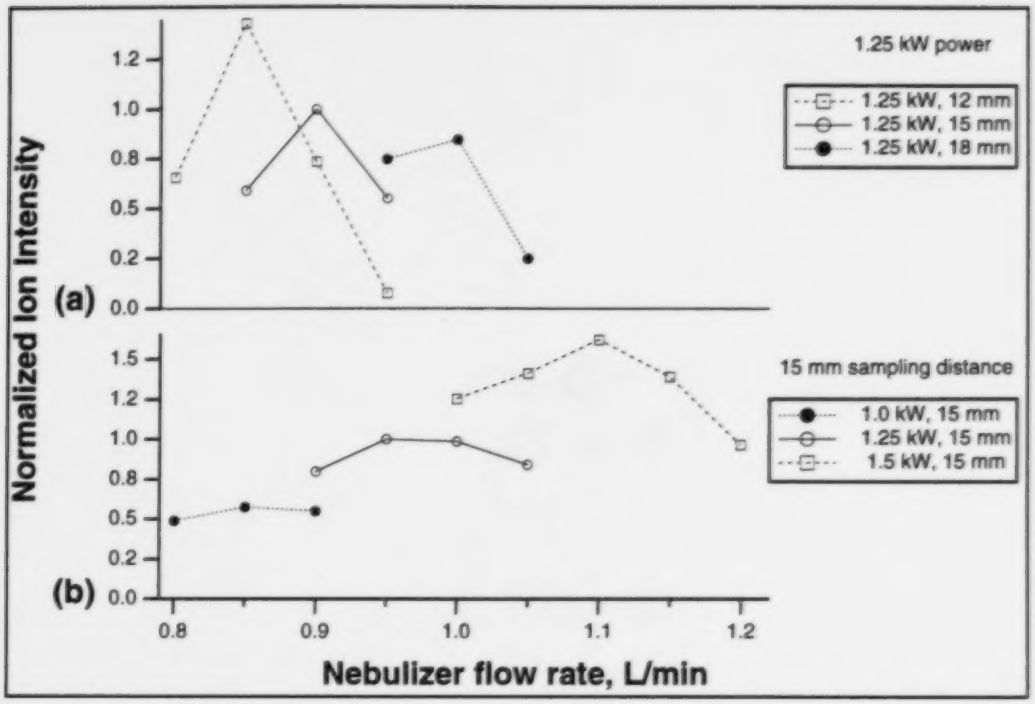

Figure 3.3
Dependence of the signal intensity for 100 ppb Rh at m/z 103 upon sampling distance, nebulizer gas flow rate, and forward power. Signals normalized to signal intensity for Rh at 1.25 kW, 15 mm, at its optimum nebulizer flow rate in 100% argon.

(a) Forward power of 1.25 kW. Sampling distance varied.
(b) Sampling distance of 15 mm. Forward power varied.

nebulizer flow rate at which a maximum signal intensity is obtained. These and subsequent plots show normalized intensity versus flow rate of the nebulizer gas in litres per minute. All data are normalized in the same way to show their values relative to the value in "standard conditions" in an argon plasma: *i.e.*, each data set for a species is divided by the value for that species in argon at 1.25 kW forward power and 15 mm sampling distance, at the optimal nebulizer flow rate for the analyte rhodium. For easier comparison of the data, many of the plots show a horizontal dotted line, indicating the value defined to be 1, *i.e.*, the normalized intensity in argon at the optimal nebulizer flow rate at 1.25 kW and 15 mm.

Figure 3.3 (a) shows the effect upon the net background subtracted Rh^+ signal of varying the sampler distance from 12 to 18 mm, holding the forward power at 1.25 kW. Figure 3.3 (b) shows the effect of varying the forward power from 1 to 1.5 kW while sampling at a fixed distance of 15 mm. To obtain the maximum analyte signal intensity, the nebulizer flow rate must increase as the sampling distance is increased; at a single sampling distance, the nebulizer flow rate must increase as the power increases. The optimal nebulizer flow rate shifts as the power increases, because the plasma plume containing analyte ions is pulled closer to the plasma core. It takes a higher flow rate to move the analytical zone of the ICP back to its initial position. Similarly as the sampling distance increases, it requires a higher flow rate to maximize the signal. This type of analyte behaviour has been widely observed in ICP-MS and similarly shaped profiles are obtained for other analyte species. Although the nebulizer flow rate corresponding to the maximum analyte signal intensity may vary slightly from element to element, it is possible to find compromise operating parameters, at least for elements close in mass. The power, sampling distance, and nebulizer flow rate must be varied in concert in order to maintain similar

signal levels and a single set of optimum conditions does not exist. On this instrument, although signal intensity is greater at 1.5 kW than at 1.25 kW, and the intensity is somewhat greater at 12 mm than at 15 mm, the background intensity and the noise increase as power increases and sampling distance decreases. In general, for the work presented here using an argon plasma, optimum values for the signal to background noise ratio (SNR) and signal to background ratio (SBR) were obtained using a forward power of 1.25 kW and a sampling distance of 15 mm. Hence these parameters will be considered the "standard" and, for convenience and clarity, the effects due to using other parameter sets will be compared to it.

3.2.2 Introduction of nitrogen into the plasma

3.2.2.a Addition of nitrogen into the coolant gas

Figure 3.4 shows the normalized net rhodium signal intensity as a function of the nebulizer flow rate while adding nitrogen into the coolant gas. Each of the plots shows the effect of increasing the nitrogen flow at a single forward power and sampling distance. Separate traces are shown for the various amounts of nitrogen added, from half a percent to ten percent of the total coolant. The horizontal dotted line indicates the value defined to be 1, *i.e.*, the normalized intensity in the "standard:" argon at 1.25 kW and a 15 mm sampling distance. Figure 3.4 (a) shows the effect upon the Rh signal as nitrogen was added at a forward power of 1.25 kW and 15 mm sampling distance; Figure 3.4 (b), shows the effect as nitrogen was added at 1.25 kW and 12 mm and Figure 3.4 (c) shows the effect at 1.5 kW and 15 mm. In each plot the trace shown in 100% argon is obtained at the given sampling distance and power for that plot. The shapes of these plots show the characteristic mountain shape for analyte species in ICP-MS. This behaviour contrasts with that of the background species investigated.

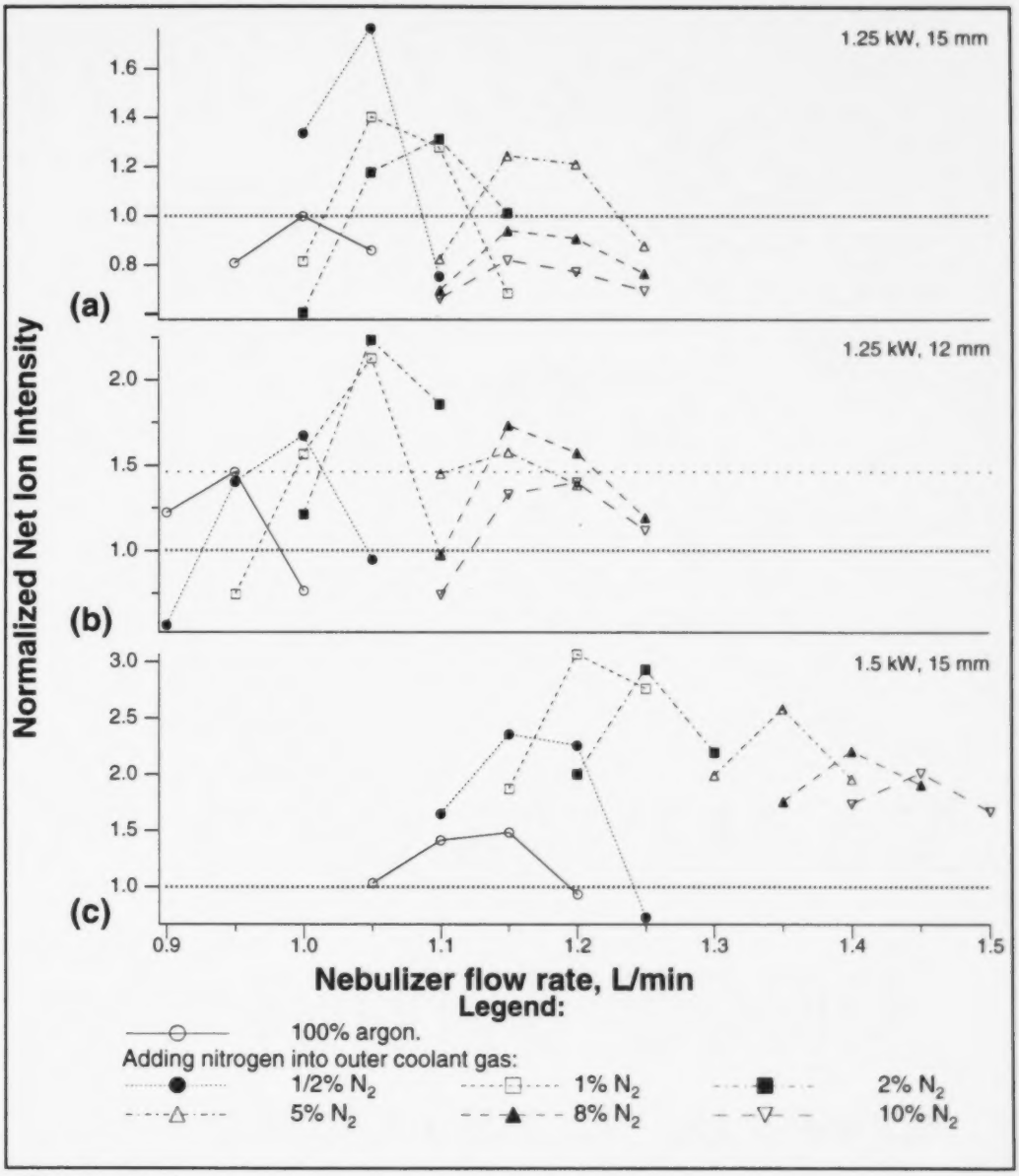

Figure 3.4
Dependence of the signal intensity for 100 ppb Rh upon sampling distance, nebulizer flow, and constitution of plasma as nitrogen added to the coolant. All signals are normalized to net signal intensity for Rh at 1.25 kW, 15 mm sampling distance, at its optimum nebulizer flow in 100% argon.

(a) Forward power 1.25 kW, 15 mm sampling distance.
(b) Forward power 1.25 kW, 12 mm sampling distance.
(c) Forward power 1.5 kW, 15 mm sampling distance.

Figure 3.4 shows nitrogen addition causing either enhancement or diminishment of the analyte signal, depending on nebulizer flow rate, power, sampling distance, and amount of nitrogen added. These parameters are interdependent, as they are in an argon plasma. In all cases the nebulizer flow required to maintain the maximum signal intensity increased as the amount of nitrogen was increased; this shift was more extreme at 1.5 kW than at 1.25 kW. In order to add more than ten percent nitrogen, it was necessary to sample closer than 10 mm and to use higher nebulizer flow rates in order to obtain the optimum analyte signals. Because equipment modifications were necessary to do either, ten percent is the maximum amount of nitrogen added in this work. This shift of the nebulizer flow rate is consistent with the visible shrinking of the plasma as nitrogen is introduced into the outer gas flow, and corresponds to increased excitation in the plasma. The region of the plasma containing the ionized species is pulled down into the plasma core.

The signal maximum is reached after only a modest amount of nitrogen is added and thereafter shows a smooth decline in intensity. The signal enhancement at 1.25 kW is more modest than at 1.5 kW. Figure 3.4 (a) shows that at 1.25 kW and 15 mm as 8 or 10% nitrogen is admitted the signal intensity is actually less than in argon only, while at 1.5 kW with 10% nitrogen, the signal is greater than in argon only. The intensity increase was due to increased power coupled with nitrogen addition into the plasma. Figure 3.4 (b) shows a pattern that looks similar to that in (a) but the signals are somewhat bigger. There is a second, more faint dotted line to mark the signal level in argon at 12 mm at its optimum nebulizer flow rate. Making this line our point of reference rather than the (heavier) line marking the intensity in argon at 15 mm, it can be seen that relative to the 12 mm line, as 8 and 10% nitrogen is added, the signal is diminished.

Figure 3.5 further shows the effect upon the rhodium signal while adding a constant ten percent nitrogen into the coolant and varying the power and sampling distance. Similar plots were obtained at other levels of nitrogen addition. The signal is largest at the closest sampling distance of 10 mm for either power. The optimum nebulizer flow rate at all sampling distances was most shifted at 1.5 kW and 15 mm sampling distance. It is clear from this figure that at this nitrogen flow, in order to see the maximum analyte signal it is necessary both to shift the sampling plate forward and to increase the nebulizer flow rate. This is especially true with increased power. In their work Beauchemin and Craig state that their analyte signals were decreased with the addition of nitrogen [39], which can probably be attributed their use of a constant nebulizer flow rate.

There is little background from the plasma and water at masses greater than that of rhodium, although depending upon the sample matrix, there may be other interferences. Of more interest is the behaviour of nitrogen plasmas in the mass range where there are more plasma background species, such as from 45 to 85 amu where the argon, argon dimers, and argon oxide species dominate and cause difficulties in the analysis of transition metals. In this work, the effect of nitrogen upon ArO^+, $ArOH^+$, $Ar_2H_2^+$, and two of the isotopes of Ar_2^+ are examined, along with its effect upon those analyte species these argides interfere with, specifically, iron (at ^{56}Fe and ^{57}Fe) and selenium (at ^{76}Se, ^{78}Se, and ^{82}Se). Although the iron isotope at 54 amu is more abundant than the isotope at 57 amu, nitrogen in the plasma increases the ArN^+ signal at 54 amu and it is virtually unusable for analyte detection.

Figures 3.6 and 3.7 give examples of intensity versus nebulizer flow rate behaviour for some of these species. Figures 3.6 shows the iron signal and background ArO^+ at 56 amu and Figure 3.7 shows selenium and background

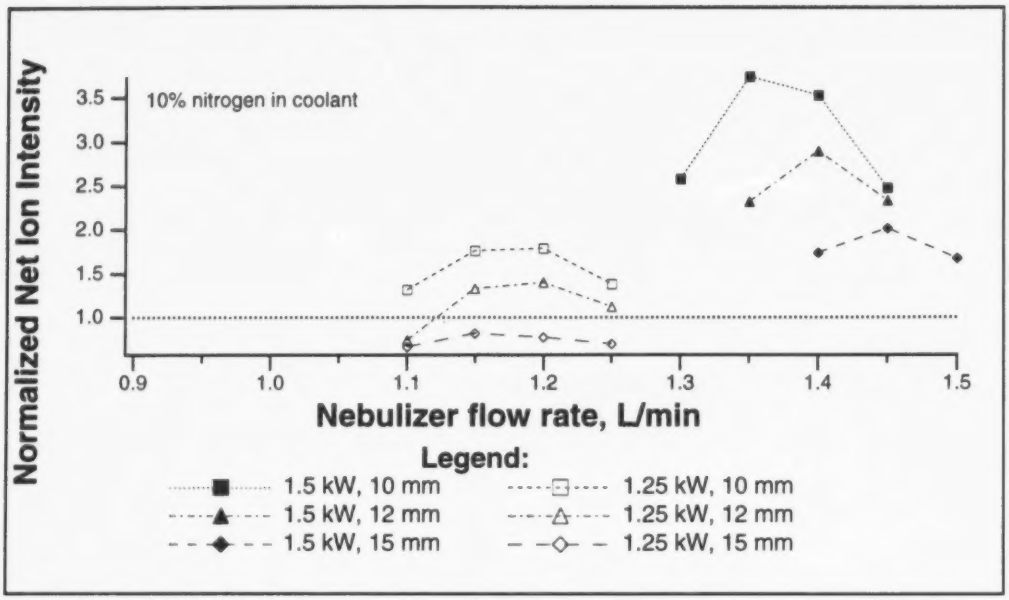

Figure 3.5
Dependence of the signal intensity for 100 ppb Rh at m/z 103 upon sampling distance, nebulizer flow rate, and forward power as 10% nitrogen added to the coolant.

All signals are normalized to the net signal intensity for Rh at 1.25 kW, 15 mm sampling distance, at its optimum nebulizer flow in 100% argon.

Ar_2^+ at 78 amu. The first two plots (a) and (b) in each of these figures show the effect of nitrogen addition upon the given background species, and the lower two (c) and (d) show the effect upon the given analyte species (iron or selenium) at that mass. Each plot in each figure shows the effect of increasing the nitrogen at a single forward power and 15 mm sampling distance upon the signal intensity for that species. These analyte signals are background subtracted and normalized. Although the shape of the plots of analyte intensity versus nebulizer flow rates is similar to that seen for rhodium, the plots for the background species do not have the same shape. For these background species, there are no signal maxima seen at the nebulizer flow rates used, although it can be seen that there is a steep slope and a strong dependence upon the nebulizer flow rate.

The intensities of the background species ArO^+ and Ar_2^+ do not behave in the same fashion as the percentage of nitrogen is increased. Figure 3.6 (a) and (b) show that at nitrogen levels less than about two percent, the ArO^+ signal is in fact somewhat enhanced relative to its intensity in argon only, and as the nitrogen is further increased, the intensity of this background species begins to drop below its intensity in argon. It is not until the percentage of nitrogen is increased to at least 8% that the background signal is reduced to less than half of its "standard" signal. Not shown are plots at 1.25 kW and 12 mm sampling distance, which are similar to those for 15 mm. The behaviour of the background species $ArOH^+$ at 57 amu is similar to that of ArO^+. Figure 3.7 (a) and (b) show that in contrast to ArO^+, Ar_2^+ at 78 amu is not reduced in intensity upon the addition of nitrogen into the coolant flow, and at 1.5 kW, actually increases slightly at all levels of nitrogen investigated. At a forward power of 1.25 kW with at least five percent nitrogen addition, the background signal is

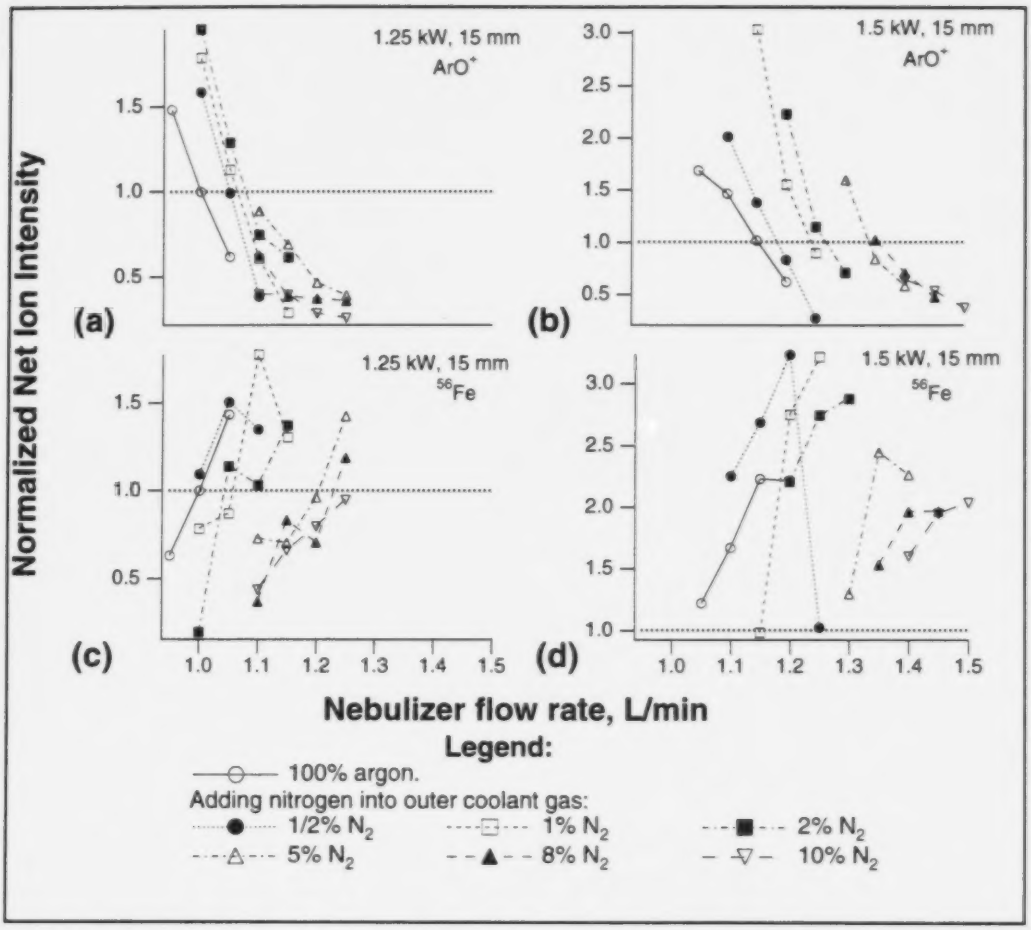

Figure 3.6

Dependence of the net signal of 100 ppb Fe^+ and the background species ArO^+ at m/z 56 upon the nebulizer flow rate and the constitution of the plasma as nitrogen is added to the coolant at two forward powers.

All signals are normalized to the signal intensity at 1.25 kW, 15 mm sampling distance, at the optimum nebulizer flow for Rh in 100% Ar.

(a) ArO^+, forward power 1.25 kW, 15 mm sampling distance.
(b) ArO^+, forward power 1.5 kW, 15 mm sampling distance.
(c) Fe^+, forward power 1.25 kW, 15 mm sampling distance.
(d) Fe^+, forward power 1.5 kW, 15 mm sampling distance.

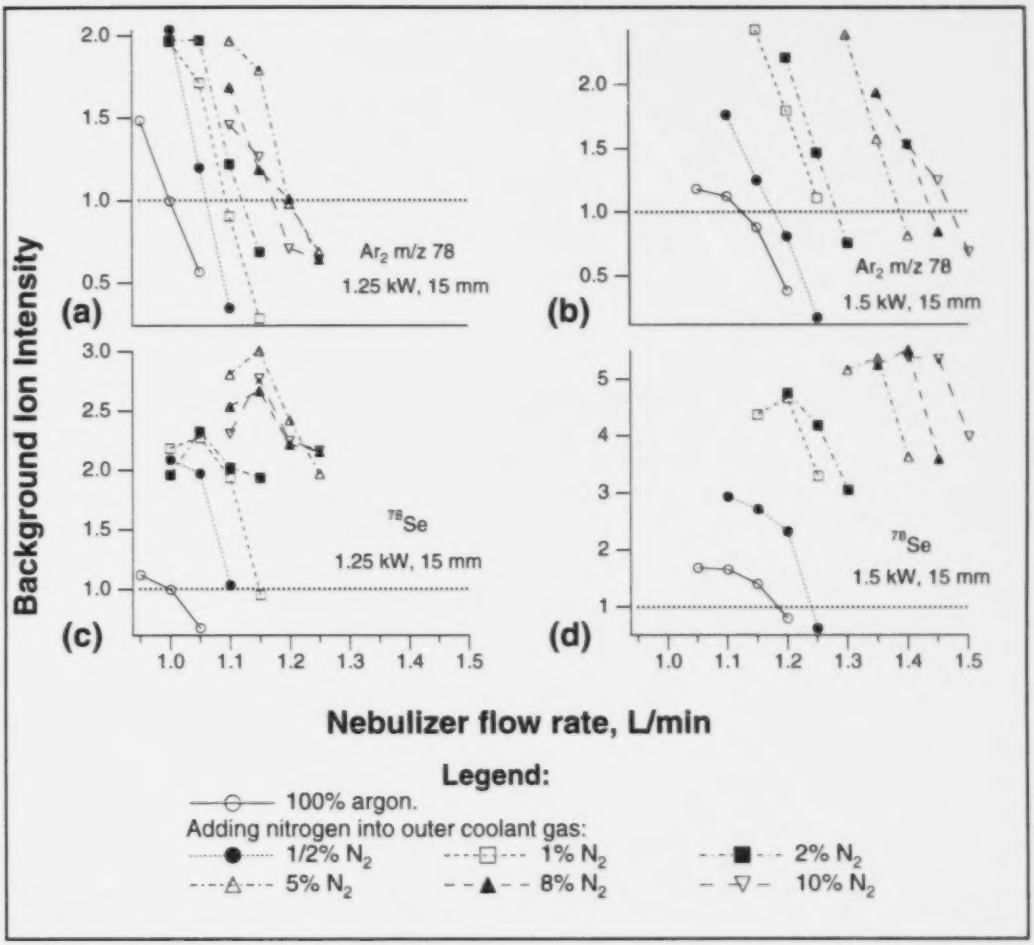

Figure 3.7

Dependence of the net signal of 100 ppb Se and the background species Ar_2 at m/z 78 upon the nebulizer flow rate and the constitution of the plasma as nitrogen is added to the coolant.

All signals are normalized to the signal intensity at m/z 78 at 1.25 kW, 15 mm sampling distance, at the optimum nebulizer flow for Rh in 100% argon.

(a) Ar_2^+, forward power 1.25 kW, 15 mm sampling distance.

(b) Ar_2^+, forward power 1.5 kW, 15 mm sampling distance.

(c) Se^+, forward power 1.25 kW, 15 mm sampling distance.

(d) Se^+, forward power 1.5 kW, 15 mm sampling distance.

about the same as in argon only. The behaviour of isotopes of Ar_2^+ at 76 and 80 amu is similar to that shown here.

Figure 3.6 (c) and (d) shows the effect of nitrogen addition upon the signal for iron at 56 amu (isotopic abundance of 91.7%). Figure 3.7 (c) and (d), shows the effect on selenium at 78 amu (isotopic abundance of 23.6%). The iron signal is enhanced about as much as rhodium in Figure 3.4. Figure 3.6 (c) at 1.25 kW shows a modest signal enhancement with small amounts of nitrogen added, and a decline in the intensity when the added nitrogen is at least five percent. Figure 3.6 (d) shows that at a power of 1.5 kW there is initially a significant increase in iron intensity as the percentage of nitrogen increases, followed by a decline to an intensity which is somewhat greater than its "standard" intensity. Iron at 57 amu behaves similarly.

Compared with the signals for rhodium and iron, the selenium signals shown in Figure 3.7 are more enhanced by the addition of nitrogen and do not decline as nitrogen increases, but rather plateau. All of the selenium signals are increased relative to their level in argon at all levels of nitrogen added at both powers investigated, despite an increase in background intensity. Selenium at 76 and 82 amu show similar behaviour. At this analyte concentration of 100 ppb, the major selenium isotope (49.7%) at 80 amu cannot be monitored because it is interfered with by the huge signal of the major isotope of the argon dimer.

For the data presented, the maximum overall signal for iron is obtained using parameters, at which the background argon oxide signal is also greatest, and increased signal intensity for selenium has also been obtained at the cost of increased background. A set of operating conditions was determined which generally increased the analyte signals, as well as the SBR and SNR values. The following table (Table 3.1) lists the parameters chosen for these sets. The

percentage of nitrogen in the total coolant flow was increased and the sampling distance was decreased as shown, at two powers. In order to facilitate comparison, the same sampling distances were used for both power levels at each nitrogen level. Each data point presented represents the mean of five replicates. The dwell time for each mass measurement was 0.3 second per point.

Table 3.1: Operating parameters as nitrogen is added to the coolant gas flow

% Nitrogen	sampling distance mm	Power kW	Power kW
0	15	1.5	1.25
0.5	15	1.5	1.25
1	15	1.5	1.25
2	15	1.5	1.25
5	12	1.5	1.25
8	10	1.5	1.25
10	10	1.5	1.25

The next figures show the trends for both the analyte signals of and the background intensities for rhodium at 103 amu, iron at 56 and 57 amu, and selenium at 76, 78, and 82 amu, for the operating conditions listed in Table 3.1. Some trends are not smooth since the sampling distance was not varied continuously. In addition, the background increases dramatically at closer distances and the plasma was less stable at 1.5 kW and as nitrogen was introduced. Each intensity value is obtained at the optimal nebulizer flow for the net rhodium signal at the nitrogen flow rate, power, and sampling distance

shown in Table 3.1. Figure 3.8 shows the net background subtracted intensity for all six analyte species, Figure 3.9 shows the background intensity at each monitored mass, Figure 3.10 shows the net signal divided by the background signal (SBR) at each mass, and Figure 3.11 shows the net signal divided by the background noise (SNR). The data are plotted with absolute values on the left hand axis versus percent nitrogen mixed into the coolant. A normalized signal for each species is obtained dividing by the intensity for that species in "standard" argon. The horizontal dotted line on each plot indicates this level for reference and, for comparison, the right hand axis is scaled using these normalized values.

Figure 3.8 shows that, using this parameter set where the sampling distance is decreased as the nitrogen is increased, analyte signals continue to rise as nitrogen levels increase. Figure 3.9 shows that background levels modestly decrease for some of these species although at both 103 and 82 amu the background levels increase. Figure 3.10 shows that these modest background reductions coupled with a rise in signal intensity increases the SBR for the all the analyte species except for rhodium. Since a decreased background will decrease the background noise if the noise is due to counting statistics, the SNR (shown in Figure 3.11) also increases for all but rhodium. Any improvements are however quite modest.

The first plots (a) of Figures 3.8 to 3.11 show the results for rhodium. Despite the net signal increase, the SBR and SNR plots show no significant improvements as a result of the similarly increased background level and accompanying noise, as can be seen from the small range of values (from around 0.5 to 1.5) in the normalized axes. There is a slight overall increase in the background intensity over the entire mass range as nitrogen increases and may be partly due to nitrogen emission in the vacuum chamber [22]. Although

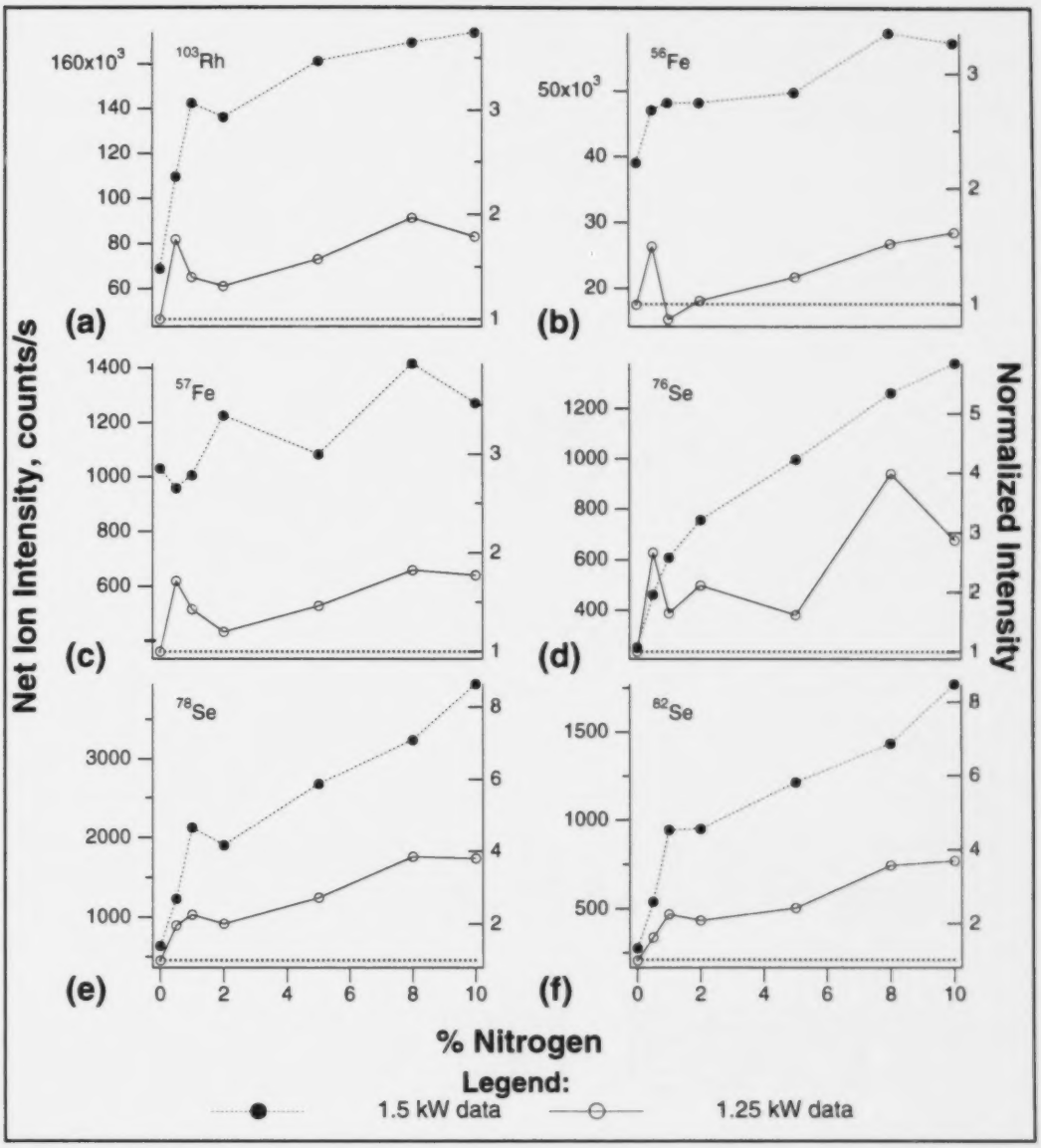

Figure 3.8
Effect of the addition of nitrogen into outer gas upon the net signal intensities for 100 ppb analytes at two forward powers. Sampling distances are as shown in Table 3.1. The left hand axis shows absolute net signal level in counts/second. The right hand axis shows values normalized to the signal level for that analyte in argon at 1.25 kW and 15 mm sampling distance.

(a) Rhodium at m/z 103
(b) Iron at m/z 56
(c) Iron at m/z 57
(d) Selenium at m/z 76
(e) Selenium at m/z 78
(f) Selenium at m/z 82.

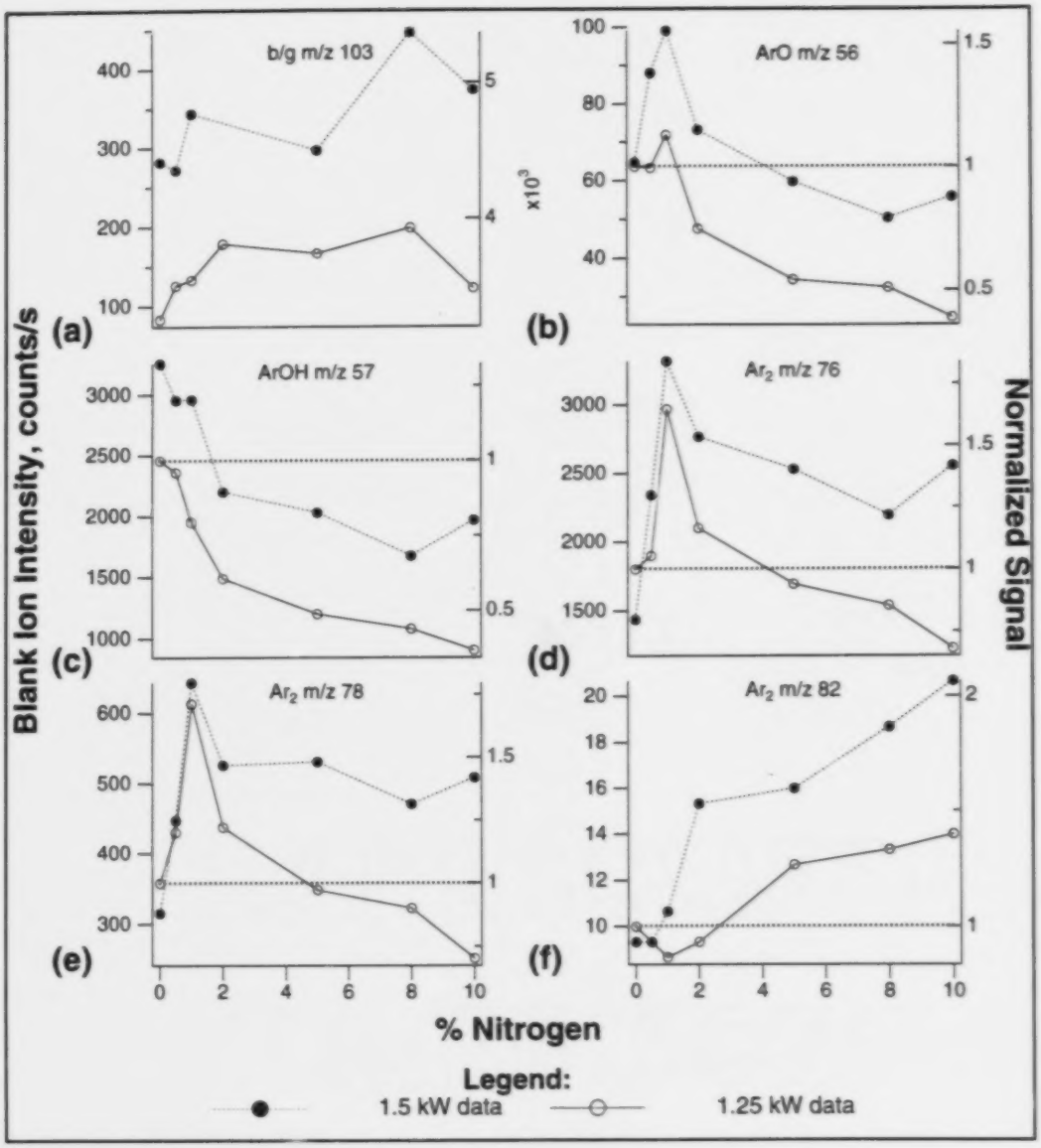

Figure 3.9
Effect of the addition of nitrogen into the coolant upon the background signal intensities at two forward powers. Sampling distances are as shown in Table 3.1. The left hand axis shows absolute background signal level in counts/second. The right hand axis shows values normalized to the background signal at that mass in argon at 1.25 kW and 15 mm sampling distance.

(a) Background at m/z 103
(b) ArO^+ at m/z 56
(c) $ArOH^+$ at m/z 57
(d) Ar_2^+ at m/z 76
(e) Ar_2^+ at m/z 78
(f) $Ar_2H_2^+$ at m/z 82.

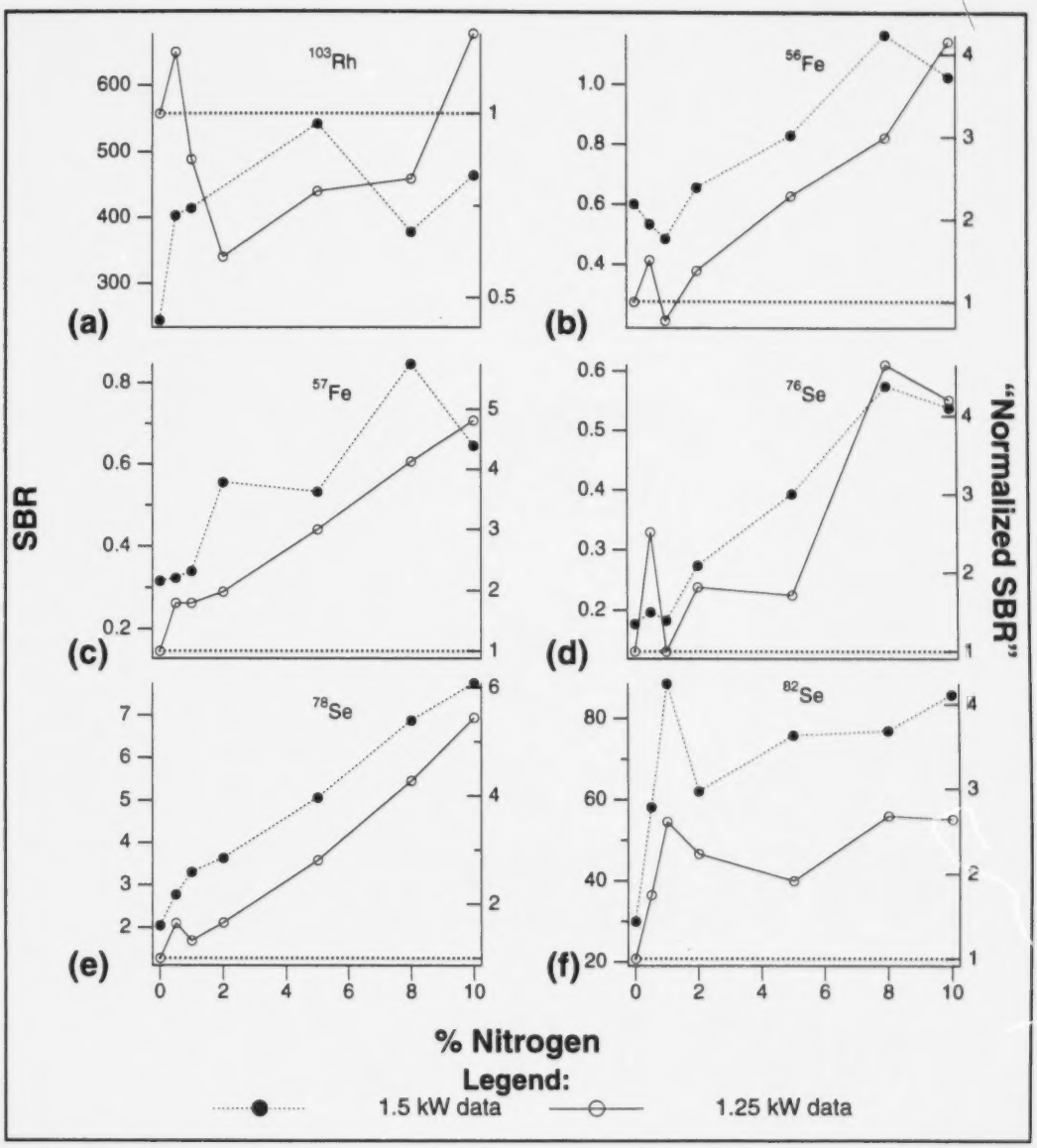

Figure 3.10
Effect of the addition of nitrogen into the coolant upon the ratio of net signal/background signal (SBR) at two forward powers. Sampling distances are as shown in Table 3.1. The left hand axis shows absolute SBR. The right hand axis shows SBR values normalized to the SBR for that analyte in argon at 1.25 kW and 15 mm sampling distance.

(a) SBR at m/z 103
(b) SBR at m/z 56
(c) SBR at m/z 57
(d) SBR at m/z 76
(e) SBR at m/z 78
(f) SBR at m/z 82.

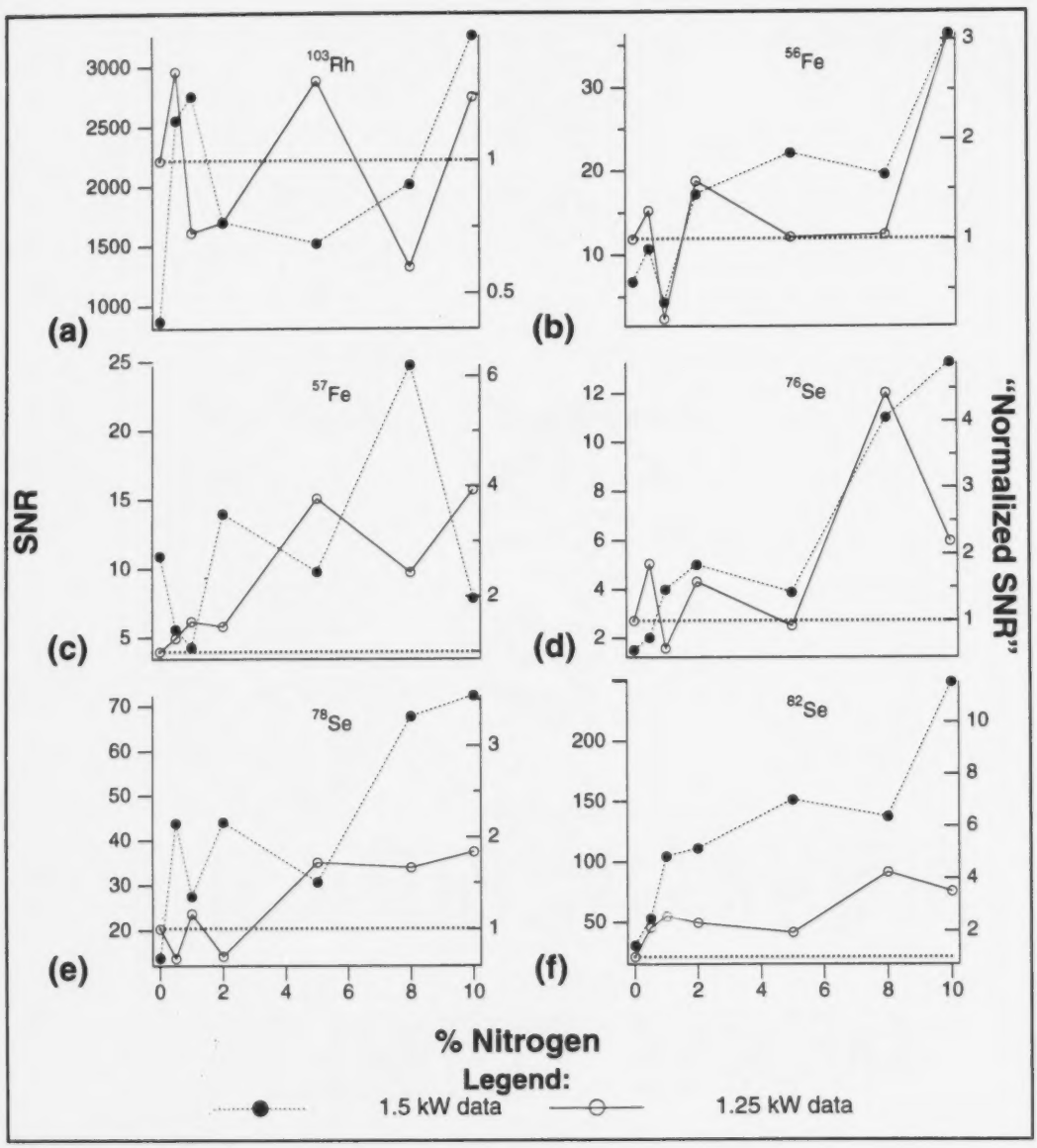

Figure 3.11
Effect of the addition of nitrogen into the coolant upon the ratio of net signal/background noise (SNR) at two forward powers. Sampling distances are as shown in Table 3.1. The left hand axis shows absolute SNR. The right hand axis shows SNR values normalized to the SNR for that analyte in argon at 1.25 kW and 15 mm sampling distance.

(a) SNR at m/z 103
(b) SNR at m/z 56
(c) SNR at m/z 57
(d) SNR at m/z 76
(e) SNR at m/z 78
(f) SNR at m/z 82.

there are photon stops, they are designed to prevent photons from entering the mass spectrometer, and may be less effective at blocking those formed inside the vacuum system itself. For an analyte such as rhodium which has no interfering argon or water background species, the addition of nitrogen to the coolant at these levels, powers, and sampling distances made no real difference to the sensitivity or precision, provided the parameter set was also optimized.

The second and third plots (b) and (c) of Figures 3.8 to 3.11 show results for iron and the background argon oxides at 56 and 57 amu. By decreasing the sampling distance, the main gain has simply been to maintain the enhanced intensity and to prevent these signals from falling as nitrogen increases beyond two percent, while the background level drops. The reduction in the background levels for these species is more modest than an order of magnitude decrease in the intensity of ArO^+ described by Lam and Horlick [75]. Although results obtained under different circumstances using different instruments and experimental parameters may not be directly comparable, it may be possible to make a general comparison. Their report does not clearly state it but it appears that what are being compared are the background intensity of ArO^+ in argon at 1.5 kW and 10 mm sampling distance and the intensity of ArO^+ with 12% nitrogen in the coolant at the same power and sampling distance. At 10% nitrogen addition and 1.5 kW and 10 mm, this species is reduced compared with its intensity "standard" argon, as shown in Figure 3.9 (b). However in argon at 1.5 kW, 10 mm sampling distance the ArO^+ signal is approximately double its "standard" intensity in argon. It is necessary to state clearly what the operating parameters were for data which is being compared. The background at 1.5 kW and 10 mm sampling distance is greater than the background at 1.5 kW and 15 mm shown in Figure 3.6, but is sufficiently reduced that the SNR and SBR both show

improvements at both forward powers. Both SNR and SBR values are improved because the gain at 1.25 kW is mainly due to decreased background, while at 1.5 kW the gain is due to increased signal. The improved SBR values are still below one, *i.e.*, the net signal and background are of the same order of magnitude at each of these masses.

The final three plots (d), (e), (f) of Figures 3.8 to 3.11 show results for selenium and background species at 76, 78, and 82 amu. The relative signal enhancement is much greater than for rhodium and iron. The signal is still increasing with ten percent nitrogen and is much greater at 1.5 kW power than 1.25 kW. The improvement of the selenium signal is probably due to increased ionization in a nitrogen plasma. Although both rhodium and iron are nearly 100% ionized in argon, selenium is only about 30% ionized and can benefit from an increase in plasma temperature. By decreasing the sampling distance, the background has also been decreased for the Ar_2^+ species with the addition of at least five percent nitrogen. The background signal at 80 amu is similarly decreased (not shown). The background level of $Ar_2H_2^+$ at 82 amu is consistently increased as nitrogen increases. The SNR and SBR show similar enhancements as for the iron.

The different behaviour of ArO^+ and $ArOH^+$ relative to Ar_2^+ suggests different formation mechanisms. Although nitrogen may compete with argon for oxygen to form NO^+ which diminishes the ArO^+ and $ArOH^+$ signals, at the low levels of nitrogen introduction seen here, the total amount of argon is scarcely reduced in the coolant. A reduction in Ar_2^+ with some parameter combinations is seen however. The dependence upon power is a reminder that these species must be ionized in order to be detected, and the dependence upon sampling depth, that it is not merely the presence or absence of a species that is measured, but also its relative location in the plasma. If the sampling position is

shifted to correspond to higher ionization of desired species and, at the same time, lower ionization of undesired species, something of practical utility has been accomplished, even if the actual balance overall in the entire plasma is unchanged.

3.2.2.b Addition of nitrogen into the nebulizer gas

When nitrogen is introduced into the nebulizer gas flow, the central channel appears wider and more diffuse, plasma instability increases, and the plasma expires more readily. The optimum nebulizer flow for maximum analyte signals shifts to lower gas flows. Figure 3.12 shows the normalized net rhodium signal intensity as a function of the nebulizer flow rate at various sampling distances while adding 3% nitrogen into the nebulizer gas. It was not possible to add more nitrogen into the nebulizer without extinguishing the plasma and conversely it was difficult to add less with the equipment available. Hence data will only be shown for addition of 3% nitrogen into the nebulizer gas.

Figure 3.12 (a) shows the effect upon the signal as nitrogen was added at a forward power of 1.25 kW while varying the sampling distance and (b) shows the effect at 1.5 kW. The optimum nebulizer flow is slightly shifted to lower flow rates, which is consistent with the widened sample channel since interaction of the sample with the plasma is reduced, and reduction of the nebulizer flow rate increases the sample residence time in the plasma. The signal falls off very quickly on either side of the optimum flow. At 1.25 kW and 15 mm sampling distance the rhodium signal intensity was slightly reduced compared to its intensity in pure argon. The increase at 1.5 kW is similar to that obtained at 1.25 kW at 12 mm. It was not possible to sample closer than 12 mm because the optimum nebulizer flow at this distance was too low for the aerosol to penetrate the plasma. Similar plots of intensity versus nebulizer flow rate for the iron and selenium analyte species at 56 and 78 amu and their respective

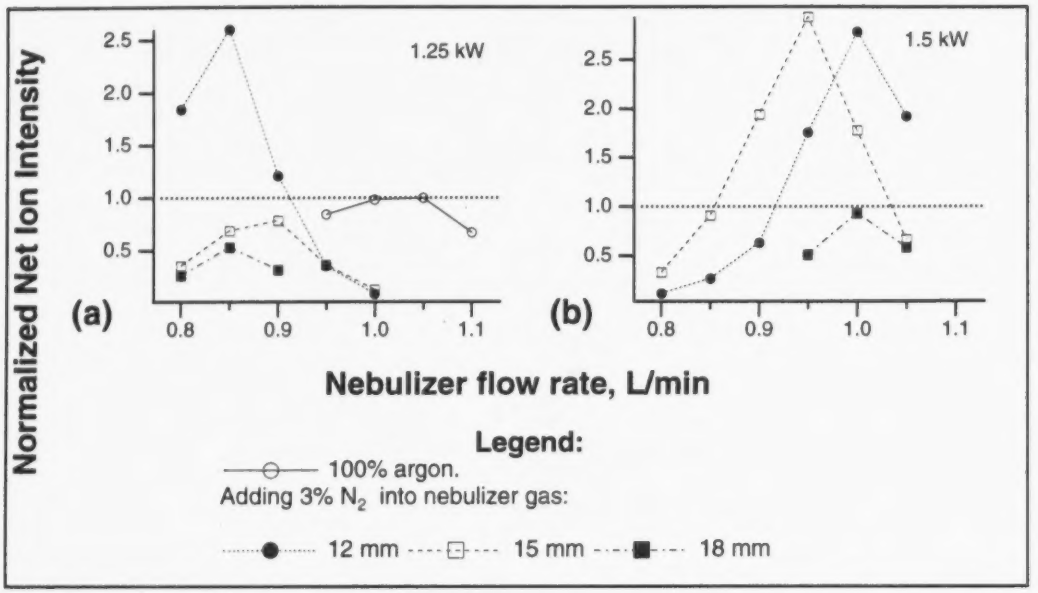

Figure 3.12
Dependence of the signal intensity for 100 ppb Rh upon nebulizer flow rate and sampling distance as nitrogen is added to the nebulizer gas at two forward powers, varying the sampling distance. All signals are normalized to the net signal intensity for Rh at 1.25 kW and 15 mm sampling distance, at its optimal nebulizer flow in 100% argon.

(a) Forward power 1.25 kW, varying sampling distance.
(b) Forward power 1.5 kw, varying sampling distance.

backgrounds are not shown, since the signal responses are similar to those shown in Figures 3.6 and 3.7 for the introduction of the lowest nitrogen flows into the coolant, but shifted to lower nebulizer flow rates as in Figure 3.12.

Figures 3.13 (a) and (b), show the effect of nitrogen in the nebulizer both upon the analytes and background intensities for rhodium at 103 amu, copper at 63 amu, iron at 56 and 57 amu, and selenium at 76, 78, and 82 amu. The power was held at 1.25 kW, the sampling distance was either 12 or 15 mm, and the measurement dwell time was one second per point. Each data point represents the mean of sixteen replicate measurements. Because there was no additional signal gain and significantly more noise and more difficulty keeping the plasma operating at 1.5 kW power, only data acquired at 1.25 kW is presented. Each intensity value is measured for that species at the nebulizer flow which is optimal for the net rhodium signal under the same circumstances, as previously outlined. Figure 3.13 (c) shows the SBR at each mass and (d) the SNR. In order to plot data for these masses together on a single scale, they have been normalized in the same manner as previous data.

At the 12 mm sampling distance all analyte signal intensities show a modest increase to about double their intensity in "standard" argon, most of the background species show a slighter increase, and there is a concomitant slight increase in SBR and SNR for all species. At 15 mm all of the signals are approximately the same intensity as in argon and the figures of merit are also approximately the same. None of the increases in any of these parameters is substantial and are insufficient to serve as incentive to add nitrogen to the nebulizer in this fashion as a routine method, given the operating difficulties.

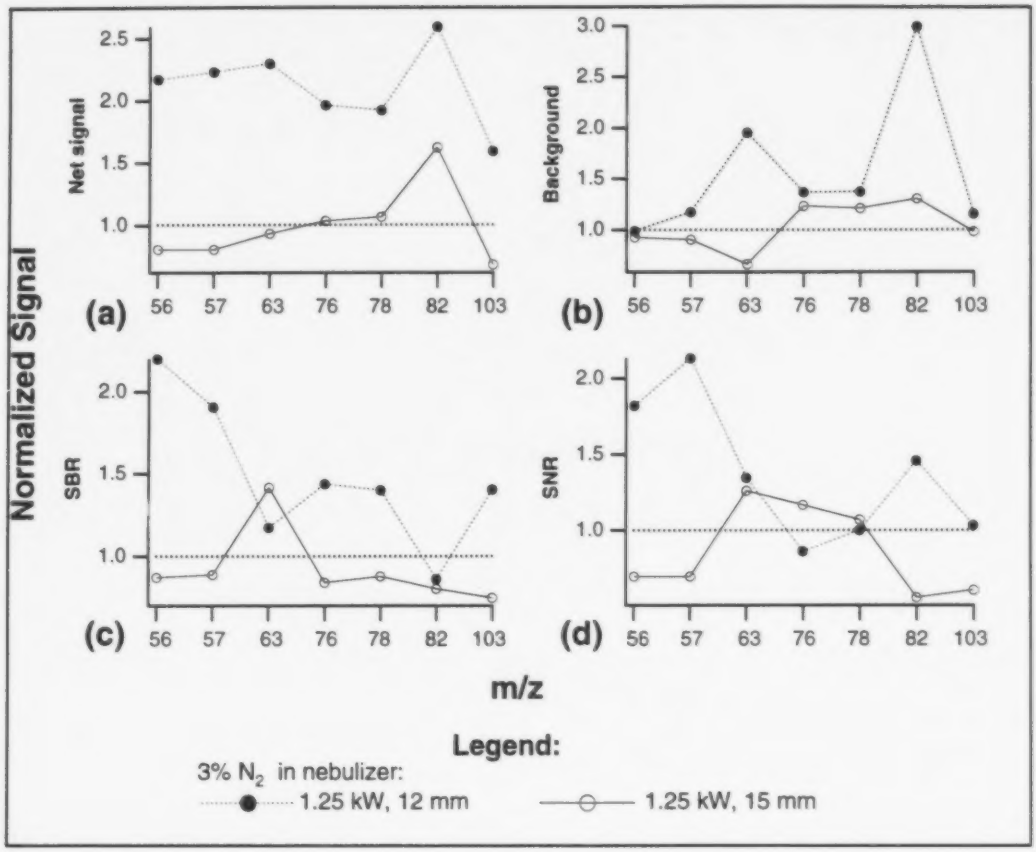

Figure 3.13
Effect of the addition of 3% nitrogen into the nebulizer gas at 1.25 kW forward power at two sampling distances at the given mass/charge (m/z) as shown, upon:

(a) the normalized net signal intensity,
(b) the normalized background intensity,
(c) the normalized ratio of net signal to background signal (SBR),
(d) the normalized ratio of net signal to background noise (SNR).

All values shown are normalized to the value for that species in 100% argon at 1.25 kW and 15 mm sampling distance.

3.2.2.c Addition of nitrogen into all plasma gases

Nitrogen was added in very small amounts into all of the gas flows in order to compare its effect with that of the other flows alone. The plasma was unstable and tended to extinguish with more than about two percent nitrogen added into all gas flows. Figure 3.14 shows the interaction of the variable parameters as nitrogen was added to a maximum of two percent. Each plot shows the effect of increasing the nitrogen at a single forward power and sampling distance, with separate traces shown for the various amounts of nitrogen added, from half a percent to two percent of the total gas flow.

The optimum nebulizer flow is shifted to slightly higher values from an all argon plasma. The rhodium signal is enhanced similarly to the observed enhancement when low levels of nitrogen introduced into the coolant only (shown in Figure 3.4). The effect of the added nitrogen into all the gas flows upon the background signals at 56 and 78 amu, and upon the iron and selenium signals at these masses, is likewise similar to what was observed when adding nitrogen to the coolant only (shown in Figures 3.6 and 3.7) for the lowest nitrogen levels and hence, are not shown again. The background signals for ArO^+ at 56 amu and for Ar_2^+ are slightly diminished relative to their intensities in argon. The iron signals at 1.25 kW are slightly smaller or are of similar intensity as in argon and at 1.5 kW, are somewhat enhanced over their intensity in argon. The selenium signals are as enhanced relative to their "standard" signals, as previously.

A set of operating parameters was determined in an attempt to find an optimal combination to enhance the analyte signal, SBR, and SNR. The following table (Table 3.2) lists the parameters chosen for these sets. The percentage of nitrogen in the total flow was increased and the sampling distance was decreased as shown, at two powers. To facilitate comparison, the

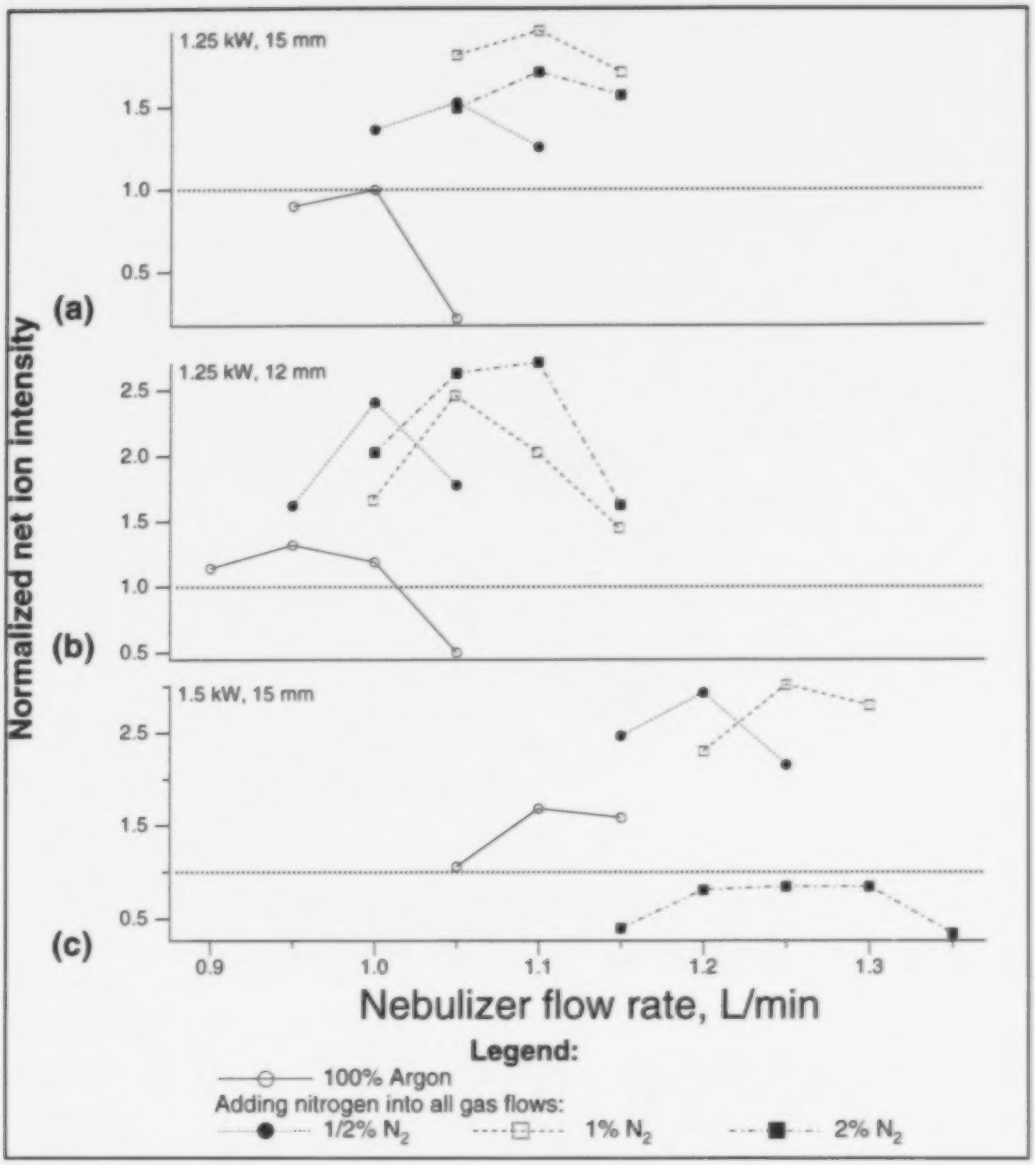

Figure 3.14
Dependence of the signal intensity for 100 ppb Rh upon nebulizer flow rate, sampling distance, and constitution of the plasma as nitrogen is added to all gas flows. All signals are normalized to the net signal intensity for Rh at 1.25 kW, 15 mm sampling distance, at its optimum nebulizer flow.

(a) Forward power 1.25 kW, 15 mm sampling distance.
(b) Forward power 1.25 kW, 12 mm sampling distance.
(c) Forward power 1.5 kW, 15 mm sampling distance.

same sampling distances were used for both power levels at each nitrogen level. Each data point presented represents the mean of five replicates. The dwell time for each mass measurement was 0.3 second.

Table 3.2: Operating parameters as nitrogen is added into all gas flows

% Nitrogen	sampling distance mm	Power kW	Power kW
0	15	1.5	1.25
0.5	12	1.5	1.25
1	12	1.5	1.25
2	10	1.5	1.25

The next figures show the trends for both the analyte signals of and the background intensities for rhodium at 103 amu, iron at 56 and 57 amu, and selenium at 76, 78, and 82 amu, for the operating conditions listed in Table 3.2. Figure 3.15 shows the effect of the addition of nitrogen into all the gas flows upon the normalized net signals of 100 ppb analyte species; Figure 3.16 upon the normalized background species at the same masses; Figure 3.17 the SBR values; and Figure 3.18 the SNR values. Normalized values for the signal and background intensities are plotted. The plots of the SBR and the SNR show absolute values on the left hand axis and values relative to their values in "standard" argon on the right hand axis.

Recall that a maximum of only two percent nitrogen has been added here, corresponding to only the first four points on the plots of Figures 3.8 to 3.11. In comparison with those figures, the analyte signals in Figure 3.15 are similar in intensity, the background signals are somewhat more depressed, and

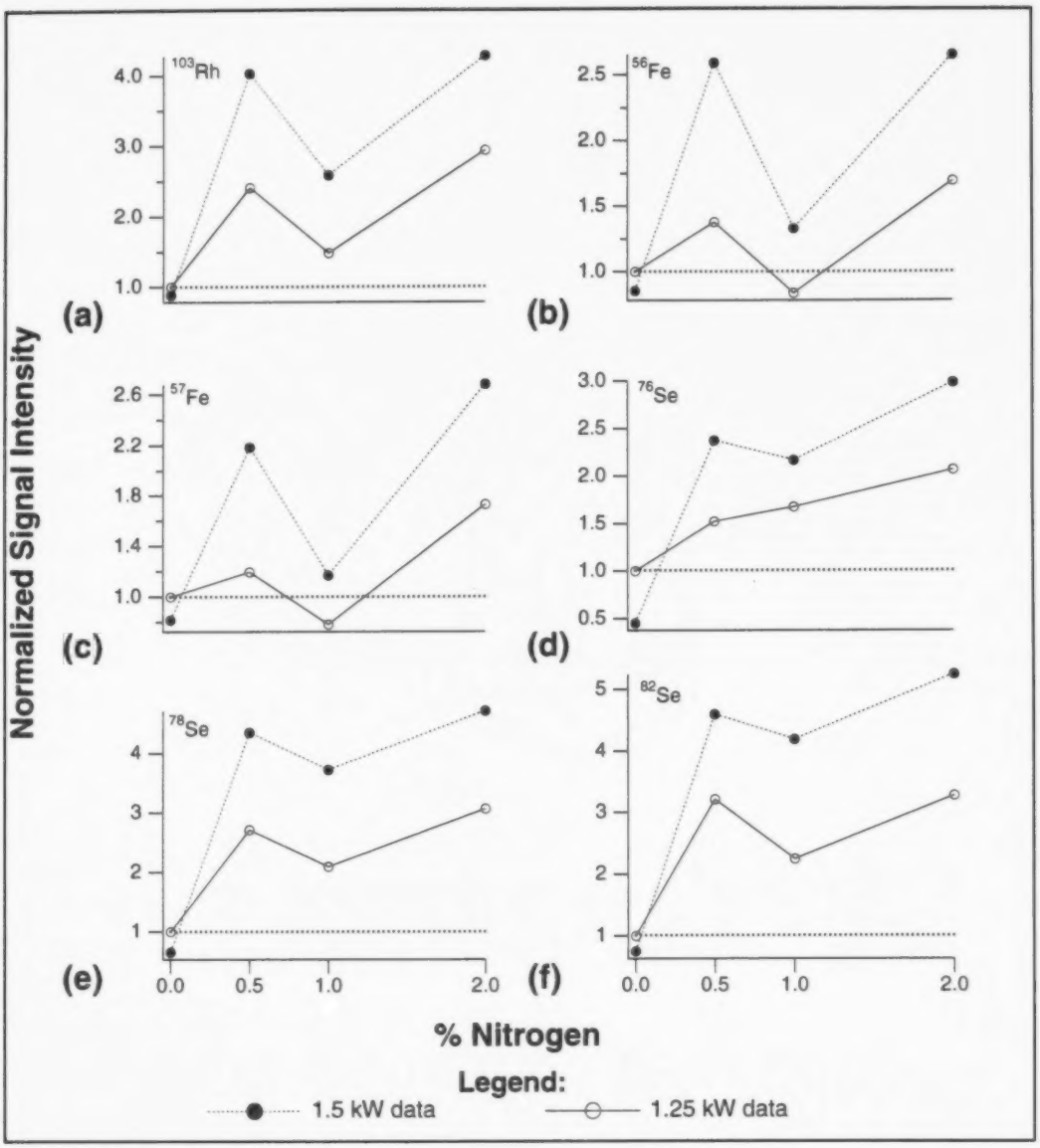

Figure 3.15
Effect of the addition of nitrogen into all gas flows upon the signal intensities for 100 ppb analytes at two forward powers. Sampling distances are as shown in Table 3.2. The axis shows the net intensity relative to its intensity in 100% argon at 1.25 kW and 15 mm sampling distance.

(a) Rhodium at m/z 103
(b) Iron at m/z 56
(c) Iron at m/z 57
(d) Selenium at m/z 76
(e) Selenium at m/z 78
(f) Selenium at m/z 82.

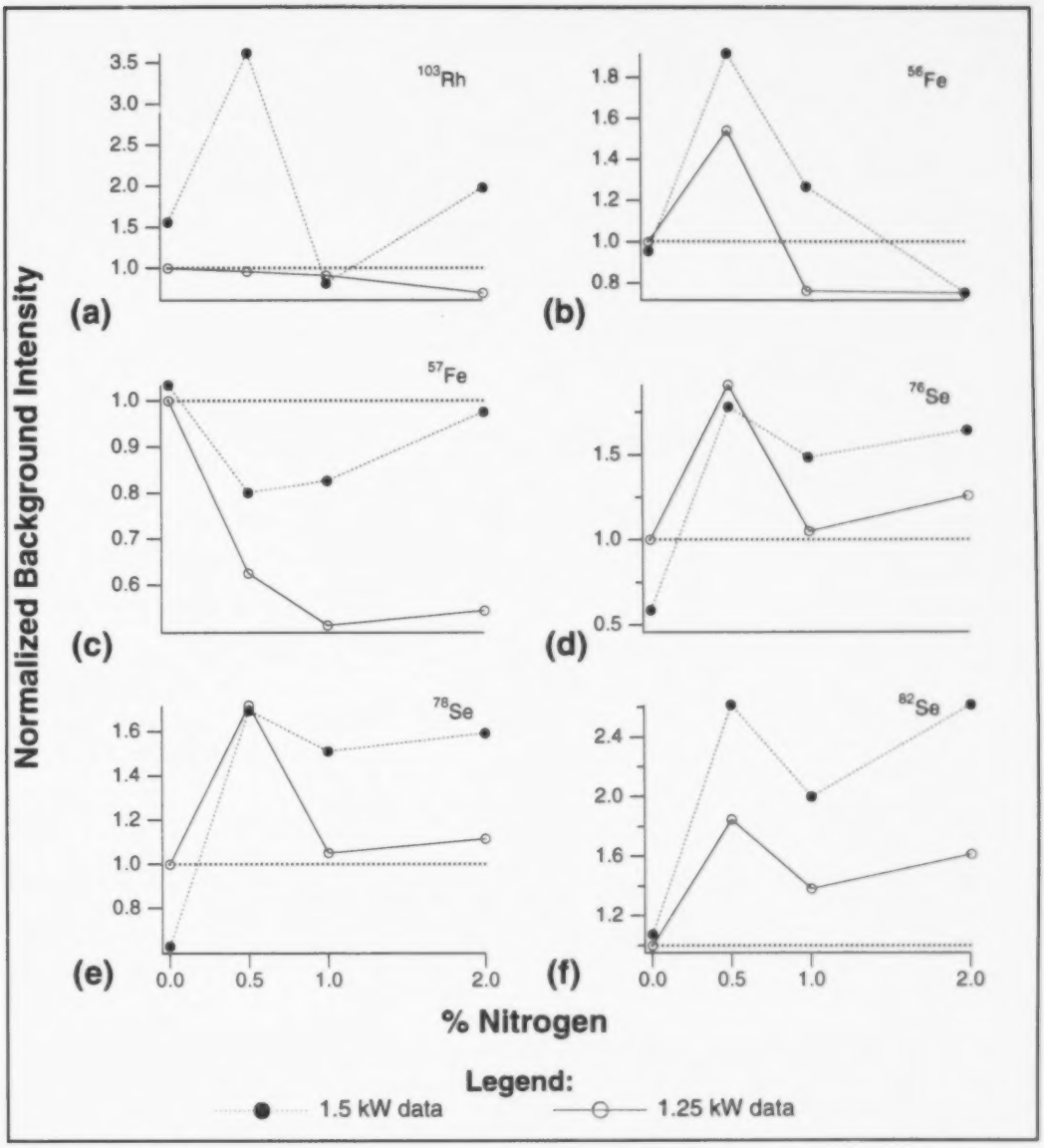

Figure 3.16
Effect of the addition of nitrogen into all gas flows upon the background signal intensities at two forward powers. Sampling distances are as shown in Table 3.2. The axis shows the blank intensity relative to its intensity in 100% argon at 1.25 kW and 15 mm sampling distance.

(a) Background at m/z 103
(b) ArO^+ at m/z 56
(c) $ArOH^+$ at m/z 57
(d) Ar_2^+ at m/z 76
(e) Ar_2^+ at m/z 78
(f) $Ar_2H_2^+$ at m/z 82.

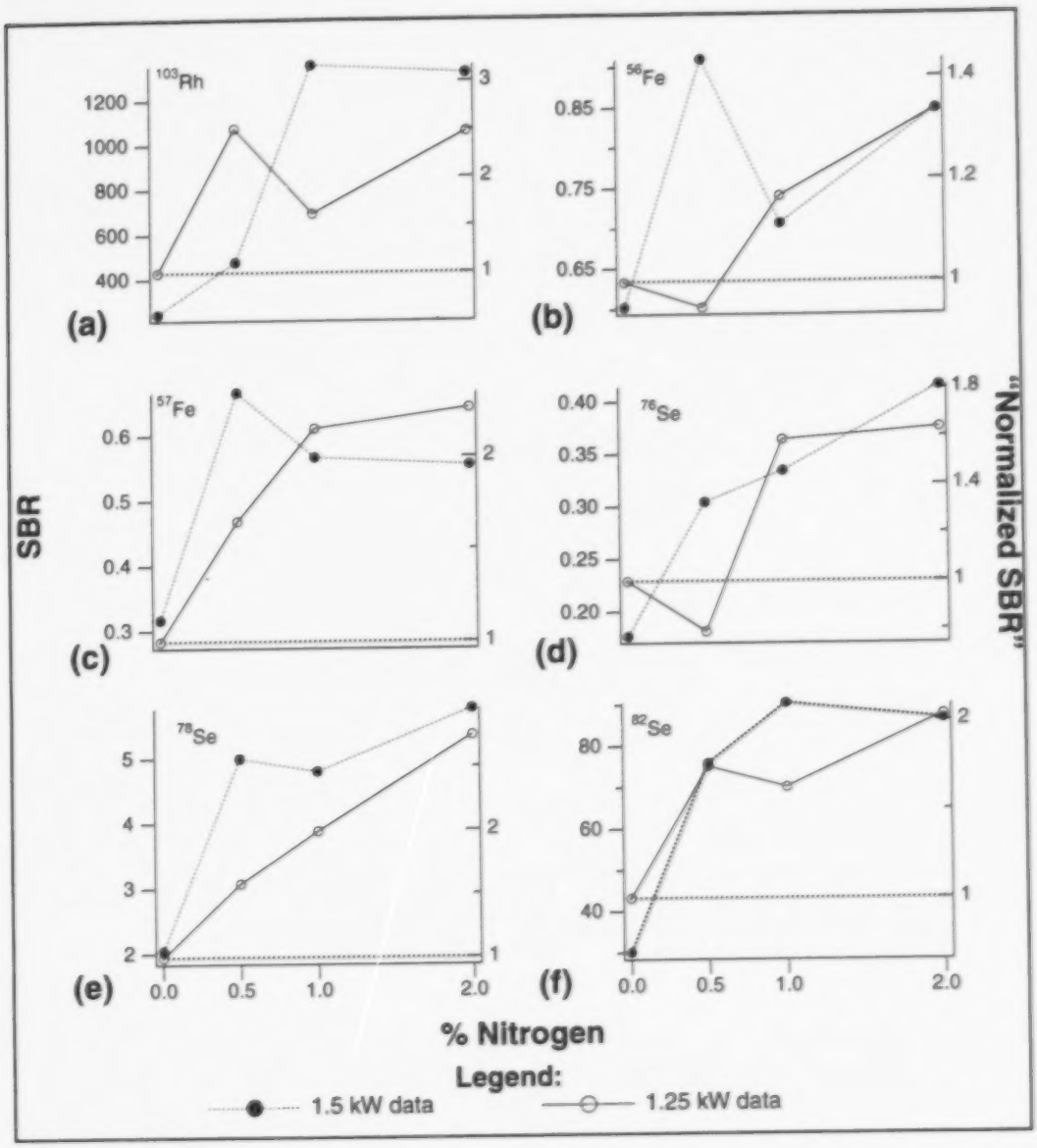

Figure 3.17
Effect of the addition of nitrogen into all gas flows upon the ratio of net signal/background signal (SBR) for 100 ppb analytes at two forward powers. Sampling distances are as shown in Table 3.2. The axis on the left hand side shows absolute SBR values while the axis on the right hand shows the SBR relative to the SBR in 100% argon at 1.25 kW and 15 mm sampling distance.

(a) SBR at m/z 103
(b) SBR at m/z 56
(c) SBR at m/z 57
(d) SBR at m/z 76
(e) SBR at m/z 78
(f) SBR at m/z 82.

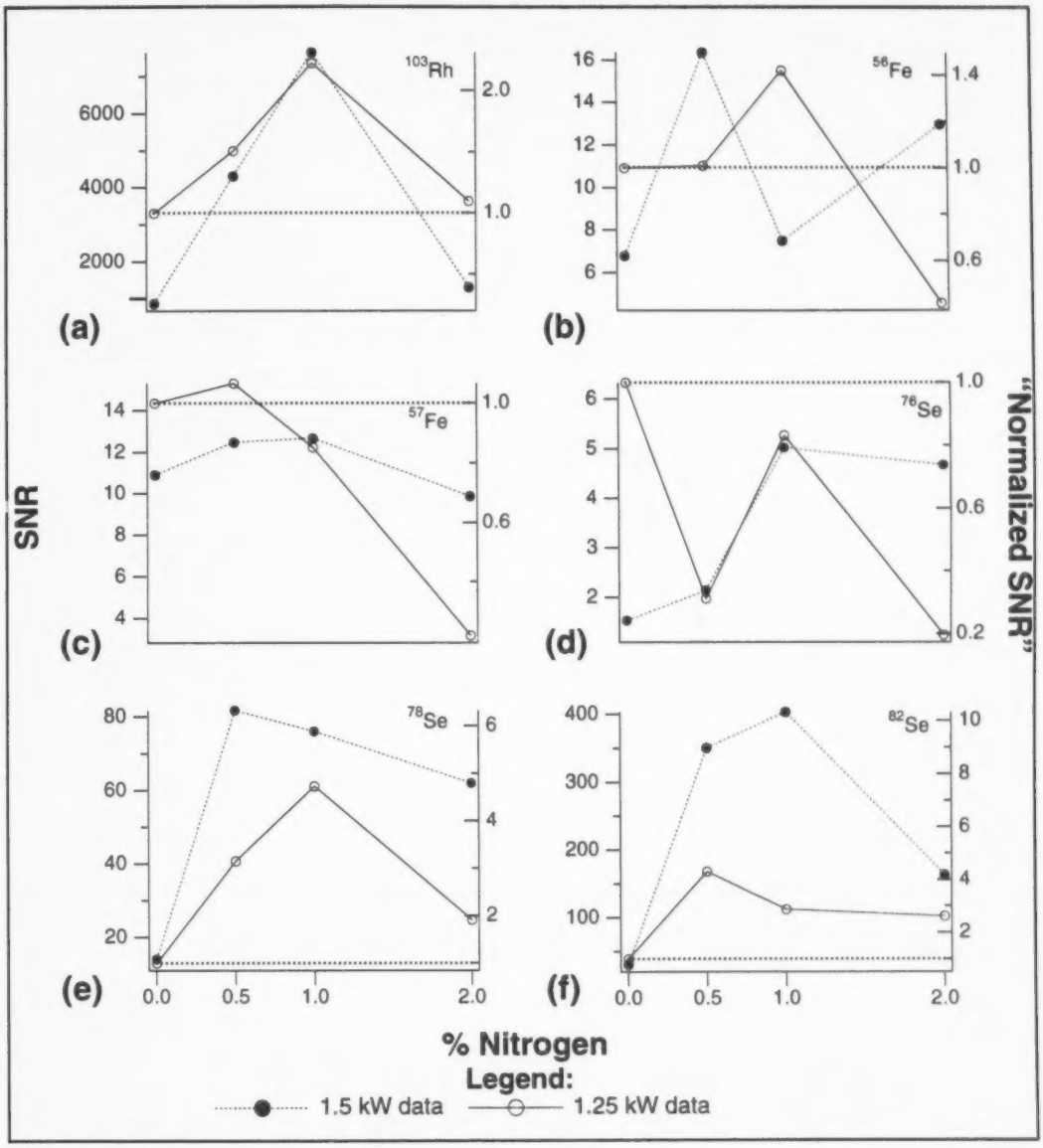

Figure 3.18
Effect of the addition of nitrogen into all gas flows upon the ratio of net signal/background noise (SNR) for 100 ppb analytes at two forward powers. Sampling distances are as shown in Table 3.2. The axis on the left hand side shows absolute SNR values while the axis on the right hand shows the SNR relative to the SNR in 100% argon at 1.25 kW and 15 mm sampling distance.

(a) SNR at m/z 103
(b) SNR at m/z 56
(c) SNR at m/z 57
(d) SNR at m/z 76
(e) SNR at m/z 78
(f) SNR at m/z 82.

the SBR's are similar. Unfortunately these low levels of nitrogen addition correspond to the region of the most erratic SNR ratios for addition into only the coolant gas, and this is also seen here. The precision and noise is not improved significantly, as shown by the SNR's of Figure 3.18. These ratios reflect the plasma instability and erratic signal counts for the background species as nitrogen was introduced in all the gas flows. The close similarity of the two sets of figures, Figures 3.8 to 3.11 and Figures 3.15 to 3.18, suggests that there is little difference in the plasma whether the same amount of nitrogen is added to the coolant only or into all gas flows. Overall there seems little gained by adding a small amount of nitrogen into all of the gas flows, compared with adding slightly more nitrogen into only the outer coolant gas.

3.3 Conclusions

The effect of adding nitrogen into the various gas flows depends upon the combination of the operating conditions: the amount of nitrogen added, and into which flow, the forward power, and the sampling distance. Effects ranging from signal suppression to enhancement were obtained measuring the same solutions under different conditions. The most beneficial case examined was obtained with the addition of nitrogen into the coolant gas only. To realize much advantage, the nebulizer flow rate must be increased and the sampling distance decreased. The analyte species rhodium, which does not suffer from argon or oxide interferences in the absence of other matrix elements, showed no appreciable difference in its figures of merit. Iron and selenium, species which suffer from argon interference, show a trend of modestly improved figures of merit with addition of nitrogen into the outer flow only at levels greater than about two percent. At levels of nitrogen introduction below about two percent the plasma is less stable. The intensity of background species were most reduced at 1.25 kW and analyte species most enhanced at 1.5 kW. The

opposing effects meant that SBR and SNR at both powers showed a trend toward similar improvement for most of the species monitored. The reasons for improvement of these figures of merit may differ for iron and selenium since for iron the main effect of the addition of nitrogen was reduced enhancement of the background signal relative to signal enhancement while for selenium the main effect was signal enhancement. The improvement in the figures of merit for the species examined was not great, although in conjunction with other techniques it may be sufficient to be of analytical utility.

CHAPTER 4

OPTICAL MEASUREMENTS

4.1 Introduction

Several recent studies have specifically studied the ICP-MS sampling interface zone in order to determine the nature of the species in the region and the causes of the matrix effects described in the introduction. These include a Langmuir probe study of the expansion chamber by Houk *et al.* [46], kinetic energy studies [47, 48, 49], and a study of sampling and ion focussing by Hieftje and Chambers [5, 50, 13, 51, 52]. This is in addition to other general studies of beam formation of a supersonic expansion into an expansion chamber [53, 54, 55, 56, 57].

There have been few reports of attempts to optically view the expansion chamber of an ICP-MS interface. Houk and Lim used a flat sampling plate to sample an ICP into a low pressure chamber, and then viewed the resulting emission within the chamber at right angles to the ICP torch and reported on its capability as an analytical excitation source [58]. Their experimental set-up was similar to that shown in Figure 2.4 (b) and described in the experimental chapter. They observed a very weak argon and water emission spectrum. The most prominent features were the OH bandhead in the ultraviolet (300 to 310 nm), many Ar (I) lines in the far red (beyond 700 nm), and a visible H_α line (656.3 nm)—a line not usually reported in ICP studies. Many of the lines usually seen when viewing the NAZ of an ICP were absent or extremely weak. Specifically, there were few argon lines in the range 330 to 600 nm, the H_β line at 486.1 nm and other lines of the hydrogen Balmer series were weak or absent, and the background continuum radiation was very weak. For the analyte species measured, although all emission was weak, the ion to atom line emission ratios observed were similar to those of the NAZ of an ICP. A plot of ionic emission intensity as a function of nebulizer flow rate had a shape more

typical of ICP-MS than of ICP-OES, that is a sharp intensity maximum rather than a smooth curve. However the optimum nebulizer flow rate was lower than the flow rates usual with ICP-MS.

In other work by Houk *et al.* [46], a similar set-up was used to study some of the fundamental characteristics of the extraction region. A gas kinetic temperature (T_{gas}) of approximately 2200 K was determined for the Mach disc using several measures of temperature: a rotational temperature (T_{rot}) derived from Boltzmann plots using the intensities of the OH bandhead (in the 310 nm region) viewed through the Mach disc as well as the afterglow, Doppler temperatures (T_{Dopp}) from line width measurements from Ca (II), Sr (II), and Na (I) emission. (The sodium intensities were measured using fluorescence.) Measurement of the temperatures within the zone of silence would be expected to yield much lower values. The emission intensity from 1000 ppm Ca was approximately one tenth as intense as that from 20 ppm Ca viewed from the NAZ of an ICP. In another study, Lim *et al.* [59] found the Doppler broadened linewidth from emission observed just in front of a sampling plate to be essentially unchanged from the linewidth of emission observed from the NAZ of the ICP, from which they inferred that the T_{Dopp} is unchanged as gas flows into the sampler.

Lepla *et al.* [60] viewed ICP emission just outside of an ICP-MS interface and obtained mass spectrometric signals simultaneously. The mass spectrum was obtained in the usual way. Emission was observed via a fibre optic cable. A lens was used to image the plasma zone 15 mm beyond the load coil of the ICP and 1 mm in front of the sampling plate of a mass spectrometer onto the fibre optic cable. Using this method, the optical view was similar to that of the conventional NAZ view of an ICP. Effective compromise viewing conditions for both emission and mass spectrometric signals could not be obtained

simultaneously. The dependence upon nebulizer flow rate for each of the signals monitored (atomic and ionic emission, and ionic mass spectrometry) were each typical of ICP-OES and ICP-MS measurements.

4.2 Results

Several approaches to the optical study of the ICP-sampler interface zone were taken in the work described here. The various experimental arrangements are described in the experimental chapter (Chapter 2). The first results discussed are of an end-on view of the ICP-sampler interface region as shown in Figure 2.3, which are then compared with an end-on view of the ICP alone (with no sampling plate and no chamber) as shown in Figure 2.4 (a). For these experiments the optical detector is along the same axis as the plasma. The other results discussed will be those obtained using a set-up similar to that employed by Houk and Lim [58]: *i.e.*, an ICP-sampling plate interface viewed through the extraction chamber at right angles to the plasma, shown in Figure 2.4 (b). In all of the work discussed here, the sampling plate (when present) had an orifice diameter of 0.76 mm and was situated 15 mm from the load coil. The forward power was 1.25 kW, the nebulizer flow rate was 0.6 L/min, and the monochromator slit width was 50 μm unless otherwise specified. The intensity scales on all spectra are as consistent with one another as possible. The wavelengths and excitation energies of the transitions observed are given in Table 4.1.

4.2.1 End-on view of the ICP-sampler interface

Figures 4.1 and 4.2 show background spectra emitted by water and argon in an argon plasma in the ultra-violet to visible range from 275 to 660 nm viewed end-on through the sampling plate and chamber. Some of the more prominent lines are labelled. The net intensities of the Ar (I) lines relative to one another are similar to those given in a reference work by Fassel *et al.* [61] for the

Table 4.1 Species, wavelengths, and upper energy levels of the spectral line transitions monitored by ICP-OES

Species	Wavelength (nm)	Excitation energy (eV)
Mg I	285.213	4.346
Mg II	279.553	4.434
	280.270	4.434
Pb I	261.418	5.71
	266.318	5.97
	280.199	5.74
	283.306	5.7
	287.332	5.63
	363.958	4.38
	368.348	4.34
	373.995	5.97
	405.783	4.38
Sr I	460.733	2.69
Sr II	407.771	3.04
	421.552	2.94
Ca I	422.673	2.93
Ca II	393.367	3.15
	396.847	3.12

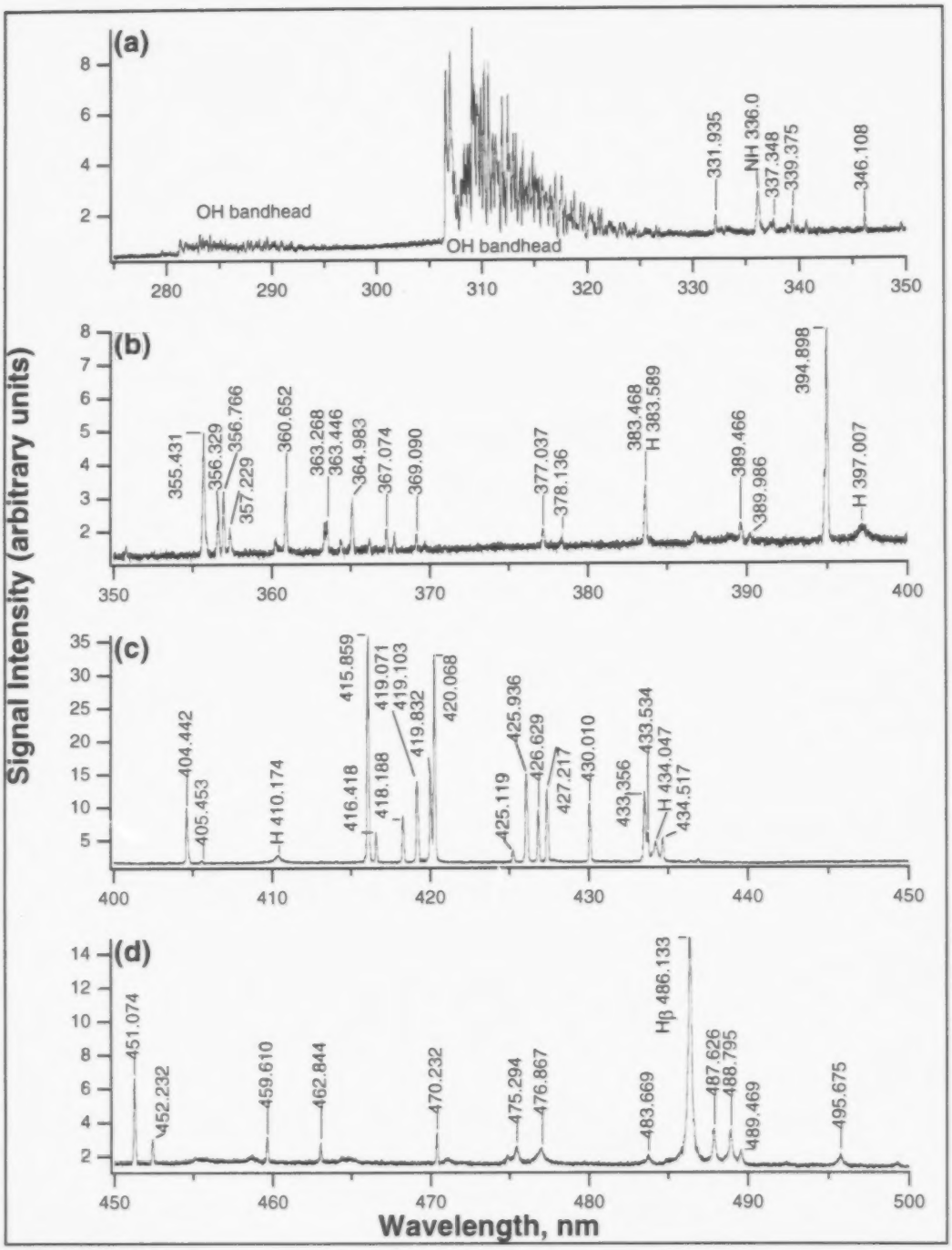

Figure 4.1
Optical emission spectrum of 100% argon and water, end-on plasma with chamber. 1.25 kW, 15 mm sampling distance, 50 μm monochromator entrance slit.

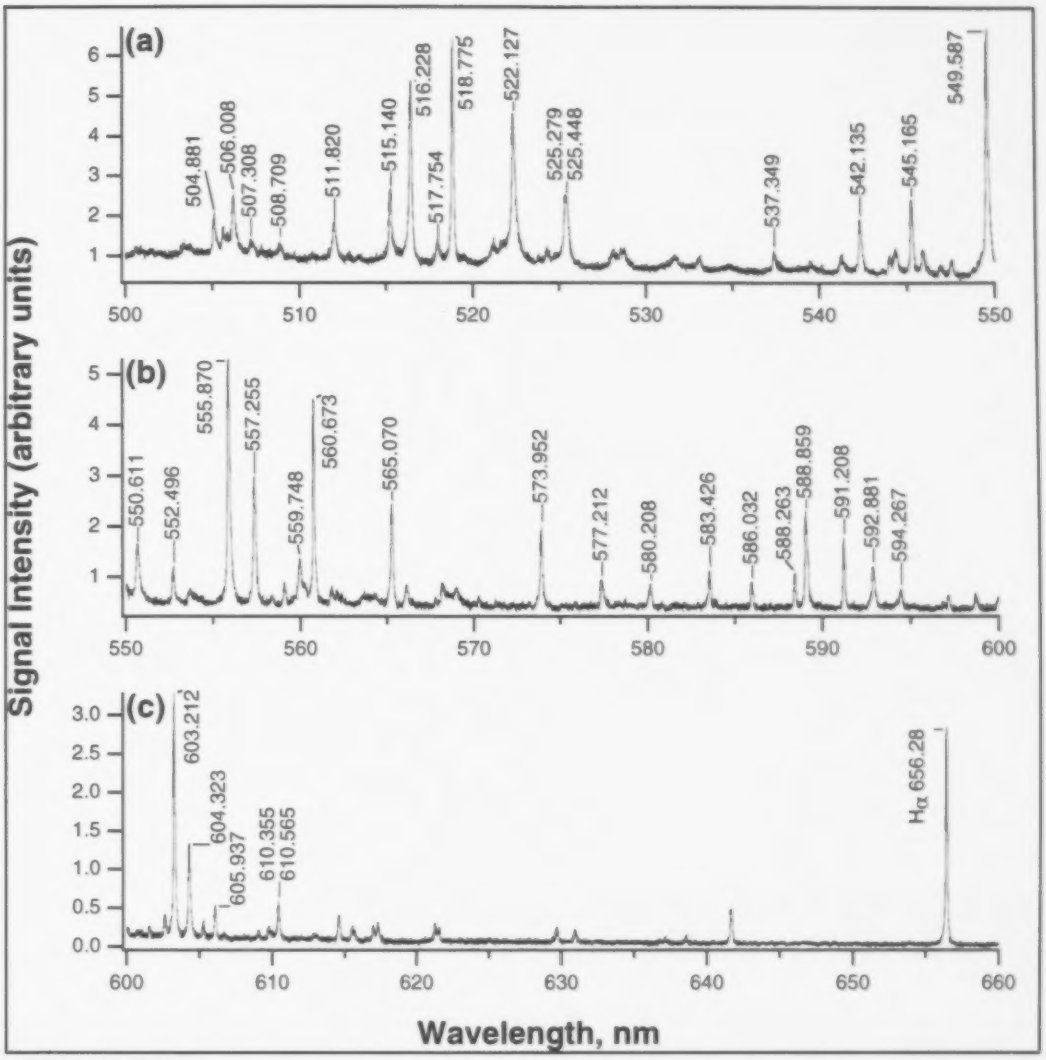

Figure 4.2
Optical emission spectrum of 100% argon and water, end-on plasma with chamber. 1.25 kW, 15 mm sampling distance, 50 μm monochromator entrance slit.

NAZ of a conventionally viewed ICP. Compared with their results, the background continuum is elevated over the entire spectral range, the ratios of net argon signal to background level are in general reduced, the OH bandhead near 310 nm is enhanced, the argon lines in the red appear enhanced, and the H_α line at 656.28 nm is prominent.

Nitrogen was added to the outer argon coolant gas and varied from 1% to 15% of the total mixed coolant gas flow. The total flow rate, power, sampling distance, and nebulizer flow rate were kept constant. Using high resolution Fourier Transform spectroscopy, Montaser *et al.* [62] have measured line widths and Doppler temperatures (T_{gas}) of similar mixed argon and nitrogen plasmas. They found the greatest Doppler temperature to be 7800 K for a mixed argon/nitrogen ICP with 11% nitrogen in the coolant flow. This is about 1000 K hotter than for a pure argon plasma and 2200 K hotter than for a pure nitrogen plasma. Similarly, they found a maximum T_{exc} with the addition of 11% nitrogen to the coolant gas and a decrease in T_{exc} as nitrogen was increased [63].

Figures 4.3 and 4.4 show sample spectra as three percent nitrogen was mixed into the coolant gas. No filter was used to block second order spectral features, hence the OH bandhead in the second order is apparent near 620 nm. An atomic argon spectrum is superimposed upon molecular bandheads of various nitrogen species when nitrogen is present. Molecular (0,0) peaks are visible at 336 nm for the NH bandhead and for the first negative system of N_2^+ at 391.4 nm, as well as the (0,0) and (0,1) peaks of the second positive neutral N_2 system at 337 and 358 nm. The intensity of NH at 336 nm quickly increases as a low level of nitrogen is introduced and then plateaus as nitrogen continues to increase. After the introduction of sufficient nitrogen, the formation of NH is limited by the amount of hydrogen present from water nebulized into the plasma. In contrast, the net intensity of the (0,0) N_2^+ peak at

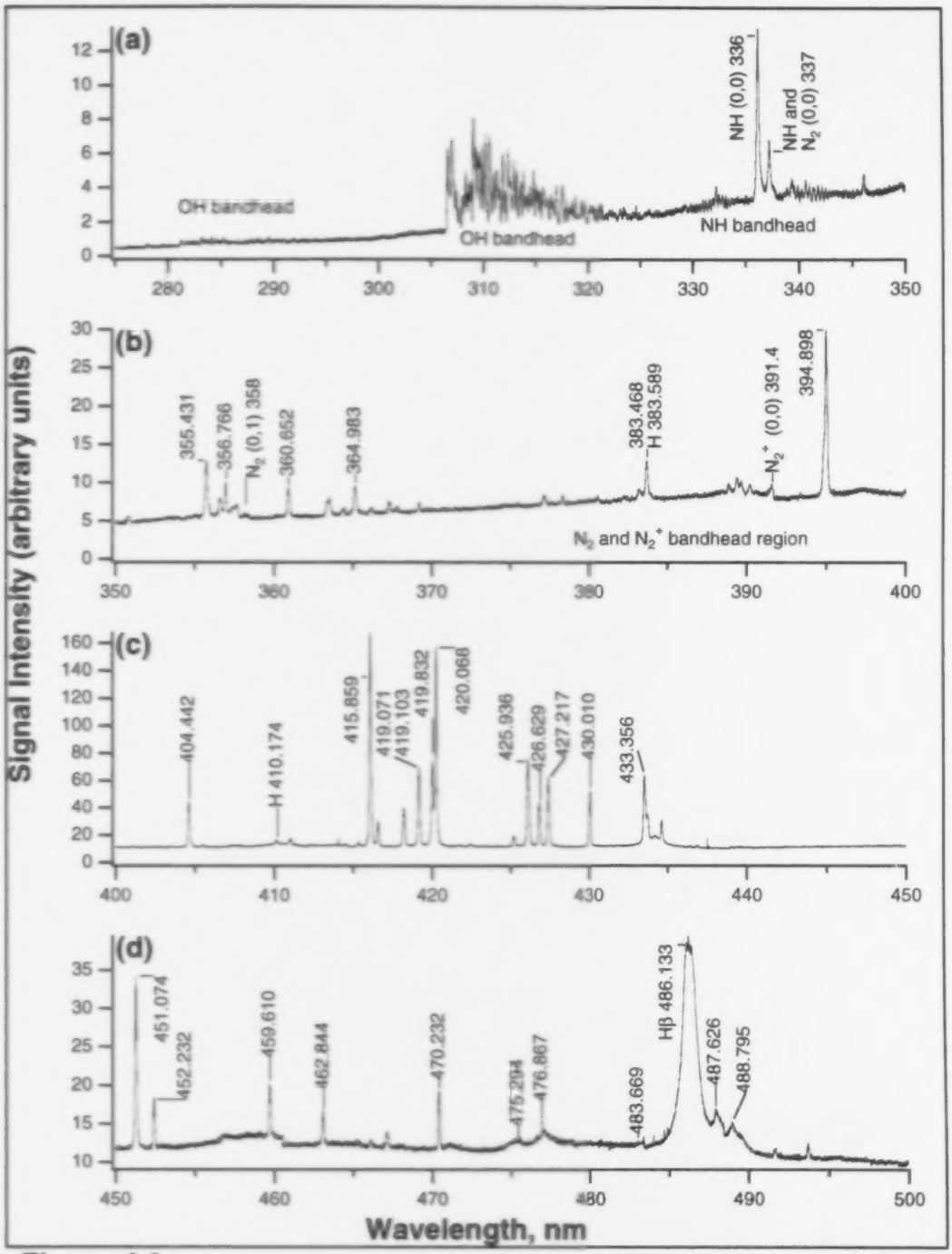

Figure 4.3
Optical emission spectrum of water in 3% nitrogen and argon in the coolant, end-on plasma with chamber. 1.25 kW, 15 mm sampling distance, 50 μm monochromator entrance slit.

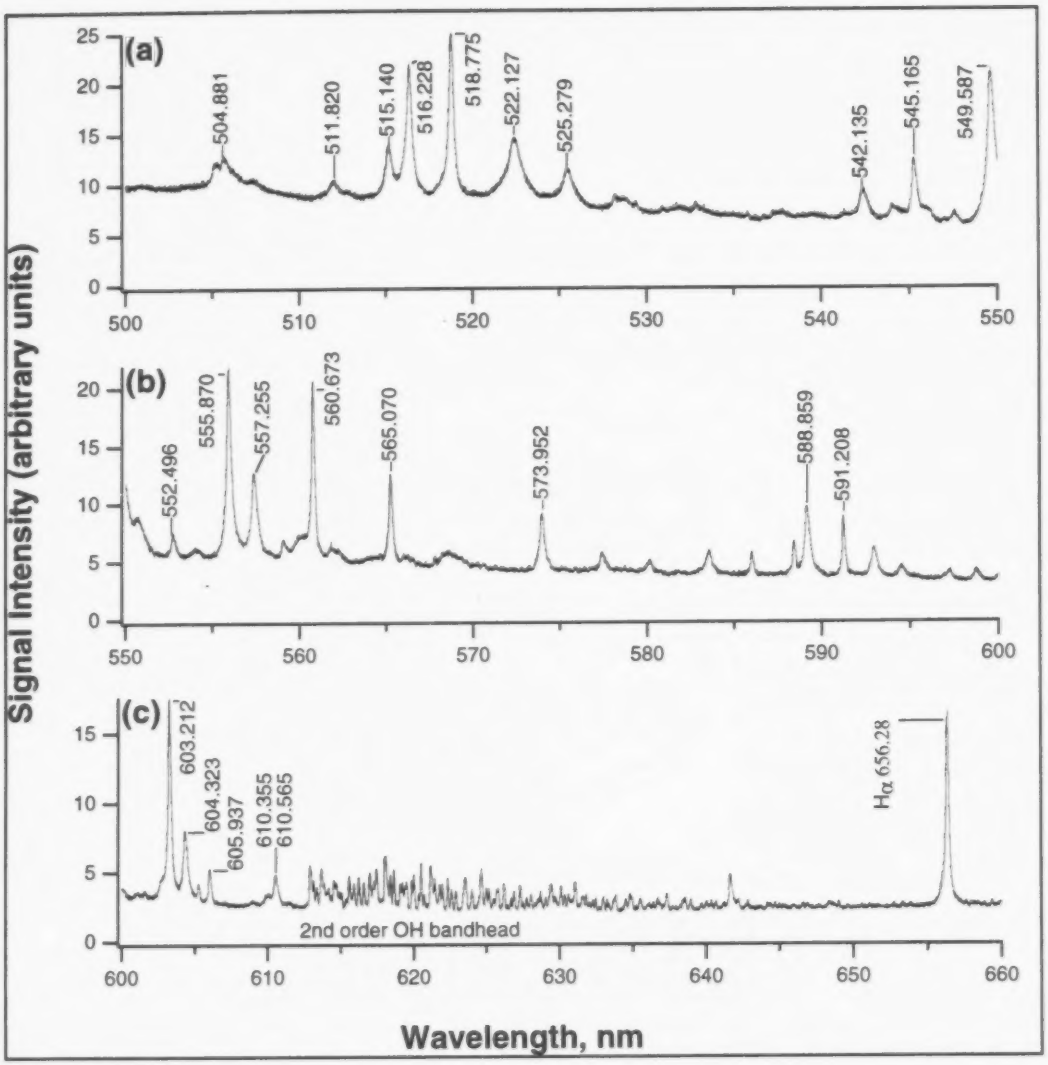

Figure 4.4
Optical emission spectrum of water in 3% nitrogen and argon in the coolant, end-on plasma with chamber. 1.25 kW, 15 mm sampling distance, 50 μm monochromator entrance slit.

391.4 nm continues to increase as nitrogen increases. When nitrogen is added the background continuum level is elevated over the entire spectral range observed, relative to that of the pure argon plasma. This enhancement is consistent with the visible bright orange glow in the chamber as the nitrogen level increases beyond ten percent and may possibly indicate the presence of a nitrogen afterglow.

The net intensity of Ar (I) at 415.8 nm, the most intense argon line in an argon ICP, quadruples with nitrogen addition. Many other atomic argon lines are similarly enhanced. In Figure 4.4, especially, it can be seen that some of the broadest argon lines are broadened still more in nitrogen and some features are lost to the baseline with this broadening. The H_α and H_β lines are very much broadened in a nitrogen containing plasma from Stark broadening [64] due to the greater excitation of the plasma, indicating a higher temperature and electron density. (As the nitrogen level increases, care must be taken to prevent the quartz torch from melting in the plasma, due to the increased energy of a nitrogen plasma.) Increased argon emission is consistent with a more energetic environment provided by nitrogen in the plasma, and an observed decrease of net argon intensity as nitrogen is increased beyond ten percent is consistent with observations by Montaser *et al.* [62]. Two of the hydrogen lines (H_α and H_β) show a moderate intensity increase with the addition of nitrogen and level off with continued addition of nitrogen. This is also consistent with a model of increased excitation, but a limited supply of hydrogen.

Figure 4.5 shows the net signal intensity as a function of the nebulizer flow rate while nebulizing 100 ppm magnesium solution into the plasma, and adding nitrogen into the coolant. A single magnesium atomic line at 285 and two ionic lines at 279 and 280 nm were monitored. The intensities have been background subtracted; the noise of the nearby background level is about 0.1%

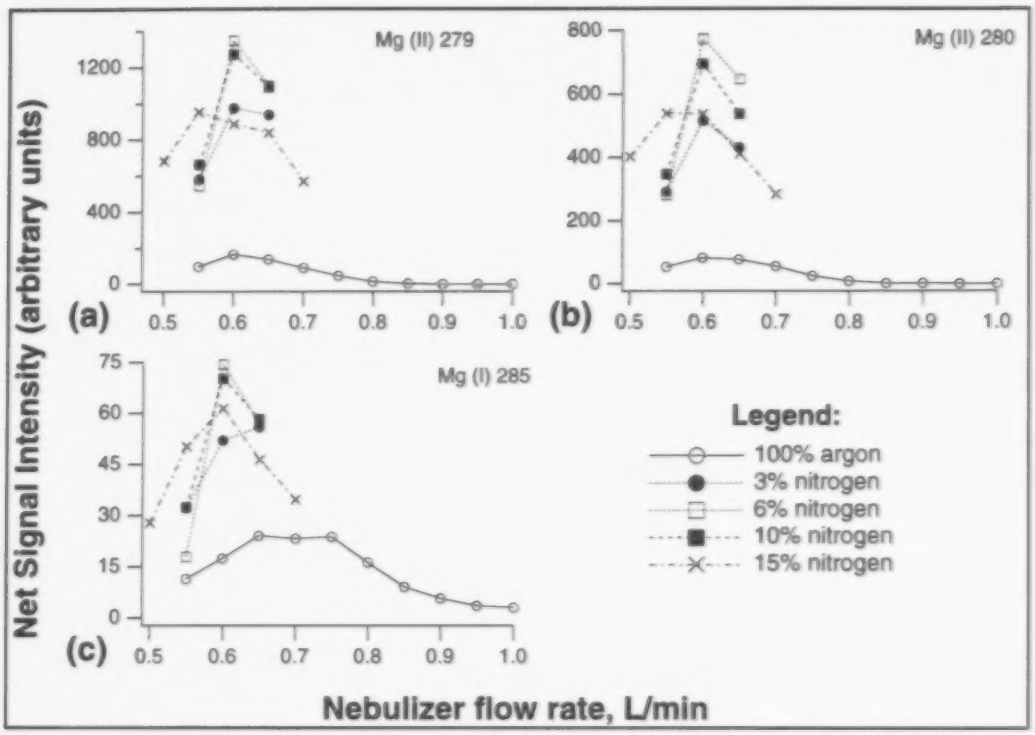

Figure 4.5
Effect upon the net spectral line intensity for 100 ppm Mg in water at (a) 279.6, (b) 280.3, and (c) 285.2 nm as nebulizer flow varied and as the fraction of nitrogen in the coolant increased from 100% argon, to 3% N_2 , 6% N_2, 10% N_2, and 15% N_2, as shown. 1.25 kW, 15 mm sampling distance, 50 μm monochromator entrance slit.

of the signal and is too small to be observable on the scale of the plot and is therefore omitted. The shape of all of these intensity versus nebulizer flow rate plots is more like the steep "mountains" seen in ICP-MS than the smoother, less steep plots generally seen in ICP-OES. The signal drops off sharply from the maximum for both ionic lines and is flatter for the atomic line which peaks at a slightly higher flow rate, corresponding to its lower position in the "initial radiation zone" of the plasma below the NAZ, where ions are typically located. These flow rates are lower than the typical optimal flow rates seen in ICP-MS and are similar to the typical rate seen in ICP-OES.

The maximum ionic signal responses occur near a nebulizer flow rate of 0.6 L/min in the argon and mixed gas plasmas observed. This contrasts with studies by Montaser [65, 66] and Choot and Horlick [67] of mixed nitrogen-argon ICP-OES viewed conventionally, which found the optimum observation height for maximum peak emission to be generally closer to the load coil as the fraction of nitrogen increased. As nitrogen is added to the coolant gas the plasma volume retracts, so that the NAZ is pushed down closer to the load coil than in an argon plasma. If the observation height is fixed, as for this work, it was expected that it would be necessary to push this zone forward and into the observation region by increasing the nebulizer flow rate. However Figure 4.5 shows that at the nitrogen levels added and viewed end-on through the sampling interface, it was not necessary to increase the nebulizer flow rate as nitrogen was added.

Figure 4.6 shows the signal change as nitrogen is added to the coolant gas at the optimal nebulizer flow rate. Scans from 279 to 286 nm for 100 ppm magnesium are shown in Figure 4.6 (a). To make it possible to see the changes to both atomic and ionic signals on the same scale, the signal intensity for each line was background subtracted and normalized to the intensity for that

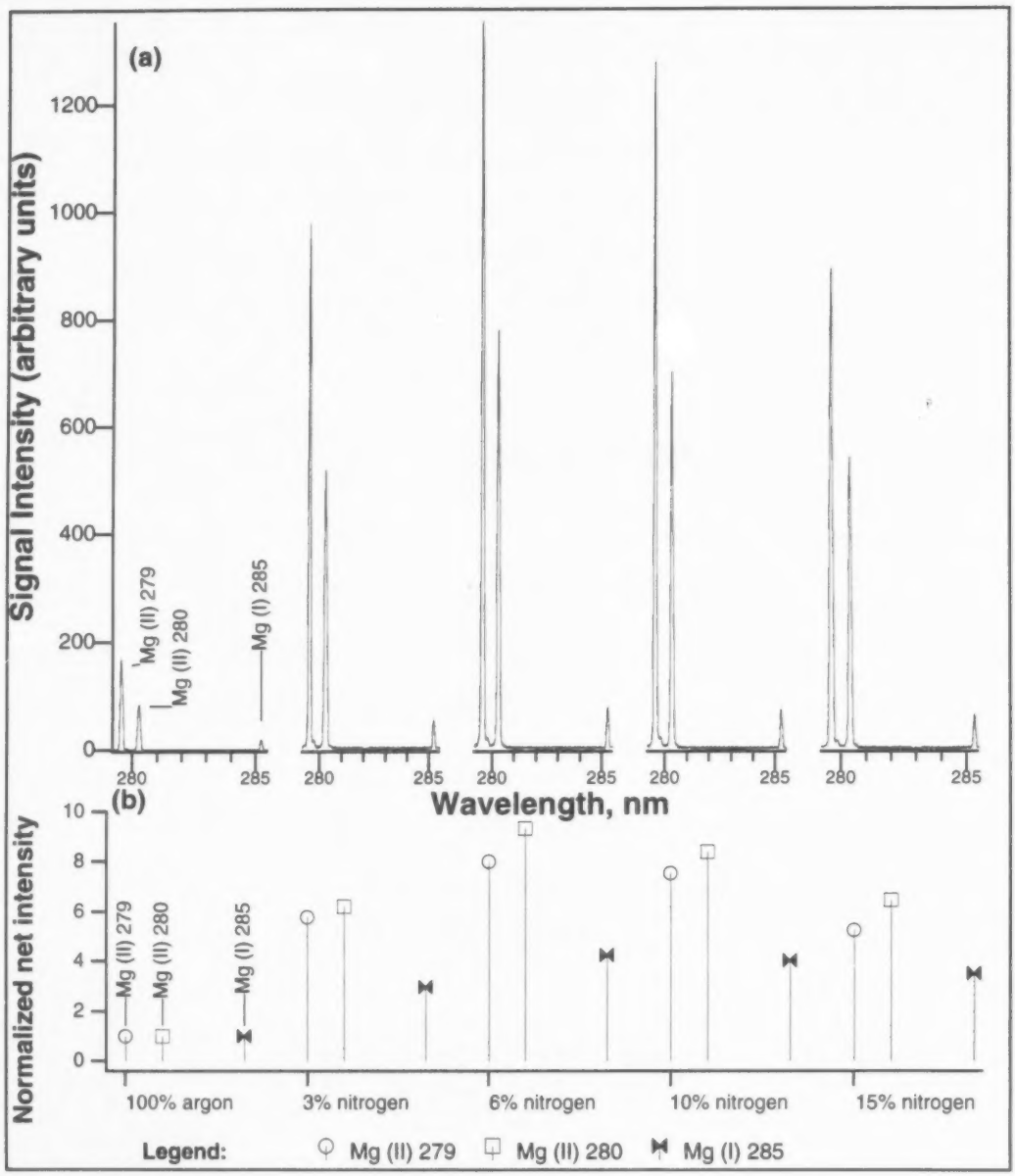

Figure 4.6
(a) Optical emission spectra from 279 to 286 nm for 100 ppm magnesium in 100% argon and with 3%, 6%, 10%, 15% nitrogen added into the coolant. (b) Net analyte signal normalized to the signal at that wavelength, as shown, in 100% argon.

1.25 kW, 15 mm sampling distance, 50 µm monochromator entrance slit. Nebulizer flow rate 0.6 L/min for all spectra. Mg (II) signals at 279.6 nm and 280.3 nm. Mg (I) signal at 285.2 nm.

line in argon and are shown in Figure 4.6 (b). It can be seen that relative to argon, both atomic and ionic emission signals increase with all levels of nitrogen added. The maximum signal enhancement was obtained with six percent nitrogen in the coolant gas. The ionic lines increase most dramatically, by almost an order of magnitude. The magnesium atomic line is approximately quadrupled, similar to the enhancement shown for the argon atomic line at 415.8 nm.

When viewed conventionally, enhanced analyte emission of a mixed nitrogen-argon plasma is generally observed only when the operating or viewing conditions are also altered, by increasing the nebulizer flow rate or shifting to a lower viewing position. For example, Choot and Horlick [67] plotted spatial profiles for various analytes in mixed gas plasmas. These plots show an increase in Mg (II) emission intensity at 279.6 nm with the addition of ten percent nitrogen to the coolant, viewed 10 to 12 mm above the load coil (ALC), whereas in pure argon, the maximum signal is viewed higher at 15 to 18 mm ALC for the same nebulizer flow and power. If the magnesium signal in ten percent nitrogen is viewed 15 to 18 mm ALC, any signal enhancement is indistinguishable from noise. Their work also showed that in ten percent nitrogen the Mg (I) emission intensity at 285.2 nm is less enhanced than the Mg (II) signal. The maximum atomic signal in nitrogen is viewed at 10 mm ALC but in argon at 15 mm ALC. If the atomic signal in ten percent nitrogen is viewed at 15 mm, the signal appears depressed relative to that in argon. It is not known if the enhancement observed in my work while operating and viewing conditions are unchanged is due to the end-on viewing of the plasma or to the sampling process, or to both.

Figure 4.7 (a) shows net normalized atomic signal intensities for 100 ppm lead as nitrogen is added at 261 nm, 280 nm, 283 nm, 364 nm, 368 nm, and

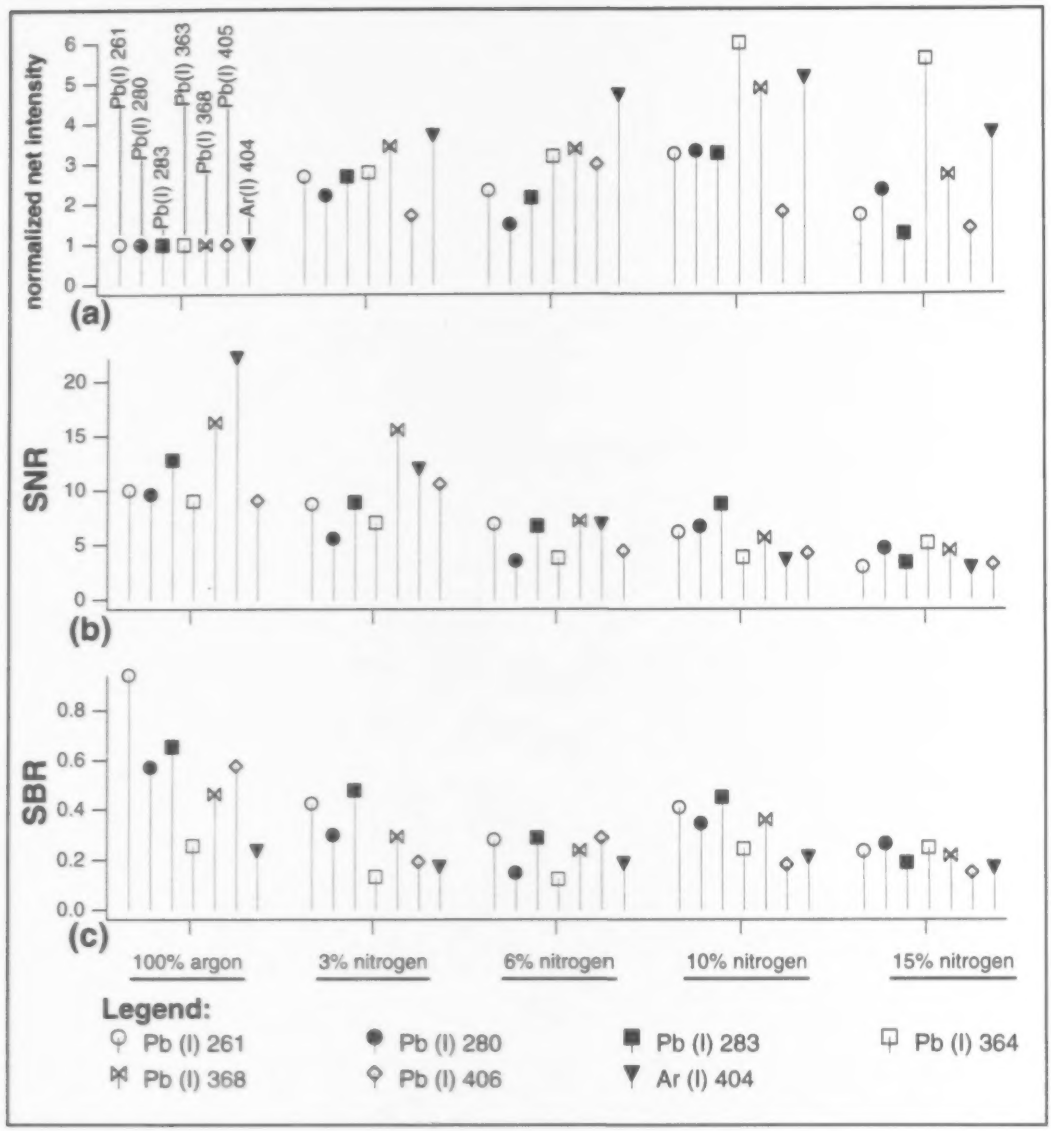

Figure 4.7
Effect upon optical emission signal intensity for 100 ppm lead at various wavelengths as shown as nitrogen increased in the coolant. Nebulizer flow rate 0.6 L/min, 15 mm sampling distance, 1.25 kW power, 50 μm monochromator entrance slit.From left to right, each set of bars represents: Pb(I) 261, Pb(I) 280, Pb(I) 283, Pb(I) 364, Pb(I) 368, Pb(I) 406, Ar(I) 404. (Argon included for comparison.)

(a) Net signal intensity normalized to line intensity in 100% argon,
(b) The ratio of analyte signal to background noise (SNR), and
(c) the ratio of analyte signal to background signal (SBR).

406 nm. The intensity of Ar (I) at 404.4 nm is added for comparison. This figure shows a similar pattern for all lead atomic lines monitored. These signal enhancements are less dramatic than those seen for magnesium: at most, the signal increased sixfold in ten percent nitrogen, similar to atomic magnesium at 285 nm. When fifteen percent nitrogen is added to the coolant gas, any gain in intensity is severely diminished for most of the lead lines observed, and signal intensity at 406 and 283 nm is actually no higher than that observed in an argon plasma. Figure 4.7 (b) and (c) also show ratios of net signal to background noise (SNR) and net signal to background signal (SBR). These plots clearly show that any gain in signal intensity is wholly lost to increases in background intensity and noise level.

Figure 4.8 shows the spectral regions monitored for 100 ppm lead as nitrogen was added to the plasma and demonstrates how atomic lead represents a somewhat unfavourable case for signal enhancement of an analyte in nitrogen. These are all atomic lines, which are in general less enhanced than ionic lines, and most are located in OH and nitrogen bandhead wavelength regions which increase in intensity as nitrogen is added. As nitrogen is added to the plasma, the background continuum emission increases, the molecular bandhead intensity increases to form a more structured noisier background, and both background and analyte signals thus become noisier. These effects cause increasing difficulty in the separation of analyte signal from background noise levels. Most of the atomic argon and analyte signals are enhanced, but unlike the case for the magnesium ions, these atomic lines are buried by the increasing bandhead background and associated noise as the nitrogen level is increased. The bandhead in the regions shown in Figure 4.8 (a) and (b) is due both to OH and NO; that in (c) and (d) is due to N_2 and N_2^+. Each pair of comparable scans in the figure are

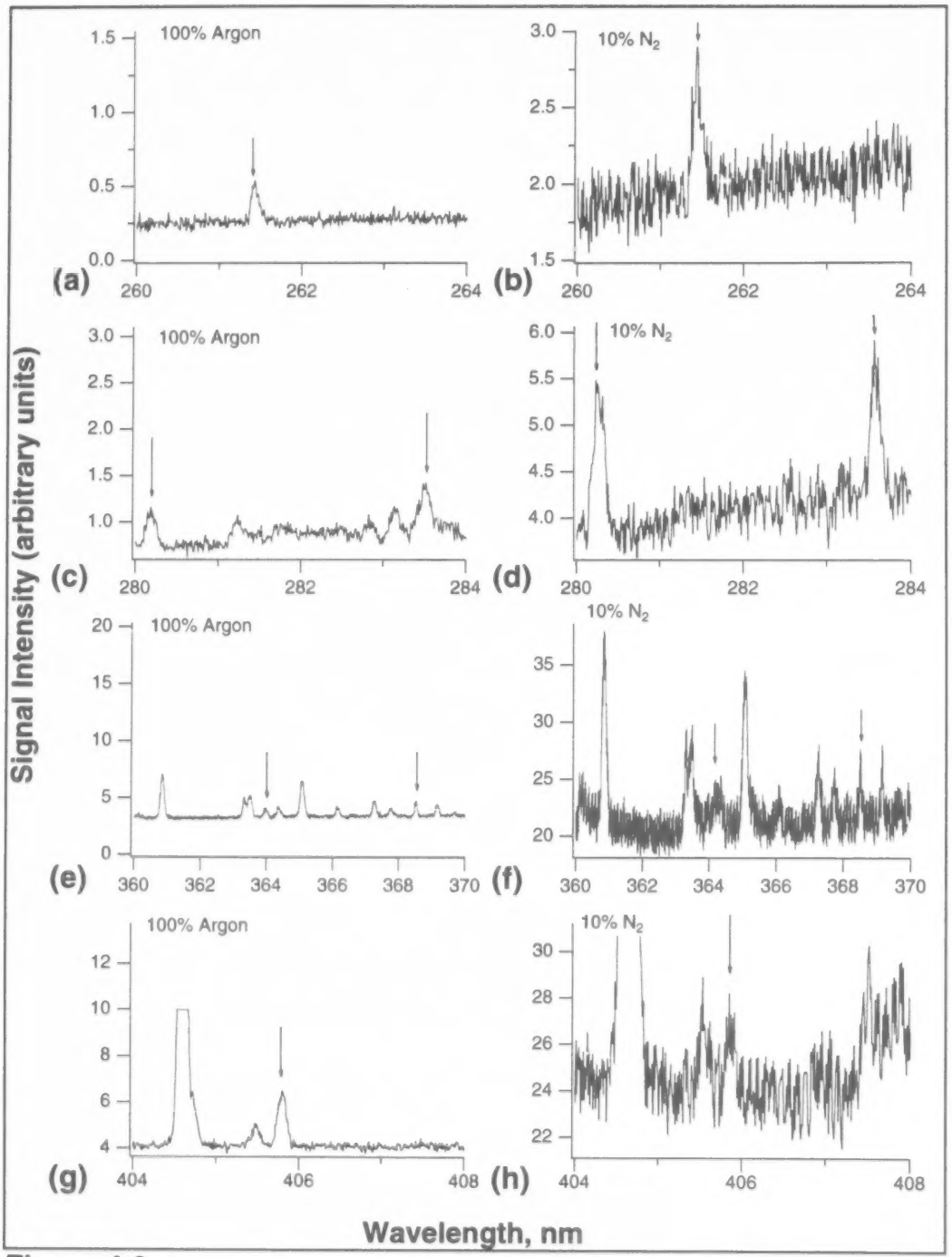

Figure 4.8
Scans comparing the optical emission signals for 100 ppm lead in 100% argon with signals as 10% nitrogen is added into the coolant for wave-length regions as shown. Arrows indicate Pb (I) signals.Nebulizer flow rate 0.6 L/min for all spectra.1.25 kW, 15 mm sampling distance, 50 µm monochromator entrance slit.

set to the same scale in order to compare them more readily despite the offset by the increased continuum of the baselines. The exact level of the continuum was very variable and sensitive to variations in any operating parameters. An increased continuum level means that net signal to background ratios deteriorate for lead as nitrogen is added, as shown in Figure 4.7 (b) and (c). The increased background structure and noise levels cause detection limits to deteriorate. In fact using this system and adding nitrogen, 100 ppm lead is near the detection limit for some of these lines.

4.2.2 End-on view of the ICP

The sampling plate and chamber were next removed from the experimental set-up, as shown in Figure 2.6 (a). Several reports have been made of studies of the ICP viewed axially in this manner and compared with the usual side-on optical view of the NAZ. Lichte and Koityohann [68] in qualitative terms in 1979, reported increased signal intensity and reduced background intensity and noise, with decreased dynamic range and more interferences. Demers [69] reported in 1979 that although analyte signal increased by five to fifteen-fold, background signal intensity also increased by three to ten-fold for aqueous samples, and background noise levels doubled, with dynamic range similar to that seen in normal optical NAZ viewing. This led to a general improvement in detection limits for many analyte species. Faires reported [70, 71] extensive end-on results using a Fourier transform spectrometer detection system. In her work, she found increased sensitivity for analytes along with unchanged background noise levels, for an improvement in sensitivity and detection limits by as much as eight times for many elements. Self-absorption was increased for low energy atomic species, hence the dynamic range was also decreased for these. Faires also reported that there was little difference in

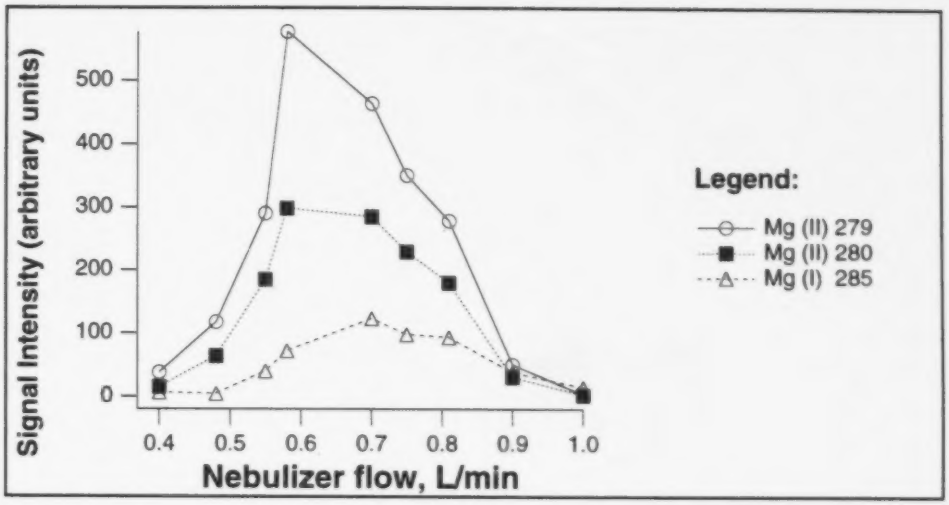

Figure 4.9
Dependence of the net spectral line emission intensity at 279.6, 280.3, & 285.2 nm for 100 ppm Mg in water upon nebulizer flow for 100% argon plasma, viewed end-on without sampling plate or expansion chamber.
1.25 kW, 50 μm monochromator entrance slit.

the relative optimum observation height for atoms and ions of the species she investigated.

In this work, the end-on view is compared not with a side-on view of the NAZ, but with the (previously discussed) end-on view through a sampling plate and expansion chamber. Figure 4.9 shows the net signal intensity for 100 ppm Mg as a function of the nebulizer flow rate in an argon plasma. Two ionic and one atomic magnesium lines were monitored. Measured noise levels of the nearby background are limited by the bit resolution of the amplifier (about 0.02%) and are not distinguishable on the scale of the plot, and hence are not shown. There is a steep signal drop when the nebulizer flow is altered from the optimum flow; the optimum flow for ions is about 0.6 L/min; the optimum flow rate for atomic species is shifted to slightly higher values, similar to that seen in Figure 4.5 with sampler and chamber present. The net signal intensity is several times greater than with plate and chamber present.

Background argon and water spectra viewed end-on without sampler and chamber are not shown here since from 275 to 660 nm the general features are the same as those shown in Figures 4.1 and 4.2. The main differences are that the background continuum was elevated over the entire spectral range monitored, with a concomitant increase in background peak to peak noise levels, the OH bandhead at 310 nm is reduced to about half its intensity, and there is somewhat more NH bandhead activity near 336 nm which may be due to the air cut-off stream, and the argon intensity is enhanced over the entire spectrum. The net intensities of the argon signals relative to one another are similar to those shown previously in Figures 4.1 and 4.2, and are also similar to those shown by Fassel *et al.* [61].

In Figure 4.10 spectra of various wavelength ranges monitored as 1000 ppm lead was nebulized into the plasma are compared with and without the

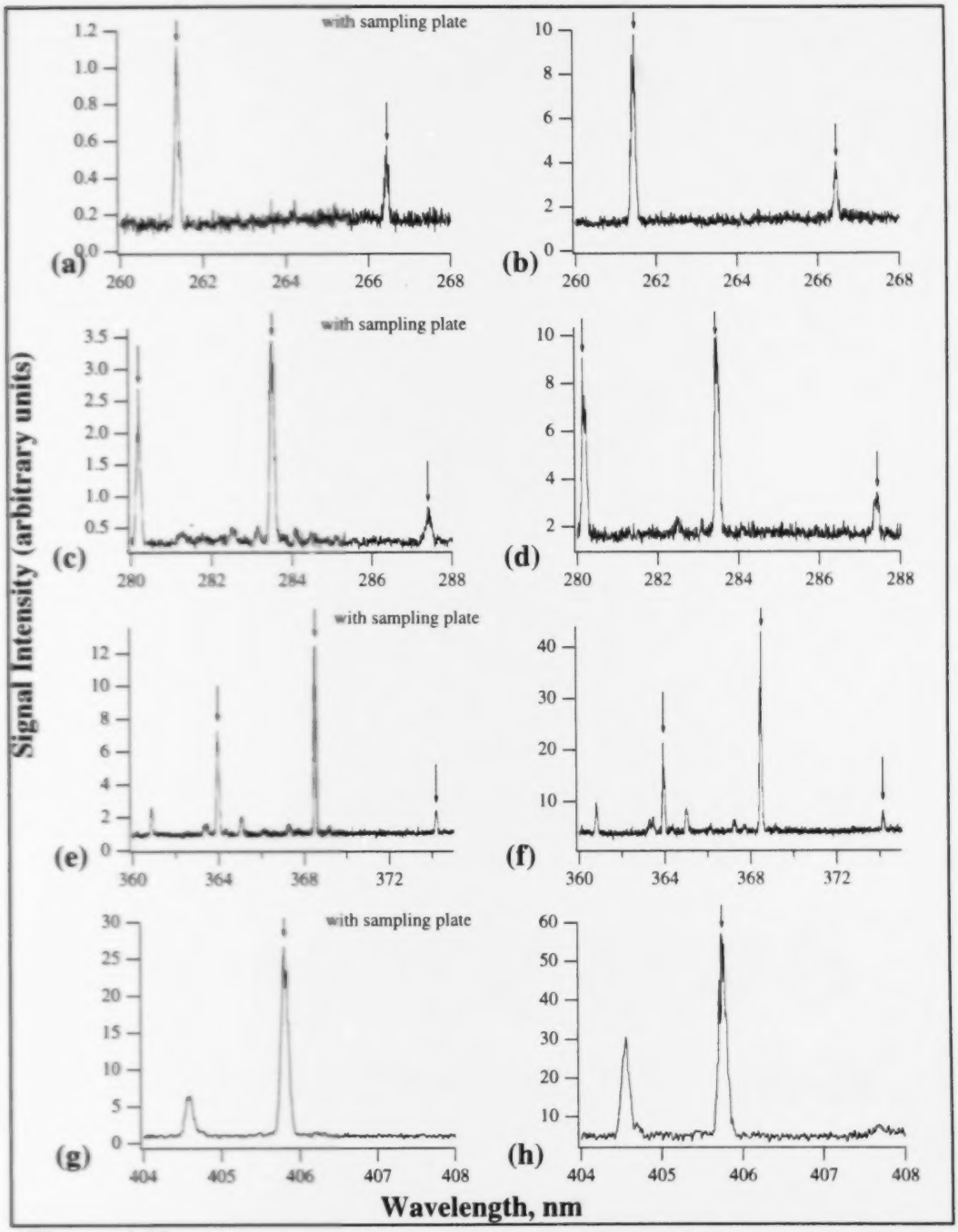

Figure 4.10
Scans comparing the optical emission signal intensities for 1000 ppm lead in argon, viewed "end-on" with sampler & expansion chamber (left) and the "end-on" view without sampler (right). Arrows indicate Pb (I) signals.

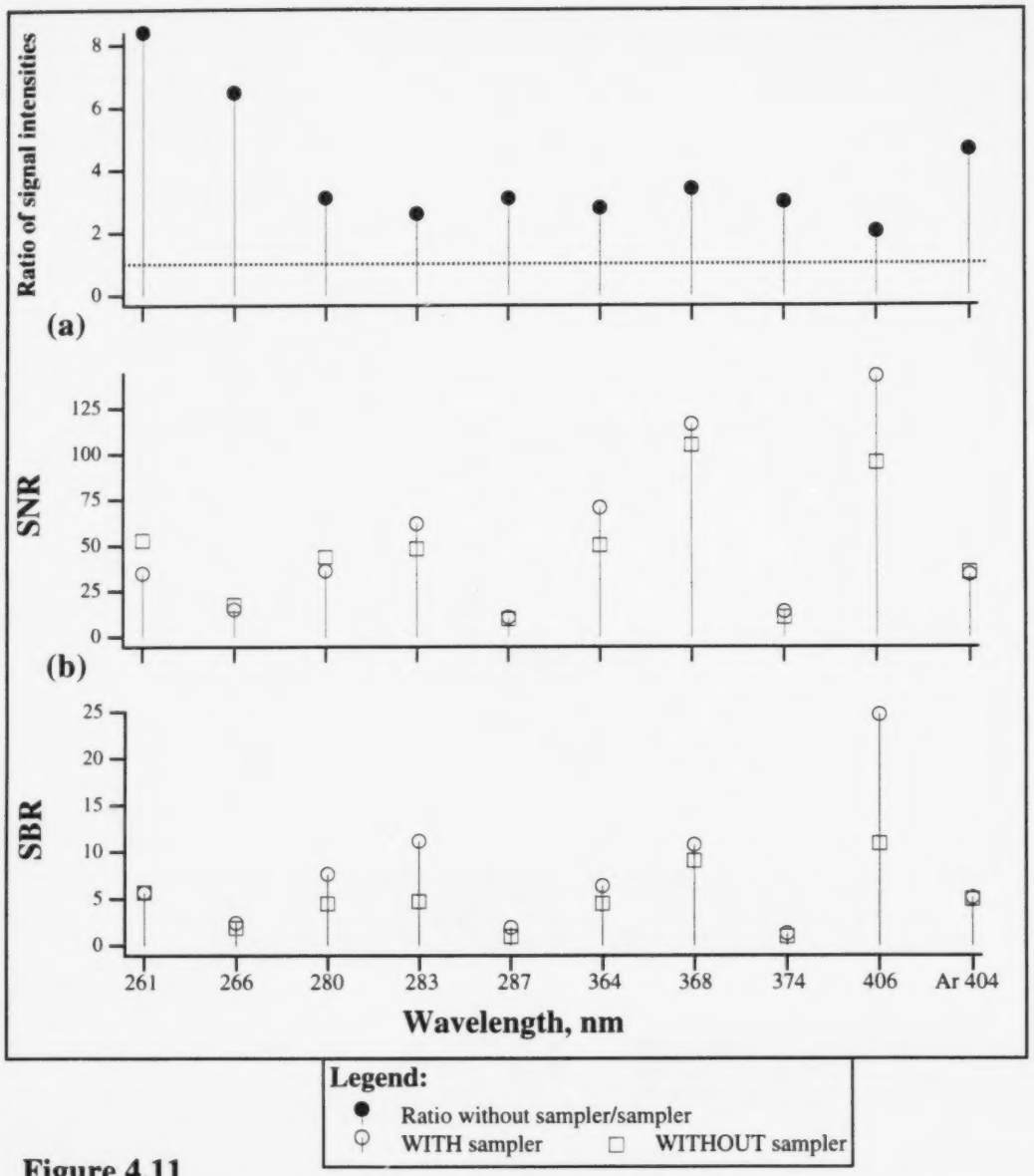

Figure 4.11
Comparison of emission signals for 1000 ppm lead at nominal wavelengths as shown, viewed "end-on" with and without sampler and chamber. Ar (I) 404 nm included for comparison.

(a) Ratio of net signal intensities for Pb(I) and and Ar (I)
(Net signal without plate & chamber / net signal with plate & chamber);
(b) SNR of Pb(I) and Ar (I); (c) SBR of Pb (I) and Ar (I).

sampling orifice and expansion chamber in place. Comparing the two sets of spectra, it is clear that without the sampler and chamber present, the signals, the background continuum, and noise level, are all higher. There are no new features visible. The ratio of background subtracted net intensities (the net signal "without plate and chamber" divided by net signal "with plate and chamber") were calculated and are shown in Figure 4.11 (a). This ratio ranges from two to approximately eight, in favour of the set-up "without plate and chamber." Figure 4.11 (b) and (c) show that despite this increased analyte and argon intensity, neither SBR nor SNR show substantive change. For two of the lines shown here (Pb (I) at 283 and 406 nm) the SBR is somewhat improved "with plate and chamber," due to the enhanced level of the background continuum without the sampler present. This similarity suggests that when viewing the plasma with sampler interface and expansion chamber in place, the region actually observed is the plasma near to and outside the sampler, not the plasma which has been extracted into the sampling chamber. The signal enhancement may be due to incomplete masking of the plasma surrounding the nebulization channel. I wished to also examine any matrix effects when viewing the plasma end-on in this way but further study using this set-up required extensive shielding from the radio frequency interference from the plasma and its power supply and was not done.

4.2.3 Side-on view of the ICP

The plasma, sampling plate, and expansion chamber were arranged as shown in Figure 2.4 (b) for the side-on observation of emission within the expansion zone of the chamber. The monochromator entrance slit width was increased to 100 μm since the emission was weak. Emission observed included any originating from the zone of silence and also from the surrounding barrel shock within the viewing area. The background argon and water spectrum from

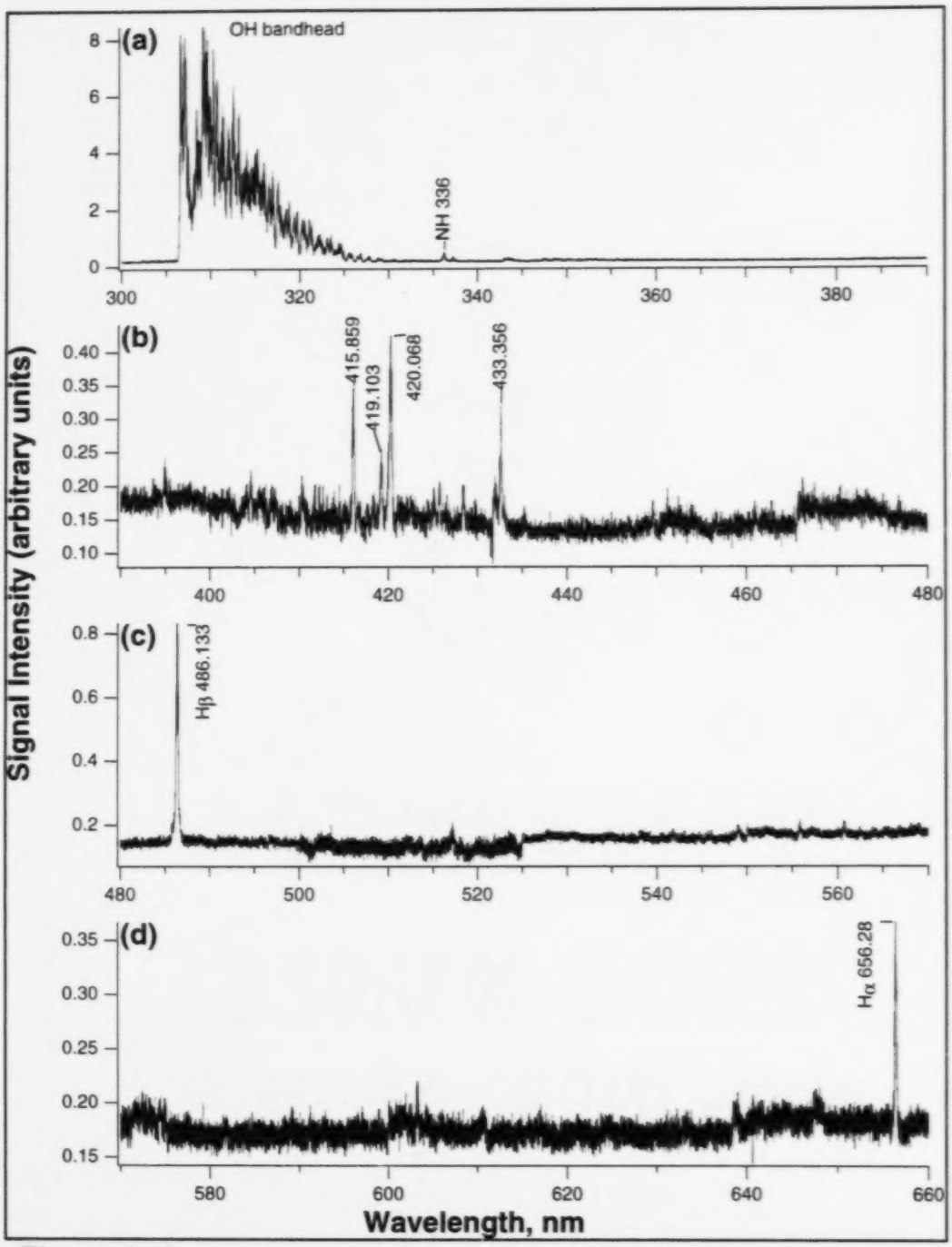

Figure 4.12
Optical emission spectrum of argon & water, viewed "side-on" through expansion chamber.1.25 kW, 15 mm sampling distance, 100 μm monochromator entrance slit.

300 to 660 nm is shown in Figure 4.12. Most notable is the severely reduced background intensity level and the absence of almost all emission, except for the most intense Ar (I) lines near 420 nm and the H_α and H_β lines at 486 and 656 nm, all severely attenuated. Only the OH bandhead near 310 nm is of comparable intensity to the OH bandheads of spectra already seen in this chapter. This spectrum is similar to that seen by Houk *et al.* [58] in the absence of strong argon emission in the visible spectral region and the presence of the H_α line at 656 nm. In their work, however, the H_β line at 486 nm was also absent and they were able to monitor the spectrum from 700 to 850 nm and observe extremely strong Ar (I) emission in this region, which was not measured in this work.

Figure 4.13 shows the effect upon the spectral line intensity for 1000 ppm magnesium at 279 nm as the nebulizer flow rate was varied. Only the strongest ionic signal was monitored because the intensity of the atomic line at 285 nm was too weak to observe any signal at the analyte concentration used, and the ionic signal at 280 nm was too weak to observe at any but the optimal nebulizer flow rate. Note that the concentration is ten times higher than that used for previous similar measurements and that the analyte signal is of the same order of magnitude as the water background. Error bars show one standard deviation. The optimum analyte signal intensity is obtained at a nebulizer flow rate of 0.5 L/min.

Figure 4.14 shows the spectra over various wavelength ranges monitored as 1000 ppm of strontium, calcium, and magnesium were separately nebulized into the plasma at 0.5 L/min. It can be seen that although the background was quiet and stable, the sensitivity is extremely low. Observing the signal from 1000 ppm magnesium at its most intense ionic line at 279 nm, we are approaching the detection limit; 100 ppm strontium is the approximate

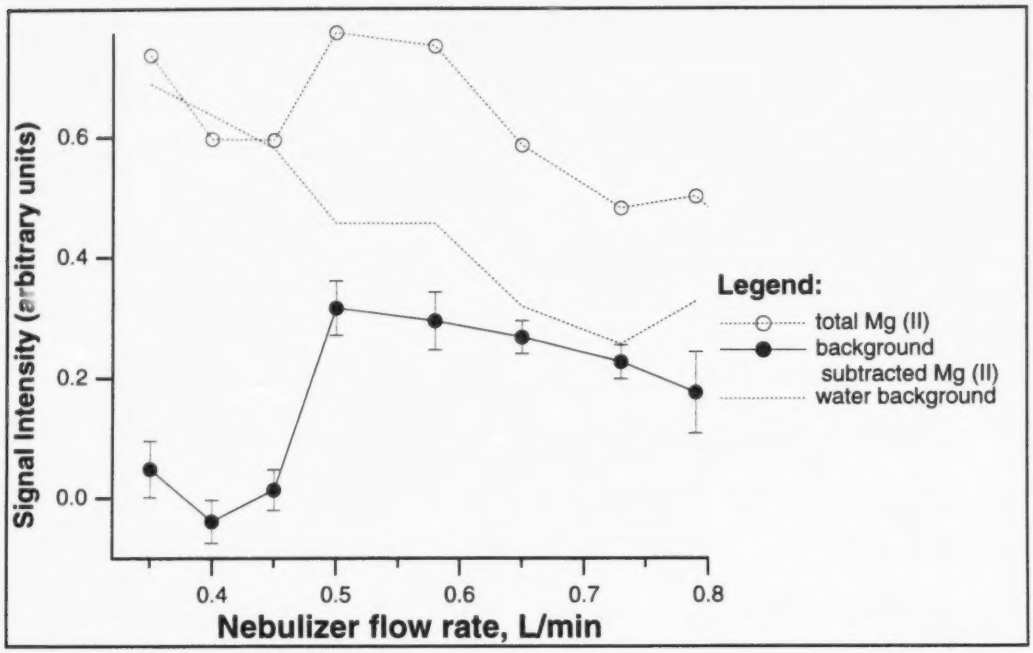

Figure 4.13
Dependence of the spectral line emission intensity at 279 nm for 1000 ppm Mg and water blank upon nebulizer flow for 100% argon plasma viewed "side-on" through expansion chamber.

1.25 kW, 15 mm sampling distance, 100 μm monochromator entrance slit.

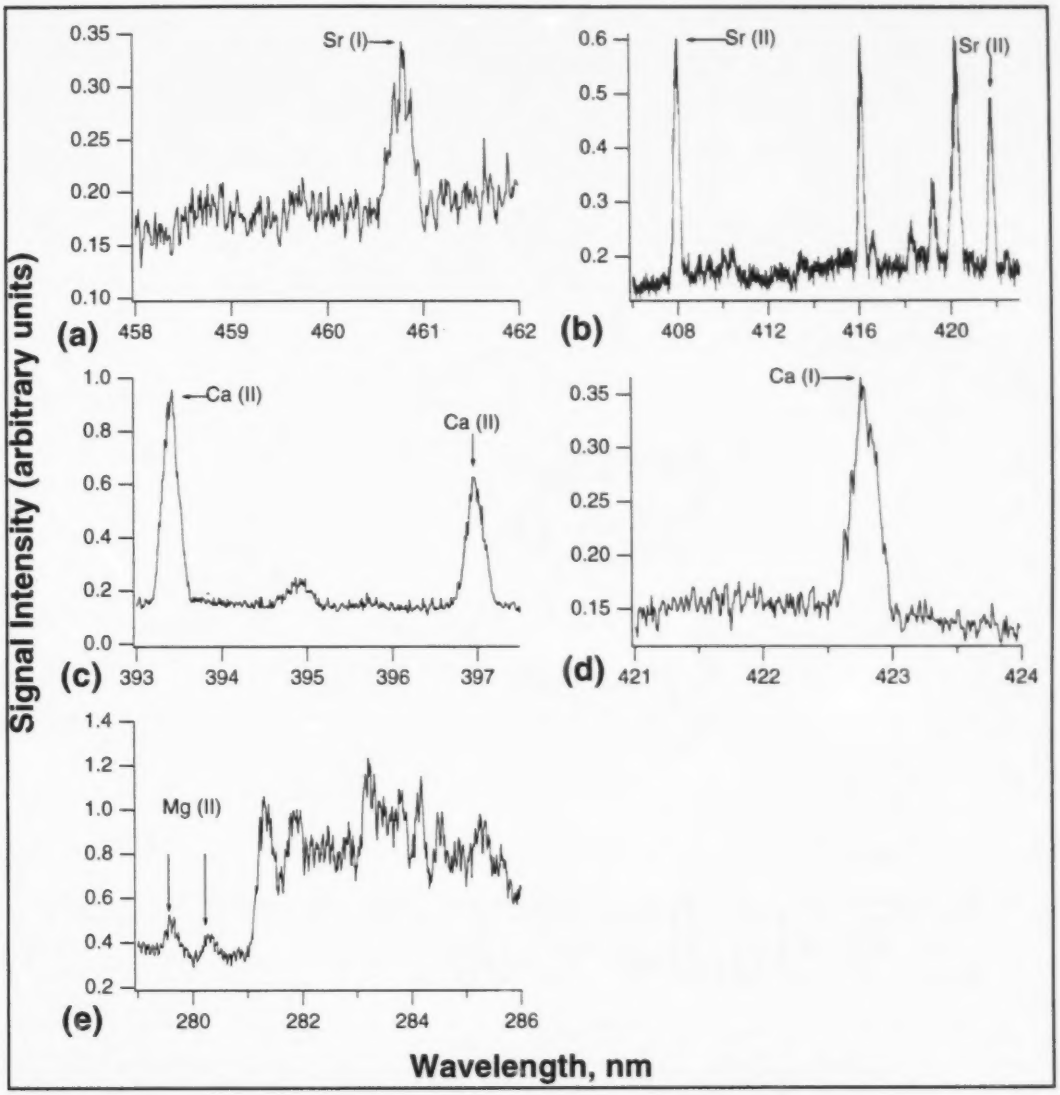

Figure 4.14
Optical emission spectra of various analytes in argon, at 1000 ppm, viewed "side-on" through expansion chamber. Nebulizer flow rate 0.5 L/min.1.25 kW, 15 mm sampling distance, 100 μm monochromator entrance slit. Arrows indicate analyte signals.

(a) 1000 ppm Sr (I) from 458 to 462 nm.
(b) 1000 ppm Sr (II) from 407 to 422 nm.
(c) 1000 ppm Ca (II) from 393 to 398 nm.
(d) 1000 ppm Ca (I) from 421 to 424 nm.
(e) 1000 ppm Mg (II) from 279 to 286 nm.

detection limit for its strong ionic lines at 407 and 421 nm and 100 ppm cannot be detected at all at its atomic line of 460 nm, nor can calcium at 100 ppm be observed at its strongest lines. This is a reduction to about 0.02% of the signals observed for other measurements in this work. This extremely weak emission observed corresponds with the earlier report by Houk [46]. It had been hoped to make a study of matrix effects viewed end-on and of the the expansion zone viewed side-on, in order to help clarify whether or not they would arise in the absence of ion optics, but it is clear that in order to have a matrix element present in an approximate matrix/analyte ratio of at least 1000/1, the matrix concentration would clog the sampling orifice. In addition, the deposition of such concentrated solutions of ionized salts on the sampling orifice causes the plasma to arc to the plate, which gravely affects the stability of the discharge.

This work seems to indicate a lack of excited magnesium, calcium, and strontium species in the zone of silence. Hence it was decided to attempt, if possible, some absorbance measurements in order to monitor ground level species to obtain information about which species are present in that zone and the surrounding shock region. Absorbance measurements of the NAZ of the ICP have been successfully made [72] by Gillson and Horlick. Unfortunately the problem of radio frequency interference from the ICP itself is far more severe when set up in the manner described, than for usual NAZ studies or for mass spectrometric studies, where the detector is electrically shielded from the plasma. It requires careful planning to reduce the interference to an acceptable level in order to establish any such study, which has not yet been done. Nonetheless, this may be a useful way to probe this region, if the electrical problems could be surmounted.

4.3 Conclusions

The spectra observed from 275 to 660 nm "end-on" with and without sampler and expansion chamber present were similar to one another and to the water and argon spectra described by Fassel *et al.* [61]. The analyte signal response to changes in the nebulizer flow rate of the two set-ups were similar to one another. The optimum nebulizer flow rate was lower than that typically seen for ICP-MS and is more typical of the rate for ICP-OES. These results indicate that the region observed visually "end-on" with the sampler plate and expansion chamber present was similar to that observed along the axis of the plasma. The presence of the sampling plate did not appear to alter the observed emission, other than to physically block emission from the brilliant plasma surrounding the central channel.

The observed analyte signal response to the addition of nitrogen into the outer plasma gas differed from that observed in ICP-MS, as reported here, and from that reported elsewhere for ICP-OES, in that the optimum nebulizer flow rate did not change although the sampling position was unchanged. Ionic emission of magnesium was enhanced almost tenfold and atomic emission of magnesium, lead, and argon were increased four to sixfold with the addition of six percent nitrogen, although a concomitant molecular background increase meant that the SBR and SNR for the atomic lead lines worsened. The spectrum viewed "side-on" through the expansion chamber was unlike the usual NAZ argon and water spectrum. Although the background was much reduced, analyte emission was also extremely weak. The measurement system used was insufficient for further diagnostic or analytical purposes.

CHAPTER 5

CONCLUSIONS

The effect of the introduction of nitrogen into various gas flows of the ICP upon the analyte species iron and selenium and the background interferent species was investigated and concurs to some extent with other reported observations. With the addition of up to 10% nitrogen to the coolant gas flow and a decreased sampling distance, the background signals of the argon oxide and dimer interferences were reduced, as has been reported by Lam and co-workers [75, 32], although the reduction seen in this work was not as large as theirs. Improvements to the SBR and SNR about the same size as that reported by Beauchemin and Craig [39] were also observed, although their reported analyte iron and selenium signals also decreased, which may be because they did not also adjust the nebulizer flow to higher values as nitrogen was introduced. This adjustment, along with a decrease in sampling distance, was shown in this work to be necessary to obtain an increased signal when nitrogen was introduced into the coolant flow or into all gas flows. An enhanced selenium signal was observed, which may be due to increased ionization from the nitrogen containing plasma. The addition of up to 2% nitrogen into all gas flows showed very similar effects as the introduction of the same amount of nitrogen into the coolant only. There is less benefit to the analyte and plasma background signals from the addition of such a small amount of nitrogen, along with the disadvantages of increased plasma noise and instability. The introduction of small amounts of nitrogen into the nebulizer flow doubled the analyte signals when sampled at 12 mm but the background and and noise were not decreased, and at a 15 mm sampling distance no significant differences were seen in analyte or background signals. This contrasts with results reported by Ebdon and Evans [41] but the operating parameters

investigated differed. The fourfold improvements to SNR and SBR with the addition of nitrogen into the coolant are not great but a trend is apparent and in combination with other techniques such as desolvation of the sample aerosol, other incremental improvements may be added to make the improvement more significant.

The optical spectra of the region near the sampling plate indicates that the region viewed was similar to that viewed along the axis of the plasma and was not altered by the presence of the sampling plate. The introduction of nitrogen into the coolant increased the ionic emission of magnesium by almost an order of magnitude. The atomic emission of argon, magnesium, and lead were increased by about four times, but the accompanying increased background molecular and continuum emission reduced the SBR and SNR for the atomic analyte species. Increased signal response with the addition of nitrogen into the plasma was seen at the same nebulizer flow rate and sampling position as for argon. This differs from the observed behaviour for ICP-MS and ICP-OES. The optical emission spectrum of the region within the expansion chamber was very weak. Spatial distribution and excitation levels of analyte species cannot be compared if only the analyte resonance lines can be observed, and requires more sensitive or selective detection methods, such as absorbance or laser fluorescence. To successfully probe this region, extensive electrical shielding from the plasma is required. The recent announcement by Thermo Jarrell Ash [73], *inter alia*, of a commercially available ICP-OES instrument incorporating an axially mounted (end-on) ICP will probably facilitate further study [76] in this area.

REFERENCES

1 D.J. Douglas, *Spectrochim.Acta*, **41B**, 197 (1986).

2 D.J. Douglas and J.B. French, *J. Anal. At. Spectrom.*, **3**, 743 (1988).

3 D.J. Douglas, "Fundamental Aspects of Inductively Coupled Plasma Mass Spectrometry," Chapter 13 in *Inductively Coupled Plasmas in Analytical Atomic Spectroscopy*, 2nd edition, A. Montaser and D.W. Golightly (Eds.), VCH Publishers New York (1992).

4 A. Montaser, *Spectrochim.Acta*, **45B**, 603 (1990).

5 D.M. Chambers, J. Poehlman, P. Yang, and G.M. Hieftje, *Spectrochim.Acta*, **46B**, 741 (1991).

6 D. Beauchemin, J.W. McLaren, and S.S. Berman, *Spectrochim.Acta* , **42B**, 467 (1987).

7 G.R. Gillson, D.J. Douglas, J.E. Fulford, K.W. Halligan, S.D. Tanner, *Anal. Chem.*, **60**, 1472 (1988).

8 G. Horlick and Y. Shao, "Inductively Coupled Plasma-Mass Spectrometry for Elemental Analysis," Chapter 12 in *Inductively Coupled Plasmas in Analytical Atomic Spectroscopy*, 2nd edition, A. Montaser and D.W. Golightly (Eds.), VCH Publishers New York (1992).

9 H.P. Longerich, B.J. Fryer, and D.F. Strong, *Spectrochim.Acta*, **42B**, 49 (1987).

10 A.R. Date, *Spectrochim.Acta Rev.*, **14**, 3, (1991).

11 J.A. Olivares and R.S. Houk, *Anal. Chem.*, **58**, 20 (1986).

12 S.H. Tan and G. Horlick, *J. Anal. At. Spectrom.*, **2**, 745 (1987).

13 D.M. Chambers, B.S. Ross, and G.M. Hieftje, *Spectrochim.Acta*, **46B**, 785 (1991).

14 M.A. Vaughan and G. Horlick, *Spectrochim.Acta*, **45B**, 1301 (1990).

15 G.M. Hieftje, manuscript (1992).

16 S.R. Koirtyohann, J.S. Jones, C.P. Jester, and D.A. Yates, *Spectrochim.Acta*, **36B**, 49 (1981).

17 B.L. Caughlin and M.W. Blades, *Spectrochim.Acta*, **40B**, 1539 (1985).

18 B.L. Caughlin and M.W. Blades, *Spectrochim.Acta*, **39B**, 1583 (1985).

19 N. Furuta, *Spectrochim.Acta*, **41B**, 1118 (1986).

20 R.S. Houk, V.A. Fassel, G.D. Flesch, H.J. Svec, A.L. Gray, and C.E. Taylor, *Anal. Chem.*, **52**, 2283 (1980).

21 J.A. Olivares and R.S. Houk, *Anal. Chem.*, **57**, 2674 (1985).

22 J.W.H. Lam and G. Horlick, *Spectrochim.Acta*, **45B**, 1327 (1990).

23 M.A. Vaughan and G. Horlick, *Spectrochim.Acta*, **45B**, 1289 (1990).

24 A.R. Date and A.L. Gray, *Analyst*, **106**, 1255 (1981).

25 D. C. Gregoire, *Spectrochim.Acta*, **42B**, 895 (1987).

26 D.C. Gregoire, *Appl. Spectrosc.*, **41**, 897 (1987).

27 J. Wang, W.L. Shen, B.S. Sheppard, E.H. Evans. and J.A. Caruso, *J. Anal. At. Spectrom.*, **5**, 445 (1990).

28 S.E. Hobbs and J.W. Olesik, *Appl. Spectrosc.*, **45**, 1395 (1991).

29 S.D. Tanner, *Spectrochim.Acta*, **47B**, 809 (1992).

30 G. King & G. Horlick, *Spectrochim.Acta*, **47B**, E353 (1992).

31 S.H. Tan and G. Horlick, *Appl. Spectrosc.*, **40**, 445 (1986).

32 J.W. Lam and J.W. McLaren, *J. Anal. At. Spectrom.*, **5**, 419 (1990).

33 R.C. Hutton and A.N. Eaton, *J. Anal. At. Spectrom.*, **2**, 595 (1987).

34 R. Tsukahara and M. Kubota, *Spectrochim.Acta*, **45B**, 581 (1990).

35 M.J. Powell, D.W. Boomer, and R.J. McVicars, *Anal. Chem.*, **58**, 2864 (1986).

36 F.G. Smith, D.R Wiederin, and R.S. Houk, *Anal. Chem.*, **63**, 1458 (1991).

37 E.H. Evans and L. Ebdon, *J. Anal. At. Spectrom.*, **4**, 299 (1989).

38 L. Ebdon, M.J. Ford, R.C. Hutton, and S.J. Hill, *Appl. Spectrosc.*, **48**, 507-516 (1994).

39 D. Beauchemin and J.M. Craig, *Spectrochim.Acta*, **46B**, 603 (1991).

40 M.A. Vaughan and G. Horlick, *Appl. Spectrosc.*, **40**, 434 (1986).

41 E.H. Evans and L. Ebdon, *J. Anal. At. Spectrom.*, **5**, 425 (1990).

42 L.L. Burton and G. Horlick, *Spectrochim.Acta*, **47B**, E1621 (1992).

43 This spectrum courtesy of Hugh Johnson.

44 G. Horlick, S.H. Tan, M.A. Vaughan, and C.A. Rose, *Spectrochim.Acta*, **40B**, 1555 (1985).

45 M.A. Vaughan, G. Horlick, and S.H. Tan, *J. Anal. At. Spectrom.*, **2**, 765 (1987).

46 H.B. Lim, R.S. Houk, M.C. Edelson and K.P. Carney, *J. Anal. At. Spectrom.*, **4**, 365 (1989).

47 J.E Fulford and D.J. Douglas, *Appl. Spectrosc.*, **40**, 971 (1986).

48 A.L. Gray, R.S. Houk, J.G. Williams, *J. Anal. At. Spectrom.*, **2**, 13 (1987).

49 R.S. Houk, J.K. Schoer, and J.S. Crain, *J. Anal. At. Spectrom.*, **2**, 283 (1987).

50 D.M. Chambers and G.M. Hieftje, *Spectrochim.Acta*, **46B**, 761 (1991).

51 D.M. Chambers, J.W. Carnahan, Q. Jin, and G.M. Hieftje, *Spectrochim.Acta*, **46B**, 1745 (1991).

52 B.S. Ross, and G.M. Hieftje, *Spectrochim.Acta*, **46B**, 1263 (1991).

53 H.C.W. Beijerinck, R.J.F. van Gerwen, E.R.T. Kerstel, J.F.M. Martens, E.J.W. van Vliembergen, M.R.Th. Smits and G.H. Kaashoek, *Chem. Phys.*, **96**, 153 (1985).

54 A. Höglund and L-G. Rosengren, *Int. J. Mass Spectrom. Ion Processes*, **60**, 173 (1984).

55 A.N. Hayhurst and N.R. Telford, *Combust. Flame*, **28**, 67 (1977).

56 A.N. Hayhurst and N.R. Telford, *Combust. Flame*, **28**, 123 (1977).

57 A.N. Hayhurst and N.R. Telford, *Combust. Flame*, **28**, 137 (1977).

58 R.S Houk and H.B. Lim, *Anal. Chem.*, **58**, 3244 (1986).

59 H.B. Lim, K.P. Carney, M.C. Edelson, and R.S. Houk, *Spectrochim.Acta*, **48B**, 1617 (1993).

60 K. Lepla, M.A. Vaughan and G. Horlick, *Spectrochim.Acta*, **46B**, 967 (1991).

61 R.K. Winge, V.A. Fassel, V.J. Peterson, and M.A. Floyd, (Eds.) "Inductively Coupled Plasma-Atomic Emission Spectroscopy: An Atlas of Spectral Information," *Physical Sciences Data 20* series, Elsevier Science Publishers B.V., Amsterdam (1985).

62 A. Montaser, I. Ishii, B.A. Palmer and L.R. Layman, *Spectrochim.Acta*, **45B**, 603 (1990).

63 I. Ishii, D.W. Golightly and A. Montaser, manuscript.

64 W.L. Wiese, "Line Broadening," Chapter 6 in *Plasma Diagnostic Techniques*, R.H. Huddlestone and S.L. Leonard (Eds.), Academic Press, New York (1965).

65 A. Montaser, V.A. Fassel, and J. Zalewski, *Appl. Spectrosc.*, **35**, 292 (1981).

66 A. Montaser and J. Mortazavi, *Anal. Chem.*, **52**, 225 (1980).

67 E.H. Choot and G. Horlick, *Spectrochim.Acta*, **41B**, 889 (1986).

68 F.E. Lichte and S.R. Koirtyohann, *ICP Inform. Newslett.*, **2**, 192 (1976).

69 D.R. Demers, *Appl. Spectrosc.*, **33**, 584 (1979).

70 L.M.H. Faires, *Thesis,* Los Alamos National Laboratory Los Alamos New Mexico 87545, 54 (1983).

71 L.M. Faires, T.M. Bieniewski, C.T. Apel, and T.M. Niemczyk, *Appl. Spectrosc.*, **39**, 5 (1985).

72 G. Gillson and G. Horlick, *Spectrochim.Acta*, **41B**, 619 (1986).

73 R. Foster, R. Crawford, A.E. Pellowe, and J.J. Sotera, Thermo Jarrell Ash, Abstract 465, 1994 Pittsburgh Conference.

74 E.H. Evans and J.J. Giglio, *J. Anal. At. Spectrom.*, **8**, 1 (1993).

75 J.W.H. Lam and G. Horlick *Spectrochim.Acta*, **45B**, 1313 (1990).

76 Y. Nakamura, K. Takahashi, O. Kujirai, H. Okochi and C.W. McLeod, *J. Anal. At. Spectrom.*, **9**, 751 (1994).